University Medical Center Hamburg-Eppendorf

Institute of Clinical Chemistry and Laboratory Medicine

Regulation of CD4+ T-cell Responses through Modulation of intracellular Polyphosphate

Dissertation

Submitted to the Department of Chemistry

Faculty of Mathematics, Informatics and Natural Sciences

University of Hamburg

In fulfilment of the requirements for the degree of

Doctor of Natural Sciences (Dr. rer. nat.)

By

Benita Kröger

July 2025, Hamburg

List of publications and presentations

<u>Kröger B</u>, Spohn M, Mengel M, Sperhake JP, Ondruschka B, Mailer RK. Expression of full-length FOXP3 exceeds other isoforms in thymus and stimulated CD4 + T cells. J Clin Immunol. 2024 Apr 27;44(5):114. doi: 10.1007/s10875-024-01715-8. PMID: 38676826; PMCID: PMC11055749.

<u>Kröger B</u>, et al., Degradation of intracellular polyphosphate promotes calcium mobilization and induces a non-suppressive regulatory T cell-like phenotype in stimulated CD4+ T cells. *in preparation*

Part of this work was presented at the following conferences:

Date	Conference	Type of presentation
September 2024	ECI Dublin	Poster presentation
May 2025	Third International Conference on Polyphosphate Biology	Oral presentation

Table of contents

1 Zusammenfassung

Polyphosphat (polyP) ist ein Biopolymer bestehend aus bis zu mehreren hundert verknüpften Phosphatmolekülen und ist in jeder Zelle vorhanden. Die Funktion von PolyP ist sehr gut in Bakterien und Hefen definiert, während die Bedeutung von PolyP in Säugetierzellen bislang weitgehend unbekannt ist. Es wurden jedoch pro-thrombotische und pro-inflammatorische Fähigkeiten von sezerniertem PolyP aus Blutplättchen, basophilen Granulozyten und Mastzellen beschrieben. In dieser Arbeit wurde PolyP aus CD4+ T-Zellen charakterisiert und die Bedeutung von PolyP für T-Zell Stimulation und Differenzierung untersucht. Zunächst konnte gezeigt werden, dass T-Zellen bei Stimulation PolyP akkumulieren, wobei diese Anreicherung von Glykolyse und T-Zelldifferenzierung abhängig ist. Während pro-inflammatorische CD4+ T-Zellpopulationen mehr PolyP anhäufen, wird bei einer Induktion anti-inflammatorischer, regulatorischer T-Zellen (Treg) weniger PolyP angereichert. Um den PolyP-Gehalt in primären CD4+ T-Zellen zu modulieren, wurde eine zell-penetrierende Polyphosphatase (CPP-Ppx1) rekombinant hergestellt, was eine effiziente und nicht-toxische Expression des Enzyms mittels Proteintransduktion ermöglichte. Durch den Verdau von PolyP durch CPP-Ppx1 wurde intrazellulär Calcium mobilisiert, welches zu einer Stoffwechselkaskade in behandelten T-Zellen führte und eine vermehrte Produktion von Aktivierungsmarkern und eine gesteigerte Proliferation zur Folge hatte. Dies konnte sowohl in Durchflusszytometrie als auch im Assay für Transposase-zugängliches Chromatin nachgewiesen werden. Des Weiteren führte der PolyP-Verdau durch CPP-Ppx1 zu einem erhöhten Metabolismus durch Glykolyse und oxidative Phosphorylierung sowie, daraus resultierend, einer gesteigerten Gesamt-ATP-Produktion. Darüber hinaus induzierte der Verdau von PolyP die Expression des Treg-Transkriptionsfaktors Foxp3. Überraschenderweise rief die Expression von Foxp3 keine immunosuppressive Treg-Funktion hervor und dies konnte mit einer instabilen Foxp3 Induktion, bedingt durch eine unzureichende Demethylierung des *Foxp3* Promoters, und einer konstant erhöhten Produktion von Interleukin-2 begründet werden. Zusammenfassend konnte in dieser Arbeit gezeigt werden, dass PolyP differentiell in unterschiedlichen T-Zell Populationen reguliert wird und dass PolyP die Aktivierung von T-Zellen durch Bindung von Calcium hemmt. Eine experimentelle Reduktion von intrazellulärem PolyP resultierte in einem Treg-ähnlichen, jedoch nicht-suppressiven, Phänotyp *in vitro*, so dass eine Modulation

von PolyP in CD4+ T-Zellen geeignet sein könnte, um Immunantworten zu beeinflussen.

2 Abstract

Polyphosphate (polyP) is a biopolymer consisting of up to several hundred linked phosphate residues and can be found in every cell type. PolyP has been associated with multiple cellular functions that are well defined in bacteria and yeasts, whereas its significance in mammalian cells remains largely unknown. However, pro-thrombotic and pro-inflammatory functions have been ascribed to extracellular polyP released from platelets, basophils and mast cells. In this study, intracellular polyP from CD4+ T cells was characterised and the role of polyP for T-cell stimulation and differentiation was investigated. PolyP was shown to accumulate in stimulated CD4+ T cells in a glycolysis-dependent manner and in response to T-cell differentiation *in vitro*, where pro-inflammatory CD4+ T-cell populations display more polyP than anti-inflammatory, regulatory T (Treg) cells. To modulate polyP in primary CD4+ T cells, a recombinant cell-penetrating peptide polyphosphatase (CPP-Ppx1) fusion protein was produced, that allows for the efficient protein transduction into viable T cells. Degradation of polyP with CPP-Ppx1 resulted in calcium mobilisation and signalling in treated CD4+ T cells that increased activation marker expression and proliferation, analysed by both flow cytometry and chromatin accessibility assays. Moreover, polyP digestion by CPP-Ppx1 led to enhanced glycolysis and oxidative phosphorylation, resulting in an elevated overall ATP production. Furthermore, expression of the Treg transcription factor Foxp3 was induced in CD4+ T cells with CPP-Ppx1 mediated polyP reduction. However, Foxp3 expression in response to CPP-Ppx1 treatment did not facilitate immunosuppressive Treg functions, which could be attributed to transient Foxp3 expression, caused by insufficient demethylation of the *Foxp3* promotor, and a constant production of elevated interleukin-2 levels.

In summary, this study demonstrated that polyP is differentially regulated in distinct T-cell subsets and that polyP inhibits T-cell activation by binding calcium. Experimental degradation of intracellular polyP results in a Treg-like phenotype *in vitro* but did not confer suppressive functions. Thus, the regulation of T-cell polyP might be a useful tool for the modulation of CD4+ T-cell responses in future applications.

3 Introduction

3.1 <u>Immune System</u>

The immune system is the first defence mechanism that protects against harmful pathogens that challenge our body every day. It consists of a complex network of organs, cells and proteins, working in unison to prevent entry and induction of disease by viruses, microorganisms and parasites. The very first physical barrier is formed by all outer and inner surfaces of the body. Pathogens that cross this first hindrance trigger an immune response that is typically divided into innate and adaptive immunity.

3.1.1 Innate and adaptive immune system

The first and unspecific response to pathogens is provided by the innate immune system, which is available early on in life. An array of different cell types, like macrophages, granulocytes, mast and natural killer cells are able to recognize conserved pathogen-associated molecular patterns (PAMPs, e.g. microbial nucleic acids, surface glycoproteins, lipopolysaccharide) on the surface of pathogens or damage-associated molecular patterns (DAMPs, e.g. cytoplasmic proteins, heat shock proteins) released by injured cells [1]. Upon recognition of these patterns, the innate immune system reacts with numerous unspecific responses like cytokine secretion or phagocytosis, leading to antigen presentation and thereby activation of the adaptive immune system.

The adaptive response is slower but highly specific for antigens and generates immunologic memory towards pathogens upon first contact. The key players are T and B lymphocytes that are derived from hematopoietic stem cells in the bone marrow. During their development, T and B cells rearrange antigen-receptor gene segments that allows them to express receptors recognizing self and non-self-antigens. During somatic recombination, the combination of a variable (V), a joining (J) and a diverse (D) region, further modified by addition and/or deletion of nucleotides at the junction sites between the gene segments, creates a virtually unlimited range of T and B cell receptor transcripts [2]. Mature B and T cells patrol blood and lymph in search for cognate antigens as naïve lymphocytes that will initiate a proliferation and differentiation program into effector cells to exert potent defence mechanisms, like antibody production, cytokine secretion or release of cytotoxic reagents upon antigen

contact. Following the eradication of pathogens, some lymphocytes will retain their acquired pathogen-specific reactivity and form a pool of memory cells that provide a long-lasting protection against already encountered pathogens.

The proper execution of immune responses is crucial for the defence against pathogens because a hyperactive or misdirected immune response can cause damage to surrounding tissues, while an insufficient immune response might lead to pathogen spreading and infectious diseases. A balanced immunologic environment providing both pro- and anti-inflammatory effects is therefore required to maintain health.

Particularly, T cells are required to control their responsiveness meticulously, firstly because the elimination of self-reactive T-cell antigen receptor (TCR)-bearing cells during development ensures immunological tolerance against self-antigens and secondly, their supportive interactions with other immune cells positions them as pivotal regulators to prevent unhinged immune reaction that would otherwise cause immunopathology and autoimmunity.

3.1.2 T lymphocytes

3.1.2.1 Development of T cells

T cells recognize and respond to antigens presented on the surface of infected cells and are crucial to support cellular and humoral immune responses. After their development from hematopoietic stem cells in the bone marrow, T cells migrate to the thymus for maturation. As a primary lymphoid organ, the thymus reaches its maximal size in humans after roughly 12 months, after which it shrinks, due to a process called thymic involution. Precursor T cells enter the thymus in a double negative (CD4-CD8-) stage and firstly commit to the expression of the α- and β- or the γ- and δ-chain of the TCR [3]. While αβ-T cells form the adaptive T-cell population, γδ-T cells present an innate-like T-cell phenotype. Further development of αβ-T cells is marked by the expression of both CD4 and CD8 receptors on the surface at the double positive developmental stage. Cells then undergo two selection processes to ensure measured signalling capacity of the individually expressed TCR. The first process is the positive selection in which recognition of major histocompatibility complex (MHC) class I or II molecules is tested. Only cells that can recognize MHC class I or II survive the selection process and become single positive CD8+ or CD4+ T cells, respectively. After

that, cells undergo the negative selection in which all cells binding to presented self-antigens with high affinity receive an apoptotic signal. The cells that survived both selection processes emigrate into secondary lymphoid organs as naïve T cells. Besides classical CD4+ or CD8+ T cells, some non-conventional T-cell lines are also produced in the thymus. Among these are the natural regulatory T cells (nTreg) characterised by a CD4+CD25+Foxp3+ phenotype or natural killer cells (NK cells) that can be either CD4+ or CD4-CD8- [4]. CD8+ T cells, also known as cytotoxic T cells, patrol the body to detect foreign proteins, e.g. virus particles and tumour neoantigens, which are bound to MHC class I molecules expressed by almost all cell types, and eliminate these cells by the release of cytotoxic granula. In contrast, the CD4 receptor supports the TCR-mediated recognition of foreign proteins of endolysosomal origin bound to MHC class II molecules, which are mainly expressed on antigen presenting cells (APCs), such as dendritic cells or B cells. After TCR engagement on naïve T cells in spleen and lymph nodes, cells proliferate, differentiate into distinctive subsets and migrate into the periphery to further scout for antigens and to facilitate important support for other immune cells. Particularly CD4+ T cells play a central role in the immune system as they elevate CD8+ T-cell-mediated cytotoxicity, antibody production in B cells, phagocytic activity in macrophages and immune cell migration through the release of cytokines and chemokines.

3.1.2.2 CD4+ T-cell stimulation

Naïve T cells circulate the lymphoid system and scout for APCs that present their respective antigen and may elicit signalling by their specific TCR. T-cell stimulation requires three activation signals: antigen-recognition, co-stimulation and cytokine signalling (**Figure 1**).
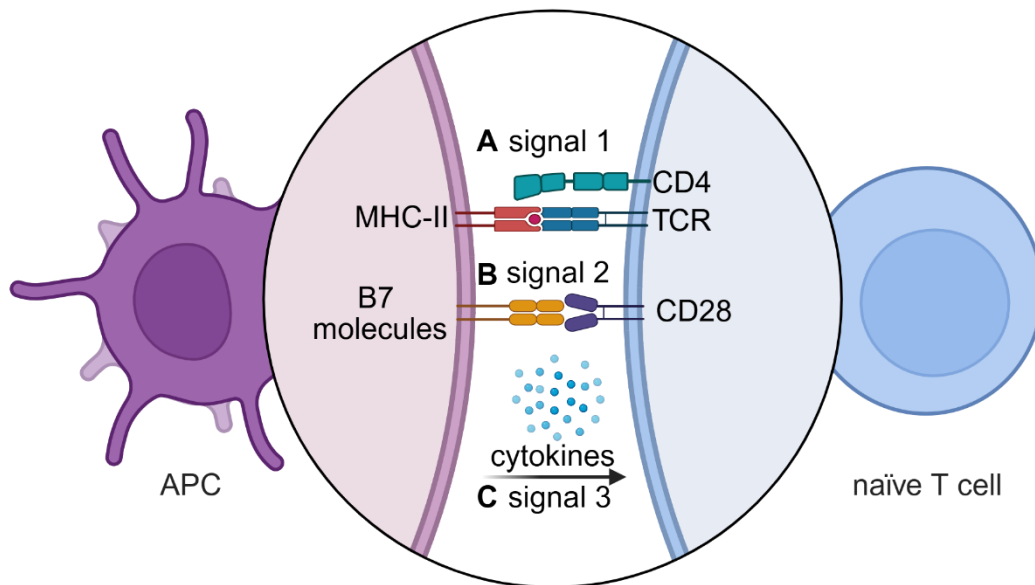
Figure 1. Stimulation of naïve CD4+ T cells. Naïve T-cell stimulation requires three activation signals. (**A**) The first signal is the binding of the T-cell receptor (TCR) to the MHC (II) receptor on APCs. (**B**) The second signal is the binding of costimulatory receptor CD28 to B7 molecules, followed by the third signal (**C**) comprised by a stimulatory cytokine environment. Created with biorender.com.

The first signal is comprised of a stable interaction between TCRs and antigens presented by MHC class II on the surface of an APC (**Figure 1A**). Membrane rearrangement provides a broad and steady T cell-APC interaction zone, known as the immunological synapse, which forms a defined sequence of TCRs, CD28 and other receptor-ligand engagements between the cells. TCR signalling results in the activation of downstream pathways that culminates in calcium release from the sarcoplasmic reticulum, amplified by further calcium influx into the cell from the outside. Calcium binds to calcineurin which then dephosphorylates nuclear factor of activated T-Cells (NFAT) to enable its passage to the nucleus, where it promotes the transcription of interleukin-2 (IL-2), an essential cytokine for T-cell proliferation. IL-2 production can further be increased, e.g. in response to activation of the RAS/extracellular signal-regulated kinases (ERK) pathway as a distal reaction to TCR activation [5].

In addition, T cells are activated by binding of co-stimulatory receptor CD28 to B7 molecules CD80 and CD86 expressed on activated APCs (**Figure 1B**) [6, 7]. CD28 signalling leads to activation of the AKT/mammalian target of rapamycin (mTOR) pathway followed by nuclear factor kappa-light-chain-enhancer of activated B cells (NFκB) translocation into the nucleus, culminating in transcription of further activation

signals. The co-stimulation therefore results in a potentiation of the TCR signalling itself [4, 5].

These two signals are sufficient to prime T cells for carrying out their effector functions. However, the activation of T cells goes hand in hand with the expression of cytokine receptors and the final differentiation of activated T cells depends largely on the third signal, the cytokine environment provided by the APC and other immune cells (**Figure 1C**). Fully differentiated T cells produce a characteristic repertoire of cytokines and transcription factors that facilitate optimal immune responses to bacterial, parasitic and fungal infections through certain adaptations, which are also used to categorize the predominant T-cell differentiation. Mossmann and Coffman were the first to characterize two distinct cytokine profiles, defining the inflammatory T helper (Th) cell subsets Th1 and Th2. While Th1 cells were defined as interferon gamma (IFNγ) producing cells, Th2 cells produce IL-4 [8]. This classification is still in use but ever more subsets like Th17 and regulatory T (Treg) cells have been defined and will be discussed in the following paragraphs (**Figure 2**). It is noteworthy however, that the scope of T-cell subpopulations remains ever growing and is even more complex due to the proposed flexibility in T-cell commitment, that allows the cell to alter its cytokine expression profile [9-11].

3.1.2.3 T-helper-cell subsets
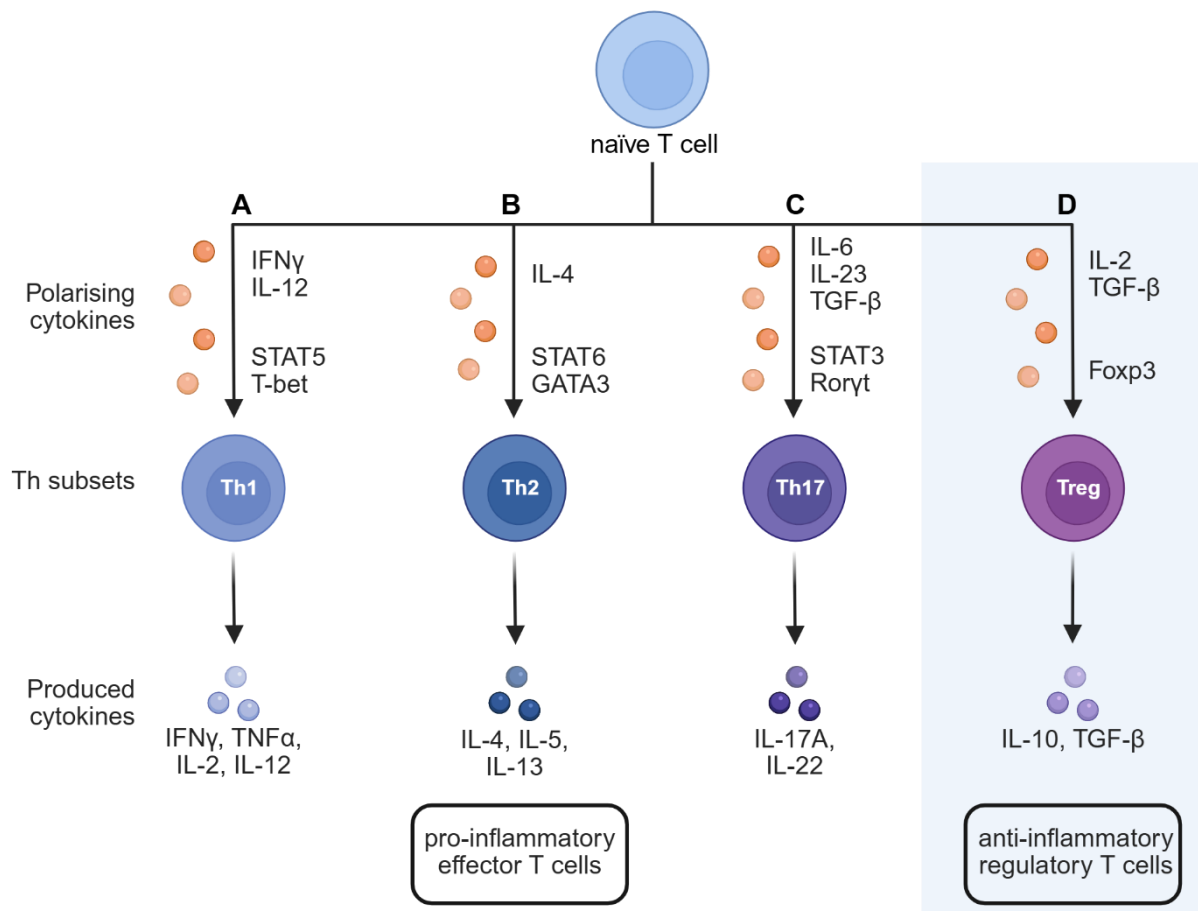
Figure 2. Differentiation of T-helper-cell subsets. (**A**) IFNγ and IL-12 prime naïve T cells to develop a Th1 phenotype which is characterised by expression of the transcription factors STAT5 and T-bet and the cytokines IFNγ, TNFα and IL-2. (**B**) IL-2 and IL-4 are the defining cytokines for the development of a Th2 phenotype expressing STAT6 and GATA3 and producing IL-4, IL-5 and IL-13. (**C**) IL-6, IL-23 and TGF-β skew a Th17 phenotype characterised by STAT3 and Rorγt expression followed by IL-17A and IL-22 expression. (**D**) IL-2 and TGF-β induce the expression of Foxp3, the characteristic marker for Treg cells which produce the anti-inflammatory cytokines IL-10 and TGF-β. Created with biorender.com.

Th1 cells mainly differentiate as a response to viral and bacterial infections which induce IL-12 and IFNγ production in natural killer and dendritic cells (**Figure 2A**). This cytokine environment results in the activation of signal transducer and activator of transcription 1 (STAT1) which in turn activates the Th1-characteristic transcription factor T-box expressed in T cells (T-bet). Th1 cells produce IL-2, IL-12, IFNγ and tumour necrosis factor α (TNFα) that support the immune response of CD8+ T cells and macrophages. The transcription factor T-bet induces the activation of STAT4 and consequently the production of IFNγ and also inhibits the formation of the Th2 lineage by inhibiting IL-4 production. Through interaction with the *Rorc* promoter the production

of retinoic acid receptor-related orphan receptor gamma (Rorγt) is inhibited, therefore T-bet also inhibits the production of Th17 cells [4, 12, 13].

IL-4 promotes the development of the Th2 lineage which plays a key role in parasitic inflammation and allergies, but also mediates the class switch important for B cell IgE antibody production. IL-4 induces the phosphorylation of STAT6 in CD4+ T cells which results in the production of GATA3 (**Figure 2B**). This transcription factor activates the cytokine production of IL-4, IL-5 and IL-13 in order to promote the humoral immunity [14]. GATA3 also inhibits the manifestation of a Th1 phenotype by downregulation of STAT4 and the IL-12 receptor [12, 13].

IL-23, transforming growth factor β (TGF-β) and IL-6 are crucial cytokines for the differentiation of Th17 cells that take part in the clearance of bacterial and fungi infections (**Figure 2C**). IL-6 mediated induction of STAT-3 results in the activation of the characteristic transcription factor Rorγt that in turn leads to the expression of the pro-inflammatory cytokines IL-17A and IL-22. In addition, Rorγt inhibits the expression of the Treg marker forkhead box P3 (Foxp3), induced by TGF-β [4, 13]. Th17 cells have been identified as key players in the development of auto-inflammatory diseases like rheumatoid arthritis [15-17], inflammatory bowel disease [18-21] and multiple sclerosis [22-25].

3.1.2.4 Regulatory T (Treg) cells

The negative selection in the thymus diminishes the amount of self-reactive T cells and provides central immune tolerance. However, some T cells may escape this selection process, which therefore demands for regulation of immune reactions in the periphery. In order to maintain peripheral tolerance, the immune system requires a way to prevent autoreactive immune activation and to dampen overshooting immune reactions. This is provided by a pool of Treg cells which exert anti-inflammatory effects. Sakaguchi first described a regulatory CD4+ T-cell subset which could prevent graft versus host disease. The IL-2 receptor α-chain (CD25) was defined as a characteristic surface marker of this immunosuppressive subset [26]. Later on, Treg cells were further characterised by their expression of the transcription factor Foxp3, whose expression results in the development of a suppressive phenotype [27, 28].

Treg cells are either thymus-derived naturally occurring Treg (nTreg) cells or peripherally induced Treg (iTreg) cells. Although the differentiation between these two subsets is phenotypically difficult, as they express almost equal levels of CD25, Foxp3 and cytotoxic T-lymphocyte-associated protein 4 (CTLA4), it has been proposed that nTreg cells can be distinguished by higher expression of Neuropilin-1 and Helios [29, 30]. TGF-β and IL-2 are required to generate iTreg cells in the periphery (**Figure 2D**), in contrast to TGF-β and IL-6 which are needed for Rorγt induction in Th17 cells. In TCR stimulated CD4+ T cells, high doses of TGF-β alone result in the expression of Foxp3 and the production of IL-10 and TGF-β [4]. In mice, the expression of Foxp3 is generally considered to be a definitive marker for the development of suppressive Treg cells, while the same cannot be said for human Treg cells, as Foxp3 is also transiently expressed in TCR stimulated CD4+ T cells that do not have suppressive capacities [31-34].

Treg cells use several different anti-inflammatory mechanisms to supress overshooting immunity, such as the production of anti-inflammatory cytokines, the deprivation of local IL-2 by high expression levels of CD25, the production of adenosine by CD39, the direct inhibition by CTLA4 and finally cytolysis due to granzyme B production. [35, 36] Furthermore, the production of the anti-inflammatory cytokines IL-10 and TGF-β are major mechanisms of Treg mediated suppression. This was previously shown by Joentham *et al*. and Assemann *et al*., as these two cytokines can reduce the burden of both allergic airway inflammation and inflammatory bowel disease [37, 38].

IL-2 is one of the most important cytokines for T-cell differentiation and function that is not only expressed as early activation marker but also consumed by T cells as a growth factor. Treg cells are unable to produce IL-2 themselves and therefore express high levels of the high affinity IL-2 receptor α chain CD25 to meet their needs. This leads to a scavenging of IL-2 from the periphery and deprives pro-inflammatory T cells of their essential growth factor [39, 40]. In addition, CTLA4 is constitutively expressed on Treg cells that interacts with CD80 and/or CD86 on dendritic cells. This interaction can prime dendritic cells to produce indoleamine 2,3-dioxygease (IDO) which produces pro-apoptotic metabolites from tryptophan that exert toxic effects on surrounding cells [35]. Deficiencies, haploinsufficiency and impaired signal transduction of CD25 and CTLA4 have been reported in patients with immune dysregulation syndrome,

underlining the importance of these suppressive mechanisms for proper Treg function in humans [41-45].

Treg cells further express CD39 which converts pro-inflammatory adenosine triphosphate (ATP) to anti-inflammatory adenosine which inhibits Th1 cytokine production and promotes Treg proliferation and the expression of CTLA4 and programmed death 1 (PD1) [46]; however the role of CD39 for human Treg cell functions is less clear as the lack of CD39 on Treg cells is not associated with autoimmunity [47]. In addition, granzyme B, a serine protease prominently found in cytotoxic T or NK cells to induce apoptosis in infected cells, has also been reported in Treg cells to suppress effector cells in mice [48, 49].

Treg-mediated suppression depends on the stable expression of the master transcription factor FOXP3 in mice and men [27, 50]. Deficiency or dysfunction of this hallmark Treg-related protein causes IPEX (immune dysregulation, polyendocrinopathy, enteropathy, and X-linked syndrome) in humans or "scurfy" phenotype in mice, in which over-proliferative CD4+ T cells, accompanied by extensive multiorgan infiltration and elevated cytokine production, trigger fatal autoimmunity due to the lack of suppressive T cells [51, 52].

Stable Foxp3 expression is essential for both nTreg and iTreg cell development and maintenance [28, 53, 54]. Foxp3 transcription is regulated by specific CpG demethylation and histone modification patterns in the non-coding region 2 (CNS2) of the *Foxp*3 gene [55-57]. Under physiologic conditions TGF-β and IL-2 induce a complete demethylation of the Treg specific demethylated region (TSDR) in the *Foxp3* locus of stimulated CD4+ T cells. *In vitro* differentiation, however, fails to induce absolute demethylation [58, 59]. Further epigenetic modifications like acetylation [60, 61], phosphorylation [62] and ubiquitination [63] also impact Foxp3 stability and therefore suppressive function.

3.1.2.5 Metabolic profiles

T-cell activation and differentiation is associated with a distinct metabolic reprogramming, in order to satisfy the arising energetic demands. This becomes especially clear when comparing the metabolic status of effector T (Teff) cells and Treg

cells. While Teff cells strongly induce glucose uptake, Treg cells rely more on lipid oxidisation (**Figure 3**) [64].
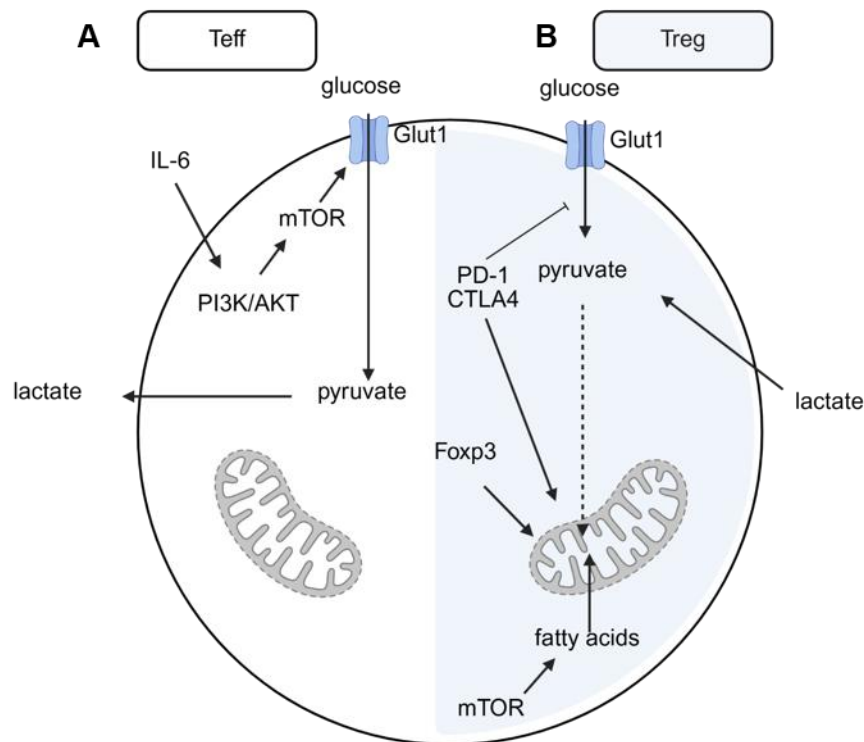
Figure 3. Metabolic profiles of Teff and Treg cells. (**A**) Upon stimulation Teff cells upregulate glucose uptake in an mTOR dependant manner and shift their metabolism towards the aerobic fermentation of glucose to lactate. (**B**) In contrast, Foxp3+ Treg cells reduce glycolysis but promote fatty acid oxidisation and oxidative phosphorylation. Signalling via inhibitory receptors like CTLA4 or PD-1 affect metabolic cues in T cells. Created with biorender.com.

Characteristic for stimulated Teff cells is the so called Warburg effect, an aerobic fermentation of glucose to lactate despite sufficient oxygen supply [65]. The cytokine environment during differentiation plays a defining role in this metabolic shift, as for example IL-6 induces the glycolysis directly and activates the PI3K/AKT signalling pathway [66]. This in turn activates the mTOR pathway which upregulates several gene sets relevant for glycolysis, the pentose phosphate pathway, steroid and fatty acid oxidisation and also induces the expression of Glucose Transporter 1 (Glut1) (**Figure 3A**) [67]. Glut1 is the most prominent glucose transporter in T cells and is more abundant on Teffs compared to Treg cells [68, 69]. In Treg cells, Foxp3-controlled gene expression inhibits the AKT/mTOR signalling with the consequence of increased oxygen consumption and pyruvate oxidisation on the cost of reduced glycolysis (**Figure 3B**) [70]. Further, inhibitory receptors like CTLA4 and PD-1 have also been

associated with a reduction in glycolytic metabolism and a fuelling of lipid oxidisation [71]. As stated before, this simple differentiation of Teff and Treg cells by metabolic activities does not hold true indefinitely. Foxp3+ Treg cells also upregulate Glut1 upon stimulation, but in contrast to Th1, Th2 or Th17 cells Treg cells utilise the glucose for generation of pyruvate, which is then processed in the Krebs-Cycle for further aerobic metabolism [72]. Glut1 overexpression has also been shown to promote the formation of a Treg phenotype but with reduced suppressive capacity [70].

An upregulation of oxidative phosphorylation will result in an increase of reactive oxygen species (ROS) within the cell, as complexes I and III of the respiratory chain have a 0.2-2% proton leak [64, 73]. Elevated ROS bears the risk of severe damage to the cell but is also used as secondary messenger for many signalling pathways. For one, ROS promote NFAT modulation and thereby encourage T cell activation. For another, ROS modulate the expression of cytokines and transcription factors [64, 73-75].

3.1.2.6 (Auto-)Inflammatory diseases

A balance between pro- and anti-inflammatory processes is required for optimal immune reaction, i.e. the timely eradication of pathogens and an adequate return to homeostatic conditions. If this equilibrium is disrupted, auto-inflammatory diseases or recurrent infections might be the consequence. Auto-reactive T cells or an overshooting immune response due to diminished function or number of Treg cells is characteristic for autoimmune reaction and chronic inflammation [76, 77]. Moreover, immune responses towards self-antigens have been associated with several (auto)immune diseases, e.g. diabetes [78], multiple sclerosis [24] and atherosclerosis [79]. Insufficient immune regulation with impaired differentiation of pro-inflammatory CD4+ T-cell populations are well described for the most common autoimmune diseases like rheumatoid arthritis [16, 80, 81], multiple sclerosis[82, 83], systemic lupus erythematosus[84, 85] and inflammatory bowel disease[19, 86-88].

3.1.2.7 Transfer of exogenous proteins into T cells

Vector-based transfection methods and excessive overexpression of exogenous enzymes are prone to toxicity and unspecifically perturbed metabolism. Specifically in

primary T cells, gene transfer has previously been shown to be a challenging task as also non-viral methods like electroporation or receptor-mediated gene transfer usually result in low transfer efficiencies accompanied by reduced cell viability [89]. However, by N-terminal addition of a tandem repeat derived from the protein transduction domain of the human transcription factor polyhomeotic-like protein 1 (HPH-1) to cargo proteins, Choi *et al.* showed that exogenous protein can be efficiently transferred into primary CD4+ T cells via protein transduction [33, 90]. Thus, protein transduction of exogenous proteins appears to be a useful strategy to target cellular pathways in which homologous genes have not been identified, yet. Particularly, the regulation of T-cell stimulation, metabolism and differentiation by inorganic polyphosphate could offer a novel approach to modulate (auto)immune responses.

3.2 <u>Inorganic polyphosphate</u>

Polyphosphate (polyP) is a linear polymer of up to several hundred phosphate moieties linked by energy-rich phosphoanhydride bonds that are present in every cell and have been reported to facilitate a plethora of different cellular functions [91]. Under physiological conditions all phosphate residues are deprotonated, forming a polyanionic structure that allows binding of basic proteins like histones or chelating of divalent metal ions [92-94]. To date, polyP is well defined in prokaryotes and unicellular eukaryotes, in mammals however, the function of polyP remains poorly defined. In bacteria and yeasts, polyP is synthesised by polyP kinases (Ppk) and digested by polyphosphatases (Ppx). Polyphosphatases can be distinguished into endo-polyphosphatases that cleave within the polyP chain, producing polyP subsets around 60 mono-phosphates in size, and exo-polyphosphatases that remove terminal phosphate residues [92]. In order to study functions of polyP, these synthesising or hydrolysing enzymes were overexpressed or knocked out to identify phenotypical changes by gain or loss of functions. Through this, polyP was found to be active as an energy storage, a calcium sink or a broad responder to environmental stress in microbiota [93].

3.2.1 Inorganic polyP in mammalian cells and tissue

In mammals, particularly high amounts of polyP are found in cells with high metabolic activity, such as cardiomyocytes, cancer cells and neurons [91, 95]. PolyP is present in every compartment of the cell or even actively stored in dense granules of platelets and mast cell granula [96].

Despite the profound insight into polyP metabolism in bacteria and yeasts, no polyP kinases or polyphosphatases exclusively producing or digesting polyP could yet be identified in the mammalian system. However, evidence arose, that the F_0F_1 ATPase of the respiratory chain may be able to both hydrolyse and synthesise polyP [97]. Diphosphoinositol polyP phosphohydrolase and alkaline phosphatase have been shown to hydrolyse the phosphoanhydride bonds of polyP *in vitro* and in osteoblast-like cells, respectively [98, 99]. However, the impact of polyP degradation for phenotype and function of targeted cells is ill-defined. Due to the current lack of knowledge regarding the distinct enzymatic machinery for polyP metabolism in mammalian cells, plasmid-based transfection of polyP kinases or polyphosphatases from bacteria or yeast remains state of the arts to show functional properties of polyP in mammalian cells. Consistent with a treatment-related response, on the one hand, polyP has been shown to be involved in mediation of cellular stress [100, 101], while on the other hand, reduction of polyP in mitochondria fuels glycolysis on the cost of oxidative phosphorylation (OXPHOS) [102, 103]. Therefore, the accumulation of polyP seems to be linked to cellular metabolism, suggesting that polyP modulation can regulate cell fate.

While intracellular functions of polyP in mammalian cells remain largely elusive, polyP-mediated mechanisms have been reported for the extracellular space. Among other functions polyP was found to play a role in contact activation [104, 105], bone mineralisation [99], inflammation [106] neurotransmission [107] and energy storage [95, 108]. Due to its polyanionic structure, polyP is able to provide a negatively charged surface for factor XII (FXII) activation, thereby triggering the contact activation pathway of the blood coagulation system [96]. The pro-inflammatory effects of released polyP are claimed to be mediated not only by induction of the contact activation system, but also by stimulating the expression of adhesion molecules on endothelial cells in an NFκB dependant manner. Furthermore, a potentiating effect on the pro-inflammatory capacities of extracellular nuclear proteins has been found [109, 110]. Because altered

polyP levels in cell lines and knockout models with targeted deletion of endogenous genes are not available due to unknown specific polyP metabolising enzymes, the role of intracellular polyP in mammalian cells remains essentially undefined. In addition, changes of polyP levels in response to cell activation, metabolism and differentiation status have been rarely determined. Nevertheless, polyP appears to be a promising target for immune modulation based on its relation to metabolism, ion homeostasis and signalling pathways.

3.3 Aim of this study

The aim of this study is to characterise polyP in T-cell subsets, to identify the role of polyP in CD4+ T cells by protein transduction of yeast polyphosphatase and to test whether changes of polyP levels in T cells are suitable to potentially modulate (auto)immune reactions.

For this, our working group devised a cell-penetrating polyphosphatase (CPP-Ppx1) by fusing the HPH-1 cell-penetrating peptide sequence (CPP) to polyphosphatase (Ppx1) from *Saccharomyces cerevisiae*. Utilising CPP-Ppx1 for intracellular targeting of T-cell polyP, this work aims to clarify polyP-dependent pathways by analyses of metabolic assays, chromatin accessibility, protein expression and functional experiments. Overall, my presented research aims to characterise polyP in murine CD4+ T cells and to gain insight into its function during T-cell stimulation and differentiation.

4 Results

4.1 PolyP accumulation in CD4+ T cells

4.1.1 PolyP accumulation is dependent on stimulation strength

PolyP is considered to be present in every cell type [92], but the content and dynamic changes of polyP levels in CD4+ T cells have not been investigated so far. Therefore, we firstly isolated polyP from CD4+ T cells using established protocols [111]. Applying minor modifications, we washed cells in TRIS buffer to avoid carry-over of phosphate/polyP from buffer solutions and culture condition, lysed the cells and removed DNA with extraction columns. The silica membrane retains any DNA within the lysate, so the flow-through can be processed by a phenol-chloroform extraction and subsequent precipitation of polyP. To validate the specificity of polyP detection in urea polyacrylamide gel electrophoresis (PAGE) by DAPI photobleaching, equal numbers of Jurkat cells were lysed in sodium dodecyl sulfate (SDS)-lysis buffer or subsequently subjected to DNA or RNA extraction protocols or polyP precipitation after phenol-chloroform extraction. Protein concentrations within each lysate sample were adjusted according to BCA assays and immunoblotting against β-actin was performed as loading control (**Figure 4**). Upon repeated UV light exposure, DAPI disintegrates in the vicinity of polyP, but not protein, DNA or RNA samples, which is discernible by a black smear in urea PAGE [112].

After photobleaching, samples with whole cell lysates and extracted DNA/RNA appear white, whereas isolated polyP shows a characteristic black banded pattern on the upper part of the gel, indicating successful isolation of long-chain polyP from Jurkat cells and its specific detection by negative DAPI staining. The synthetic polyP P30 was used as a positive control and is visible as an intensive black smear throughout the whole gel (**Figure 4**).
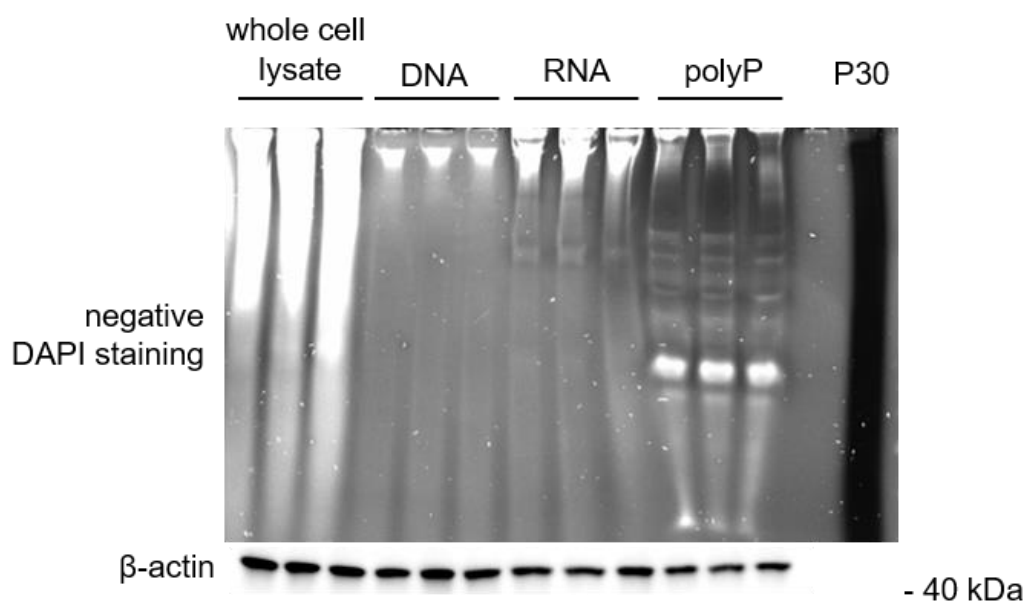
Figure 4. Specific detection of PolyP isolated from Jurkat cell lysates. Urea PAGE gel with negative DAPI staining of whole cell lysate, isolated DNA, RNA or polyP from 2×10^6 Jurkat cells per lane. Equivalent protein concentrations for each sample were loaded according to BCA assays and β-actin immunoblotting was performed as loading control. Respective protein ladder is indicated on the right. Synthetic polyP P30 (20 ng per lane) was used as a long chain polyP standard. Three technical replicates were used per sample in two independent experiments.

After validation of the protocol for polyP isolation and detection from T cells, we isolated CD4+ T cells from mouse splenocytes and stimulated them on α-CD3 coated plates with increasing concentrations of stimulus for three days (**Figure 5A**). In order to account for the increasing cell number over time due to proliferation of T cells upon stimulation, the amount of polyP extraction samples loaded to the urea gel was adjusted to protein levels in each sample. Increasing concentrations of α-CD3 resulted in a relative increase in negative DAPI staining, suggesting that murine CD4+ T cells increase polyP levels upon stimulation (**Figure 5A**). Next, a time-dependence of polyP accumulation by stimulating T cells on α-CD3 coated plates for 24 or 48 hours was analysed. Negative DAPI staining revealed, that T cells accumulate more polyP with increasing stimulation time (**Figure 5B**).

To validate these findings in a more physiological context, we used CD4+ T cells from *Marilyn* mice that express only one transgenic TCR, recognizing male H-Y antigen, on a *Rag2* knockout background. The *Rag2* gene deficiency prevents recombination of endogenous TCR chains and allows only T cells reactive against male H-Y antigen to egress from the thymus. Consistent with T-cell stimulation by antibody treatment, polyP

levels increased in CD4+ T cells from female *Marilyn* mice following stimulation with H-Y antigen for three days *in vitro*. Analysis was performed qualitatively by negative DAPI staining in urea PAGE (**Figure 5C**) or quantitatively by malachite green assay (**Figure 5D**).
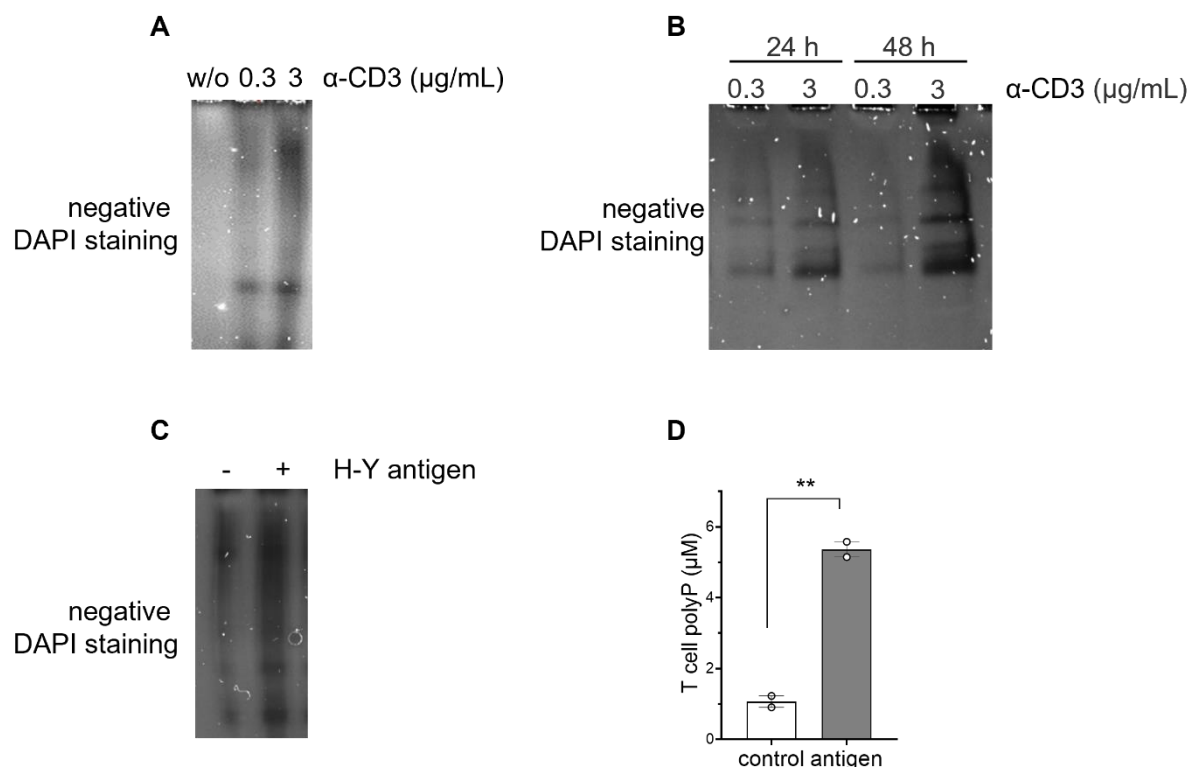
Figure 5. T cells accumulate polyP upon stimulation. PolyP was isolated from murine CD4+ T cells with phenol-chloroform extraction, separated on urea PAGE and stained in negative DAPI staining (**A-C**). (**A**) Isolated CD4+ T cells were stimulated for three days on 0.3 or 3 µg/mL α-CD3 coated plates. CD4+ T cells without stimulation were used for comparison. (**B**) Isolated CD4+ T cells stimulated for three days on 0.3 or 3 µg/mL α-CD3 coated plates and 1 µg/mL soluble α-CD28 for 24 or 48 hours. (**C-D**) Splenocytes from female *Marilyn* mice were stimulated with (**C**) 0.6 µg/mL male H-Y antigen or (**D**) 10 µg/mL male H-Y antigen for three days *in vitro*. Splenocytes cultured without male H-Y antigen served as control samples. CD4+ T cells were subsequently isolated from splenocyte cultures and polyP content was analysed by negative DAPI staining in (**C**) urea PAGE or (**D**) malachite green assay. Data represent mean ± SEM, *p*-value by Student's t-test, **$p < 0.01$, represented as n=2 independent experiments.

4.1.2 PolyP is stored in the cytosol of CD4+ T cells

PolyP is discussed to be present in every compartment of the cell and has even been shown to be compartmentalised in dense granules of platelets [113]. We therefore aimed to identify the localisation of polyP in T cells using transmission electron microscopy (TEM). Due to its negative charge and associated metal ions at physiologic

pH, polyP should be detectable in electron dense regions in TEM, as described before for platelets [114] and T cells with lysosomal trafficking deficiency [115]. TEM can be coupled to energy dispersive X-ray spectroscopy (EDX) to identify the element composition of the image detail in view. Isolated CD4+ T cells were stimulated for three days, fixated in paraformaldehyde and glutaraldehyde and analysed at the Center for Molecular Neurobiology Hamburg (ZMNH). However, stimulated T cells did not show any visible electron dense structures in our analyses (**Figure 6A**). Also, EDX analysis did not reveal any phosphorus rich regions (data not shown).

In a different approach to localise polyP storage in CD4+ T cells, Jurkat cells were fractionated into cytosol, membrane, mitochondria and nucleus/cytoskeleton fractions (**Figure 6B**). We used Jurkat cells for the fractionation as they contain a higher basal level of polyP and can therefore be analysed for polyP localisation without prior stimulation. Successful fractionation was validated by immunoblot analysis of marker proteins. Glyceraldehyde-3-phosphate dehydrogenase (GAPDH) as a prominent cytosolic protein was used to indicate cytosolic fractions. Calnexin is an integral protein of the endoplasmic reticulum and can be used as a membrane marker. Cytochrome c oxidase subunit IV (COX IV) is a component of the cytochrome c oxidase, an enzyme of the mitochondrial respiratory chain, and was used as a mitochondrial marker. Histone H3 is one of the five major histone proteins of the genome and was used as a marker for the nuclear and cytoskeletal fraction. The fractionation showed an enrichment of the cytosolic marker GAPDH, the membrane marker calnexin and the nucleus marker histone H3 in their respective fractions. The mitochondrial protein COX IV was predominantly found in the membrane fraction with a less intensive band visible in the mitochondrial fraction. While this indicates insufficient separation of the mitochondrial fraction, no other marker proteins were found in the mitochondrial fraction (**Figure 6B**).

We next performed phenol-chloroform extraction of each fraction to determine the polyP content. Urea PAGE analysis with subsequent negative DAPI staining showed that the cytosol of Jurkat cells was especially rich in polyP. The membrane fractions contained less polyP compared to the cytosol. Mitochondria and nucleus/cytoskeleton fractions did not show any characteristic polyP staining on urea PAGE, which suggests that these compartments have relatively low polyP amounts that were below the detection level.

Taken together these data indicate that CD4+ T cells accumulate polyP upon stimulation and store the majority of intracellular polyP diffusely in the cytosol or bound to the membrane compartment.
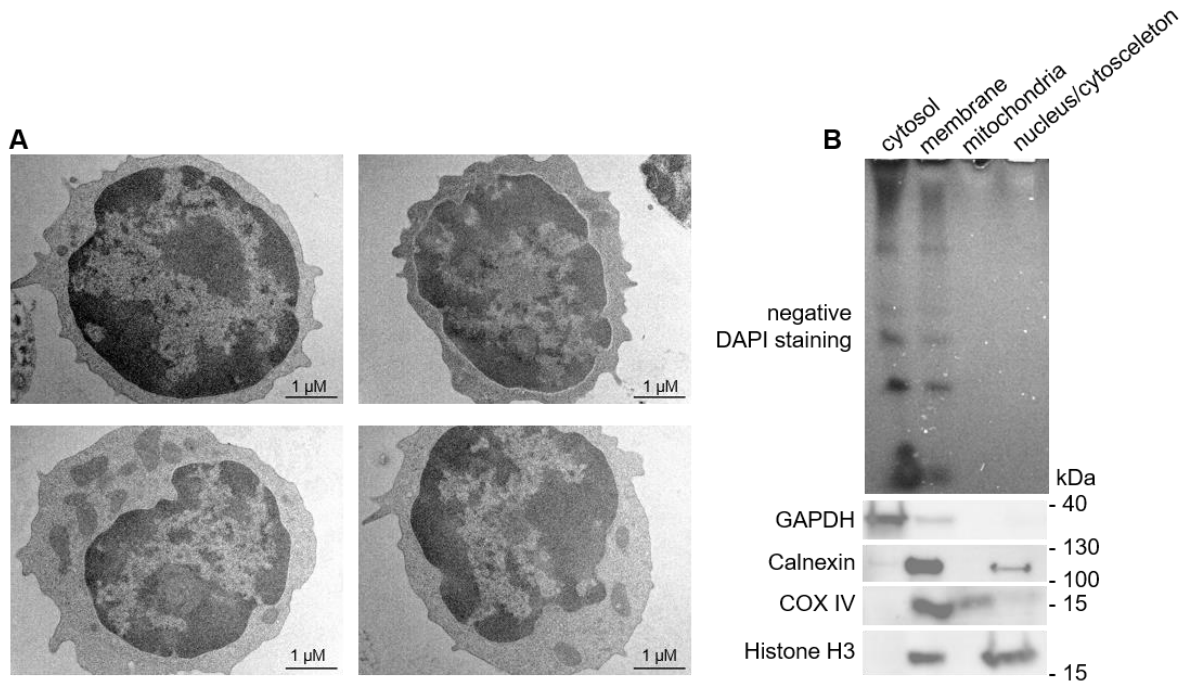
Figure 6. Subcellular localization of polyP in stimulated CD4+ T cells. (**A**) Representative electron microscopic images of CD4+ T cells isolated from murine splenocytes and stimulated on α-CD3/α-CD28 (2 µg/mL / 0.5 µg/mL) coated plates for three days for maximal polyP accumulation. Cells were analysed at the Center for Molecular Neurobiology Hamburg (ZMNH). (**B**) Urea PAGE of polyP isolated by phenol-chloroform extraction from cytosol, membrane, mitochondria and nuclear and cytoskeletal fractions. Fractionation was validated by immunoblot analysis for marker proteins of each fraction (GAPDH: cytosol, calnexin: membrane, COX IV: mitochondria, histone H3: nucleus/cytoskeleton). The respective protein ladder is indicated on the left; representative results from n=4 independent experiments are shown.

4.1.3 CD4+ T-cell subsets acquire different polyP levels

PolyP accumulation has been shown to be tightly linked to cellular metabolism [100, 102]. Murine CD4+ T cells were stimulated on α-CD3/α-CD28 coated plates and incubated with inhibitors of glycolysis or oxidative phosphorylation to investigate whether polyP accumulation depends on certain metabolic pathways (**Figure 7**). To inhibit glycolysis, 2-Deoxy-D-glucose (2-DG) as a glucose analogue that prevents the enzymatic isomerisation of glucose-6-phosphate to fructose-6-phosphate, and iodoacetate which blocks GAPDH were used. For inhibition of oxidative

phosphorylation, oligomycin and Bam15 were used. While oligomycin inhibits the ATP-synthase, Bam15 uncouples the electron transport chain by enabling protons to pass the inner mitochondrial membrane, without fuelling the ATP-synthase. Analysis of polyP levels showed that stimulated T cells were unable to accumulate polyP when glycolysis was blocked, while equal amounts of polyP could be produced with inhibitors of the oxidative phosphorylation compared to control cells. These data indicate that the polyP production in CD4+ T cells is more reliant on glycolysis than on oxidative phosphorylation.
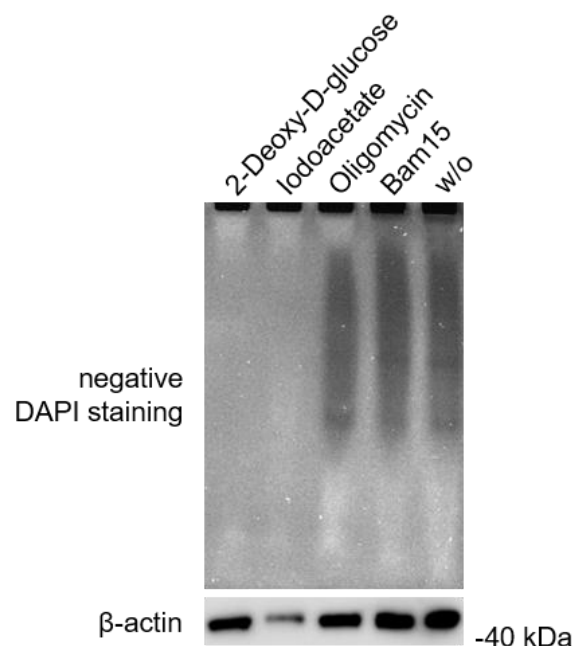
Figure 7. PolyP accumulation is fuelled by glycolysis. Urea PAGE of polyP isolated from CD4+ T cells stimulated on α-CD3/α-CD28 (2 µg/mL / 0.5 µg/mL) coated plates in inhibitor-supplemented medium. 2-Deoxy-D-glucose (50 mM) and iodoacetate (100 mM) were used as inhibitors of glycolysis, oligomycin (1 µM) and BAM15 (2.5 µM) were used as inhibitors of the oxidative phosphorylation. Equivalent protein concentrations for each sample were loaded according to BCA assays and β-actin immunoblotting was performed as loading control, respective protein ladder is indicated on the right; representative results from n=3 independent experiments are shown.

Upon stimulation CD4+ T cells differentiate into their respective T-cell subsets depending on the cytokine environment. This differentiation is tightly linked to a pronounced metabolic reprogramming, through which pro-inflammatory T cells shift their metabolism towards glycolysis followed by aerobic fermentation, a process providing ATP by production of lactate from pyruvate [65]. On the contrary, Treg cells mainly shift their metabolism from glycolysis to lipid oxidation and oxidative

phosphorylation of pyruvate [70]. As polyP accumulation appears to depend on T-cell metabolism (**Figure 8**), we hypothesised that distinct polyP levels may be present in *in vitro* differentiated T-cell subsets.

To test this hypothesis, CD4+ T cells were isolated from mouse splenocytes and stimulated in IL-2 supplemented (Th0) or subset specific T-cell differentiation medium. Proper differentiation was validated by flow cytometry analysis of characteristic cytokines or transcription factors (**Figure 8**). Appropriately, increased IFNγ production was revealed in T cells stimulated in Th1-differentiation medium (**Figure 8A**), whereas a pronounced increase in the production of IL-4 was observed in Th2-differentiated cells (**Figure 8B**). The characteristic transcription factor Rorγt and Foxp3 were used to determine successful differentiation into Th17 and iTreg cells, respectively. A prominent increase in Rorγt production was visible in Th17-differentiation medium (**Figure 8C**), whereas elevated Foxp3 expression indicated effective differentiation of iTreg cells (**Figure 8D**).
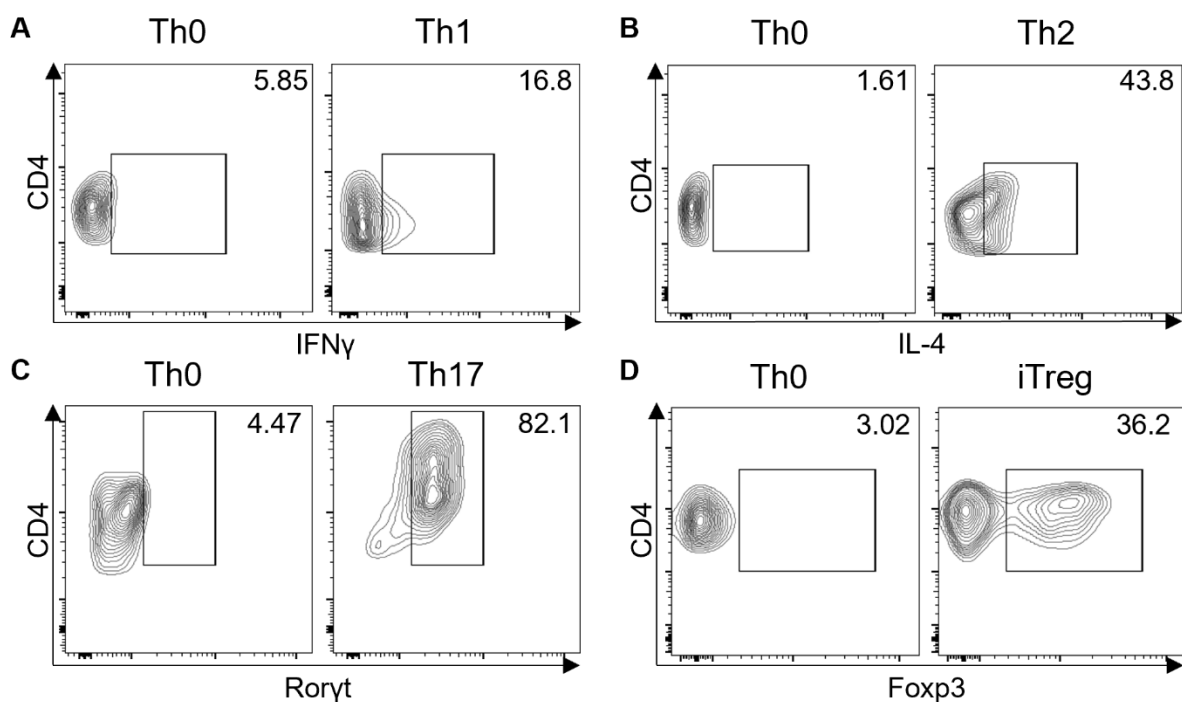
Figure 8. Validation of *in vitro* T-cell differentiation. Representative flow cytometry plots for T-cell differentiation from n=6 independent experiments. CD4+ T cells were isolated from mouse splenocytes and stimulated on α-CD3/α-CD28 (2 μg/mL / 0.5 μg/mL) coated plates in differentiation medium for three (**A, B, D**) or five (**C**) days. Gating strategy provided in 7.2.31.2. Analysis of intracellular cytokine production following PMA (50 ng/mL) and ionomycin (1 μg/mL) restimulation for two hours and protein

transport inhibition for four hours. (**A**) IFNγ expression in T cells cultured in Th1-skewing conditions. (**B**) IL-4 expression in T cells cultured in Th2-skewing conditions. Induction of transcription factor Roryt (**C**) and Foxp3 (**D**) in T cells cultured in Th17- and iTreg-skewing conditions, respectively.

The polyP content of differentiated T-cell subsets was quantified via malachite green assays, in which values were normalised to respective numbers of living CD4+ T cells measured for each subset in flow cytometry analysis (**Figure 9A**). Our analysis showed that T-cell subsets differ in their accumulation of polyP with Th17 cells containing significantly more polyP on average compared to Th1, Th2 and iTreg cells. iTreg cells showed the lowest amount of polyP although the difference to Th1 or Th2 cells was not significant. Moreover, specific differences of polyP content in T-cell subsets were also confirmed by urea PAGE (**Figure 9B**). In equally sized sample preparations, larger amounts of polyP were isolated from Th17 cells in comparison to Th1, Th2 and iTreg cells, detectable as an intensive black smear in negative DAPI staining (**Figure 9B**).

The differentiation of both Th17 and iTreg cells is largely dependent on TGF-β signalling. While high levels of TGF-β alone induce a Treg phenotype, the interplay of IL-6 and TGF-β will lead to a Th17 phenotype [4]. IL-6 is further known to stimulate the mTOR pathway, thereby enhancing the glycolysis in T cells [66]. Based on our results that metabolism and differentiation of CD4+ T cells affects intracellular polyP levels, we hypothesised that IL-6 may increase, whereas TGF-β may counteract polyP accumulation. To test this, murine CD4+ T cells were stimulated on α-CD3/α-CD28 coated plates for three days in the presence of varying mixtures of IL-6 and TGF-β ranging from 0 - 20 ng/mL (**Figure 9C**). We found that TGF-β alone and at high concentrations (5 - 20 ng/mL) resulted in comparably low polyP levels. IL-6 alone showed an optimum in polyP accumulation at around 2.5 - 5 ng/mL. Mixtures of the two cytokines did not show a definite optimum for polyP accumulation, however in the range of 10 - 20 ng/mL IL-6 and 1.25 - 5 ng/mL TGF-β a tendency towards higher polyP levels was observed.

Together with IL-6, IL-23 plays an important role in the differentiation of Th17 cells. We therefore asked the question whether treatment with IL-23 has an additional effect on polyP accumulation. Following incubation of CD4+ T cells with mixtures of both cytokines in a concentration range from 0 - 20 ng/mL, we found that the addition of IL-23 resulted in no definite concentration dependent polyP increase (**Figure 9D**).

In summary, these results indicate that subset differentiation and the cytokine environment upon differentiation impact polyP levels in CD4+ T cells. Especially for the anti-inflammatory cytokine TGF-β a negative concentration-dependent correlation was evident for the accumulation of polyP, whereas a modest positive association was found for the pro-inflammatory cytokine IL-6. However, no obvious effects could be observed for IL-23, suggesting that the polyP accumulation in Th17 cells is not exclusively regulated by the cytokine environment.
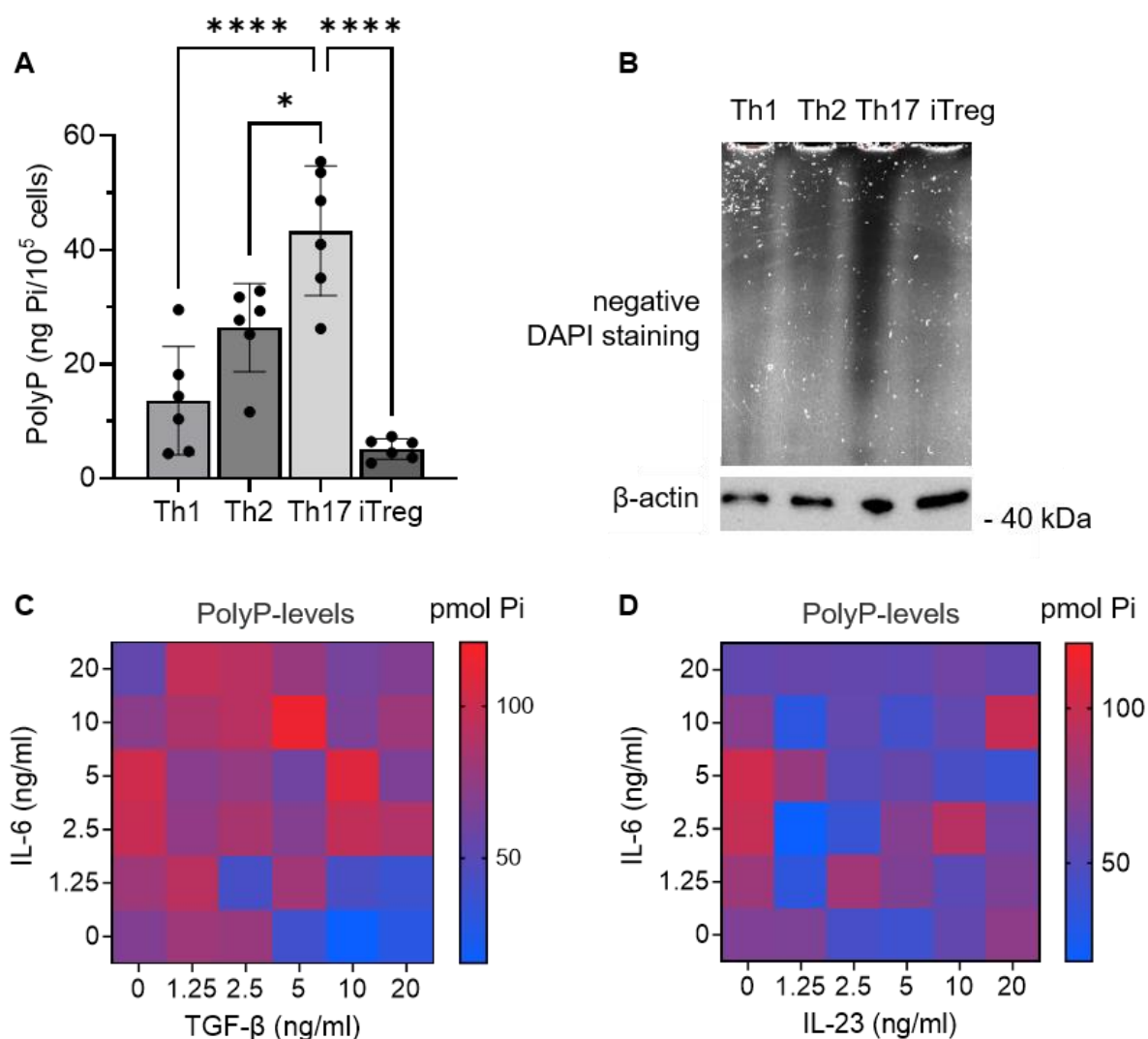
Figure 9. CD4+ T-cell subsets display differential polyP levels. (**A-B**) CD4+ T cells were isolated from mouse splenocytes and stimulated on α-CD3/α-CD28 (2 µg/mL / 0.5 µg/mL) coated plates in differentiation medium for three (Th1, Th2 and iTreg cells) or five (Th17 cells) days. PolyP content of *in vitro* differentiated T-cell subsets was analysed by (**A**) malachite green assay normalised to the percentage of living CD4+ T cells as determined in flow cytometry analysis; combined from n=6 independent experiments and by (**B**) urea PAGE. Representative negative DAPI staining from n=2

independent experiments. Equivalent protein concentrations for each sample were loaded according to BCA assays and β-actin immunoblotting was performed as loading control, respective protein ladder is indicated on the right. (**A**) Data represent mean ± SEM, *p*-value by ordinary One-Way ANOVA, *p < 0.05, and ****p < 0.0001, non-significant changes are not indicated. (**C-D**) Heat map of malachite green assay data for quantification of polyP from murine CD4+ T cells stimulated on α-CD3 coated plates (5 µg/mL) with soluble α-CD28 (1 µg/mL) supplemented with indicated concentrations of (**C**) IL-6 and TGF-β or (**D**) IL-6 and IL-23 for three days. Data represent mean of n=3 independent experiments.

4.2 Characterisation of CPP-Ppx1

4.2.1 Generation of a cell-penetrating Ppx1 (CPP-Ppx1)

Modulating polyP in mammalian cells is typically performed by overexpression of yeast or bacterial enzymes degrading (Ppx) or producing (Ppk) polyP. T cells unfortunately respond poorly to usual transfection methods like lipofection, electroporation, retroviral transduction or microinjection [89].

Cell-penetrating peptides (CPPs) have been established as novel agents for drug delivery. CPPs are small peptide sequences that enable the transport of proteins across membranes, e.g. the trans-activator of transcription (Tat) of the human immunodeficiency virus (HIV). By fusing a tandem repeat of the membrane-permeable peptide domain from HPH-1 to Foxp3 Choi *et al*. demonstrated that efficient protein transduction into murine CD4+CD25- T cells could be achieved and that the transfer of the transcription factor induced a stable and suppressive Treg phenotype without compromising cell viability [33].

Building on previously work with protein transductions of Foxp3 and CTLA4 into CD4+ T cells [33, 90], our working group set out to devise a cell-penetrating polyphosphatase to modulate intracellular polyP levels in primary CD4+ T cells. For this, the tandem repeat of the membrane-permeable peptide domain from HPH-1 was fused to the polyphosphatase Ppx1 from *S. cerevisiae* encoded within the pTrcHis-B plasmid (**Figure 10A**). Cloning of the vector was performed in the bachelor work of B.Sc. Banafsheh Afshar and includes a His-tag at the N-terminus of the CPP-Ppx1 construct that allows for affinity chromatography purification of the recombinant enzyme. Initial transformation of the vector into *E. coli* strain DH5α, cryopreservation of a glycerol stock, induced overexpression of CPP-Ppx1 with

isopropyl-ß-D-thiogalactopyranoside (IPTG) and preliminary protein transduction experiments were performed during the master thesis of M.Sc. Lydia Zhan.

Bacterial lysates containing CPP-Ppx1 were at first isolated using standard affinity chromatography protocols. In brief, bacteria were dissolved in Äkta binding buffer and sonicated to disrupt bacterial cell walls. Lysates were then applied to nickel columns, washed and recombinant protein was eluted using imidazole containing Äkta elution buffer. This standard protocol resulted in very poor protein yields, therefore we hypothesised that CPP-Ppx1 might be stored in inclusion bodies. In order to dissolve these, 8 M urea was added to the Äkta binding buffer and the sonicated lysate incubated for one hour with constant agitation at 4 °C. After this, the lysate was added to the nickel column. The flow-through of the column was added to the column two more times to ensure complete binding of the overexpressed protein (**Figure 10B**). Since urea as a chaotropic agent not only dissolves inclusion bodies but also reduces any secondary or tertiary structure of the protein, the nickel bound protein was washed with Äkta binding buffer of decreasing urea concentrations in order to refold the protein on the column. The refolded protein was then eluted from the nickel resin with an imidazole containing buffer. Imidazole competes with the His-tag for binding to nickel and due to its higher affinity for nickel replaces the tagged CPP-Ppx1.

In order to ensure proper purification of CPP-Ppx1, SDS PAGE followed by Coomassie brilliant blue staining or immunoblot analysis were performed (**Figure 10C** and **D**). Coomassie Brilliant Blue staining showed a protein band at approximately 50 kDa in the crude lysate which is reduced in intensity in the flowthrough fraction, showing binding of the protein to the nickel resin (**Figure 10C**). The first wash fraction contained some protein bands of various sizes indicating that unspecifically bound proteins were washed off the resin. The following wash fractions were devoid of any proteins. The elution fraction 2 contained a single protein at the expected hight of 50 kDa (**Figure 10C**). In immunoblot analysis a protein band at 50 kDa could also be detected by staining for the His-tag (**Figure 10D**).

Taken together these data show successful purification of the His-tagged CPP-Ppx1 with the improved protein isolation protocol.
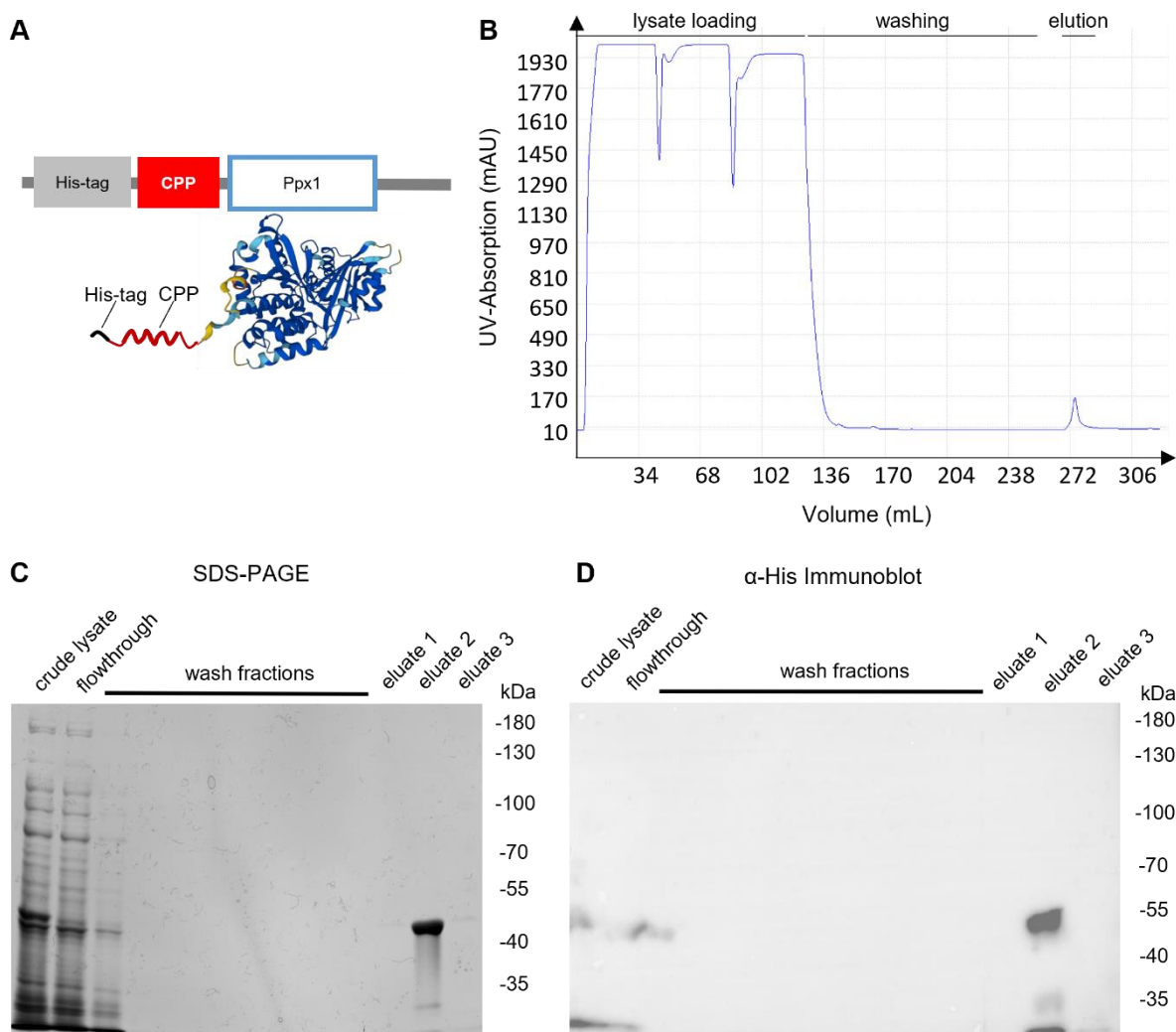
Figure 10. Purification of CPP-Ppx1 by affinity chromatography. (**A**) Schematic overview of functional regions and the structure of CPP-Ppx1 (from AlphaFold [116]): the N-terminus consists of a His-tag and two cell-penetrating peptide sequences of the human transcription factor HPH-1 fused to Ppx1 from *S. cerevisiae*. (**B**) Chromatogram of CPP-Ppx1 protein isolation by affinity chromatography using His-trap nickel columns and Äkta Start instrument. Purification and enrichment was validated by SDS PAGE with subsequent Coomassie Brilliant Blue staining (**C**) and immunoblots using an α-His-tag antibody (**D**). Protein ladder is indicated on the right.

.

4.2.2 Protein transduction of CPP-Ppx1 into CD4+ T cells

To show that recombinant CPP-Ppx1 maintains its enzymatic activity after protein purification, synthetic polyP was incubated with either purified CPP-Ppx1, hydrochloride acid as positive control, or heat-denatured CPP-Ppx1 as negative control, and analysed on urea PAGE. The synthetic long-chain polyP (P30) was visible as a black smear in negative DAPI staining that was completely reduced after acidic

hydrolysis (**Figure 11A**). As expected, CPP-Ppx1 inactivated by thermal denaturation did not have any effect on synthetic polyP. In contrast, incubation with native CPP-Ppx1 resulted in a complete enzymatic digestion of synthetic polyP (**Figure 11A**). Moreover, incubating synthetic polyP with increasing concentrations (10 - 50 µg/mL) of CPP-Ppx1 showed a concentration-dependent polyP degradation (**Figure 11B**). Based on the complete digestion of 20 ng P30 by 100 µg/mL CPP-Ppx1 (**Figure 11A)** and CPP-Ppx1 titration data (**Figure 11B**), we estimated that a concentration between 50 and 100 µg/mL of CPP-Ppx1 should be used for intracellular polyP degradation in CD4+ T cells.

To analyse a polyP digestion over time, isolated polyP from Jurkat cells was digested with CPP-Ppx1 for one to three hours. A time-dependent effect in CPP-Ppx1 mediated digestion of T-cell polyP could be observed (**Figure 11C**).
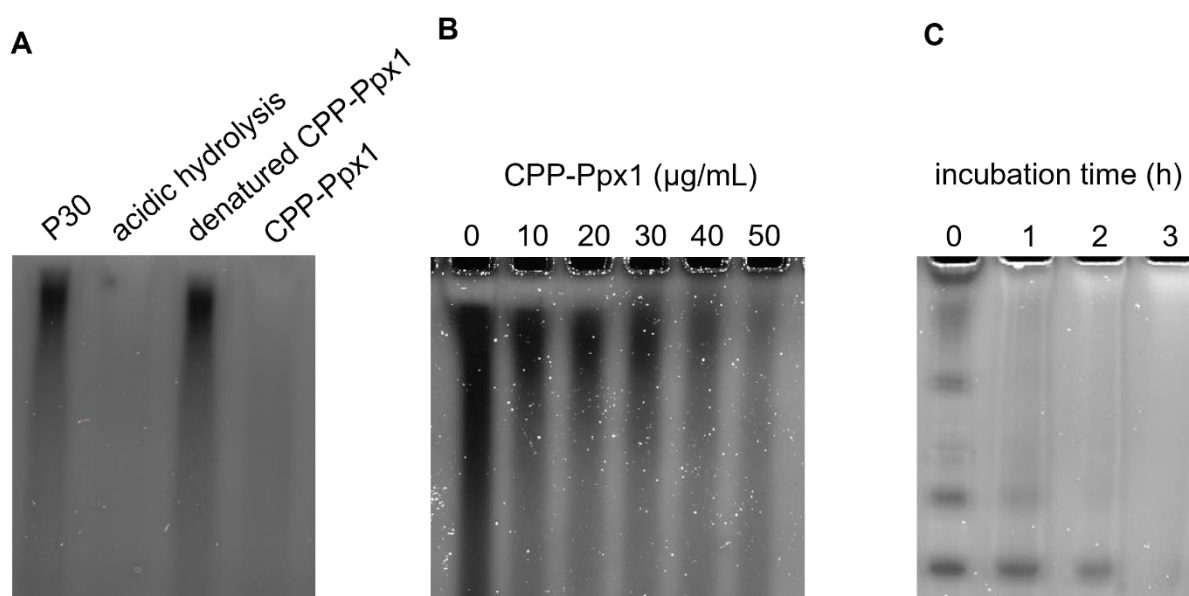
Figure 11. Recombinant CPP-Ppx1 effectively degrades polyP. Urea PAGE with negative DAPI staining of polyP incubated with purified CPP-Ppx1. (**A**) 20 ng synthetic polyP (P30) in 50 mM TRIS buffer (pH 7.0) without treatment or incubated with 4N hydrochloric acid, heat denatured CPP-Ppx1 or native CPP-Ppx1 (100 µg/mL, 30 min, 37 °C). (**B**) 20 ng polyP in 50 mM TRIS buffer (pH 7.0) incubated with 10 - 50 µg/mL CPP-Ppx1 (30 min, 37 °C). (**C**) T-cell polyP isolated by phenol-chloroform extraction from 1x10^6 Jurkat cells incubated with CPP-Ppx1 (100 µg/mL, 37 °C) for one to three hours.

Next, protein transduction of CPP-Ppx1 into living cells was tested. For this, murine CD4+ T cells were isolated and incubated with CPP-Ppx1 or denatured CPP-Ppx1 as a control (**Figure 12A**). Immunoblot analysis using a primary antibody directed against the His-tag showed a prominent band at the expected height of 50 kDa in the

CPP-Ppx1 treated T cells, demonstrating that native, but not denatured, CPP-Ppx1 actively enters the cell. Some minor bands can be detected at a lower molecular weight in the CPP-Ppx1 treated samples and can also be seen in those cells treated with denatured CPP-Ppx1. These bands could either be the effect from unspecific binding of the antibody or a degradation product of the cell-penetrating protein. This would also mean that some of the heat denatured protein was taken up but quickly degraded, while the native enzyme is mostly stable after membrane permeabilization.

For identification of subcellular localization of CPP-Ppx1, CPP-Ppx1 treated Jurkat cells were fractionated and separated into cytosol, membrane, mitochondria and nucleus/cytoskeleton fraction (**Figure 12B**). Marker proteins were used for validation of successful fractionation. The immunoblot showed a higher level of GAPDH and calnexin in the cytosolic and membrane fractions, respectively. COX IV was detected as dim bands across the membrane, mitochondrial and nuclear/cytoskeleton fraction, but no definite mitochondrial fraction was discernible. Histone H3 however was clearly detectable in the nucleus/cytoskeleton fraction. The His-tag of CPP-Ppx1 could be detected most prominently in the nucleus/cytoskeleton fraction with some protein also visible in the membrane fraction.

From these data we conclude that the Äkta purification provided us with an active polyphosphatase that integrates into murine CD4+ T cells via protein transduction while its heat-inactivated form barely crosses the cell membrane. We further assume that CPP-Ppx1 crosses the cell-membrane in an endocytic manner, as the protein was found in the cytoskeletal and membrane fraction in our fractionation experiments.
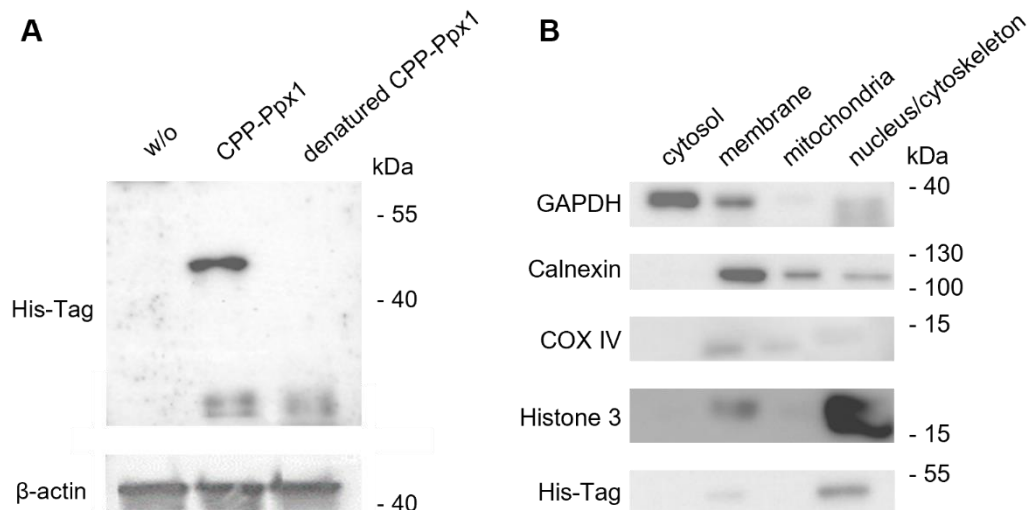
Figure 12. Transfer of CPP-Ppx1 into CD4+T cells by protein transduction. (**A**) Immunoblots of murine CD4+ T cells treated with native or denatured CPP-Ppx1 (100 µg/mL, 15 min, 37 °C). Control samples are untreated CD4+ T cells. Detection of CPP-Ppx1 was carried out by immunoblotting with an α-His-tag-antibody, β-actin immunoblotting was performed as loading control. (**B**) Fractionation of Jurkat cells treated with CPP-Ppx1 (100 µg/mL, 15 min, 37 °C) and fractionated into cytosol, membrane, mitochondria and nucleus/cytoskeleton fractions. Fractionation was validated by immunoblots for marker proteins of designated fraction (GAPDH: cytosol, calnexin: membrane, COX IV: mitochondria, histone H3: nucleus/cytoskeleton) and CPP-Ppx1 localisation was analysed by α-His-tag immunoblotting.

Common transfection methods like lipofection, electroporation or retroviral transduction usually result in high cytotoxicity to lymphocytes [89]. To investigate the viability of CPP-Ppx1 treated cells, murine CD4+ T cells were isolated, stimulated for three days and incubated with denatured or native CPP-Ppx1 for three hours at 37 °C. Treated cells were then extracellularly stained with two separate live/dead markers. We used annexin V which binds to phosphatidylserines only exposed on the cell surface when the cell goes into early apoptosis, and LIVE/DEAD™ Fixable Aqua Dead Cell Stain Kit which detects intracellular free amines only accessible to the dye once the cell membrane has become permeable. Flow cytometry analysis revealed that 90% of untreated control cells, were still viable (**Figure 13**). Neither the treatment of cells with denatured CPP-Ppx1 nor the treatment with native CPP-Ppx1 reduced the cellular viability. Overall, these data show that protein transduction of exogenous CPP-Ppx1 into murine CD4+ T cells did not affect their viability.
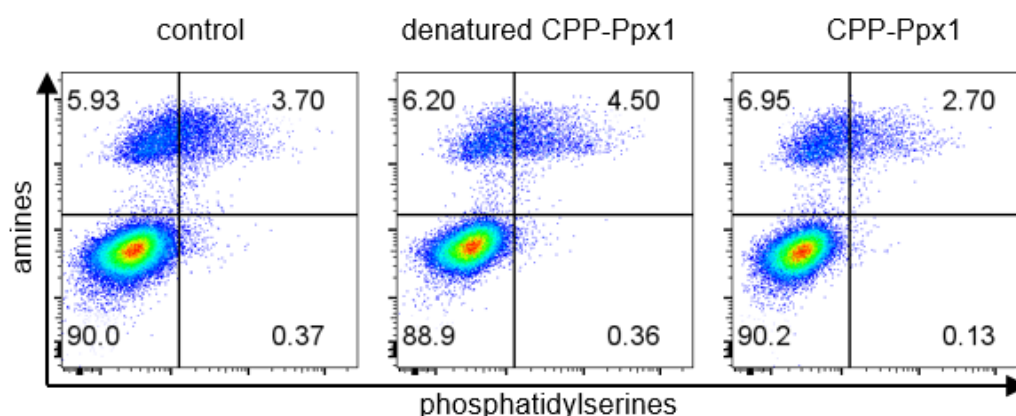
Figure 13. T-cell viability is not reduced upon CPP-Ppx1 treatment. Representative flow cytometry plots of stimulated murine CD4+T cells treated with CPP-Ppx1 or denatured CPP-Ppx1 (100 µg/mL, for three hours, 37 °C). Control samples were untreated CD4+ T cells. Viability of cells was analysed by LIVE/DEAD™ Fixable Aqua Dead Cell Stain Kit that stains intracellular free amines and Annexin V that stains phosphatidylserines as an early apoptosis marker, respectively.

To address whether CPP-Ppx1 treatment reduces intracellular polyP levels, we first tested the system on Jurkat cells, as they possess higher basal levels of polyP and we expected a reduction would be more easily detectable. For this, Jurkat cells were incubated with CPP-Ppx1 for 15 min at 37 °C prior to intracellular staining with a fluorescently labelled polyP-binding probe (enzymatically inactive PpxΔ12, derived from unrelated *E.coli* Ppx), which binds but does not degrade polyP and is suitable for flow cytometry analysis [117]. Surprisingly, the treatment of Jurkat cells with CPP-Ppx1 did not show any significant changes in intracellular polyP stainings (**Figure 14A**). We hypothesised that, Jurkat cells, as an immortalised cancer cell line, are highly metabolically active and might quickly compensate the CPP-Ppx1-mediated loss in polyP by enhanced polyP production. We therefore added 2-DG to the medium to inhibit the replenishment of polyP. As a result, a significant reduction of polyP median fluorescence could be observed in cells treated with CPP-Ppx1, but not with control treatments. (**Figure 14B**).

In the murine system, we used CD4+ T cells that had been isolated from splenocytes and were stimulated for three days with phorbol 12-myristate 13-acetate (PMA) and ionomycin in order to accumulate maximal amounts of polyP. Inhibiting *de novo* polyP synthesis with 2-DG, we could show that a one-time treatment of CD4+ T cells with CPP-Ppx1 for up to one hour already resulted in almost complete digestion of

intracellular polyP (**Figure 14C**), in which residual polyP detection might indicate some polyP replenishment. We therefore hypothesised that a repeated treatment of T cells with CPP-Ppx1 might reduce polyP levels even more efficiently. To test this, CD4+ T cells, that had been stimulated for three days, were incubated with three hourly doses of CPP-Ppx1 without the influence of 2-DG. Using this protocol, polyP levels decreased by almost 50% (**Figure 14D**). In summary, we showed that repetitive treatment with CPP-Ppx1 effectively reduces polyP in CD4+ T cells.
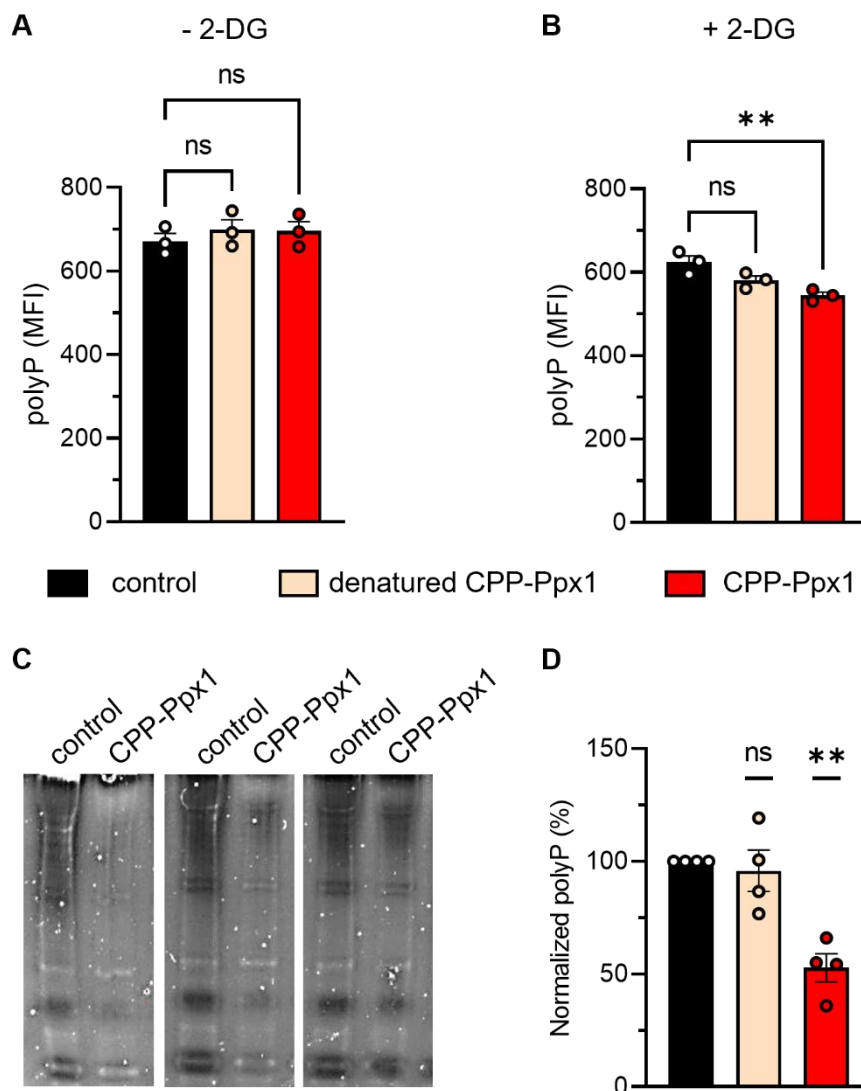
Figure 14. CPP-Ppx1 degrades polyP in T cells. Polyphosphatase activity of CPP-Ppx1 was assessed in Jurkat cells (**A** and **B**) and murine CD4+ T cells (**C** and **D**) by staining with the polyP-binding probe PpxΔ12 labelled with AlexaFluor647 represented by median fluorescence intensities (MFI). Jurkat cells treated with native or denatured CPP-Ppx1 (80 µg/mL, 15 min, 37 °C) or buffer controls in (**A**) absence or (**B**) presence of 2-Deoxy-D-glucose (2-DG) (2.5 µM). (**C**) Urea PAGE gel with negative DAPI staining

of polyP isolated with phenol-chloroform extraction from stimulated murine CD4+ T cells (PMA/ionomycin (50 ng/mL / 1 µg/mL), 3 days, 37 °C) with or without CPP-Ppx1 incubation (80 µg/mL, 15-60 min, 37 °C) and 2-DG (2.5 mM). (**D**) Statistical analysis of flow cytometry data for stimulated CD4+ T cells (PMA/ionomycin (50 ng/mL / 1 µg/mL), 3 days, 37 °C) treated with CPP-Ppx1 (80 µg/mL, three hourly doses, 37 °C) stained with the polyP-binding probe PpxΔ12 labelled with AlexaFluor647. Data represent mean ± SEM, *p*-value by (**A** and **B**) ordinary One-Way ANOVA, or (**D**) by one sample t-test to 100, **$p < 0.01$ and ns=non-significant. (**A** and **B**) represented as n=3 independent experiments, (**D**) represented as n=4 independent experiments.

4.3 <u>Identification and characterisation of CPP-Ppx1 mediated effects on CD4+ T cells</u>

4.3.1 PolyP degradation induces calcium mobilisation

Under physiologic conditions, polyP is deprotonated and therefore highly negatively charged, with divalent cations like calcium (Ca^{2+}) or proteins attached to this negative surface. A digestion of polyP by CPP-Ppx1 could therefore potentially result in a Ca^{2+} mobilisation within the cell. To test if CPP-Ppx1 mediated polyP degradation induces Ca^{2+} mobilisation in T cells, we stained Jurkat cells with the ratiometric Ca^{2+} dye Fura-2-AM. Fura-2 AM can readily cross the plasma membrane and enter the cytosol. Here, the AM-ester will be hydrolysed and Fura-2 will bind free Ca^{2+}.

For this experiment, we used human Jurkat cells as they possess a higher basal level of polyP compared to smaller murine T cells. Injection of denatured CPP-Ppx1 lead to a small but not significant increase in intracellular Ca^{2+}. In contrast, injection of native CPP-Ppx1 elevated intracellular Ca^{2+} levels lastingly (**Figure 15**). The mechanisms of protein transduction via cell-penetrating peptides remain largely elusive but are discussed to be either endocytic or based on direct translocation [13]. To assess the shuttling of Ca^{2+} from the outside into target cells by protein transduction, we included the Ca^{2+} ionophore ionomycin as control. Ionomycin treatment also increased Ca^{2+} mobilisation, but significantly less than CPP-Ppx1 treatment, suggesting that polyP degradation liberates Ca^{2+} intracellularly (**Figure 15**).

It has been shown that not only the amplitude, but also the duration of Ca^{2+} signalling plays an important role in its downstream signalling [118]. We noticed that Ca^{2+} levels after treatments did not return back to baseline levels, with CPP-Ppx1 treated samples

displaying especially high steady-state concentrations that may contribute to T-cell activation.

Taken together our data show that polyP degradation by CPP-Ppx1 treatment induces sustained Ca^{2+} mobilisation in CD4+ T cells.
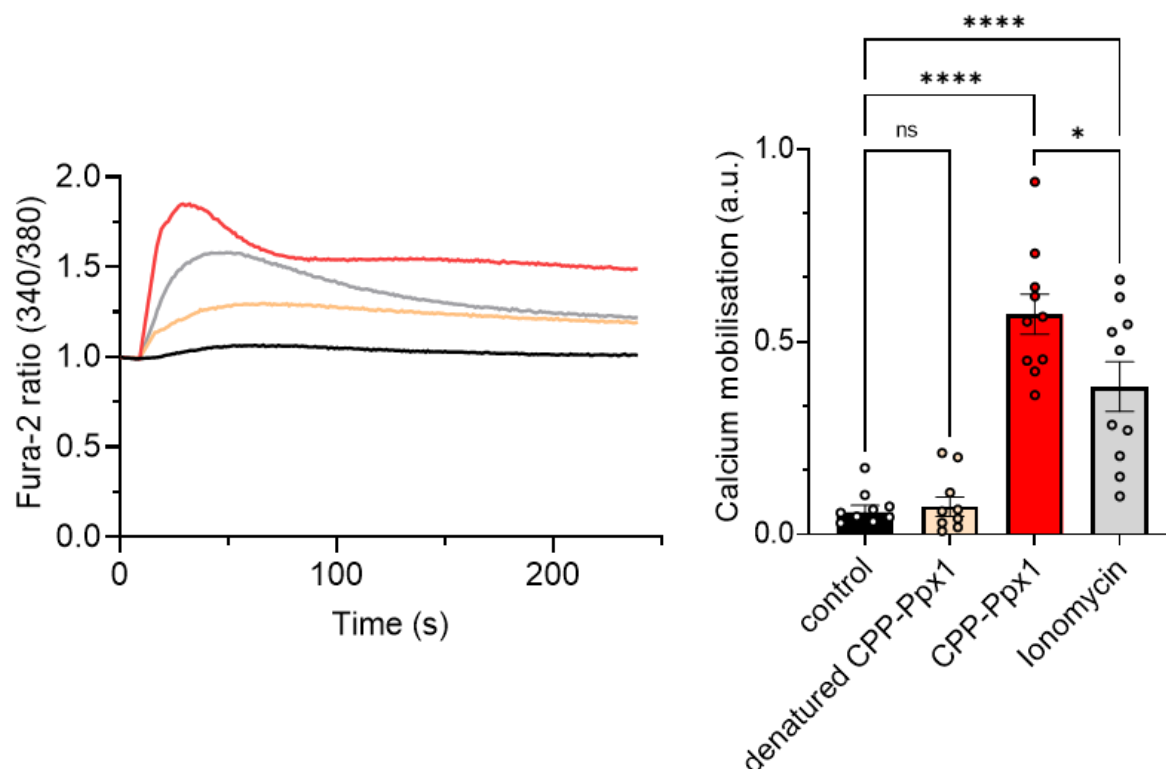
Figure 15. PolyP degradation induces Ca^{2+} mobilisation. Ratiometric Ca^{2+} measurement of Jurkat cells stained with Fura-2-AM ester (2 μM) and subjected to Ca^{2+} measurement. Representative diagram of Fura-2 ratio (340/380) plots from Jurkat cells treated with experimental reagents (buffer control, denatured or native CPP-Ppx1 (both 80 μg/mL) or ionomycin (1 μg/mL)) after 11s of baseline measurement (left). The Ca^{2+} flux data were calculated from fluorescent data, blank corrected and presented as mean ± SEM from n=10 independent experiments; *p*-value by ordinary One-Way ANOVA, *$p < 0.05$, ****$p < 0.0001$ and ns=non-significant.

4.3.2 PolyP degradation results in higher activation status

Upon stimulation of CD4+ T cells Ca^{2+} is mobilised in the cytosol and acts as second messenger for a plethora of different cellular pathways. One of those downstream pathways depends on the phosphorylation of ERK 1 and ERK 2. ERK signalling is

proposed to be involved in many different cellular processes like cell survival, growth, proliferation and differentiation [119]. Based on CPP-Ppx1 mediated Ca^{2+} mobilisation, we investigated the role of polyP degradation on ERK phosphorylation via immunoblot analysis. For this, murine CD4+ T cells were treated with CPP-Ppx1 or buffer control for 15 min to enable cell entrance and an additional 0 - 15 min for the signalling cascade to begin. Even though quantification of four independent blots did not show any significant differences, CPP-Ppx1 treated cells had a tendency towards more ERK1 and ERK 2 phosphorylation (pERK1, pERK2) after 5 min and a higher ERK 2 phosphorylation after 10 min compared to control samples (**Figure 16A** and **B**).
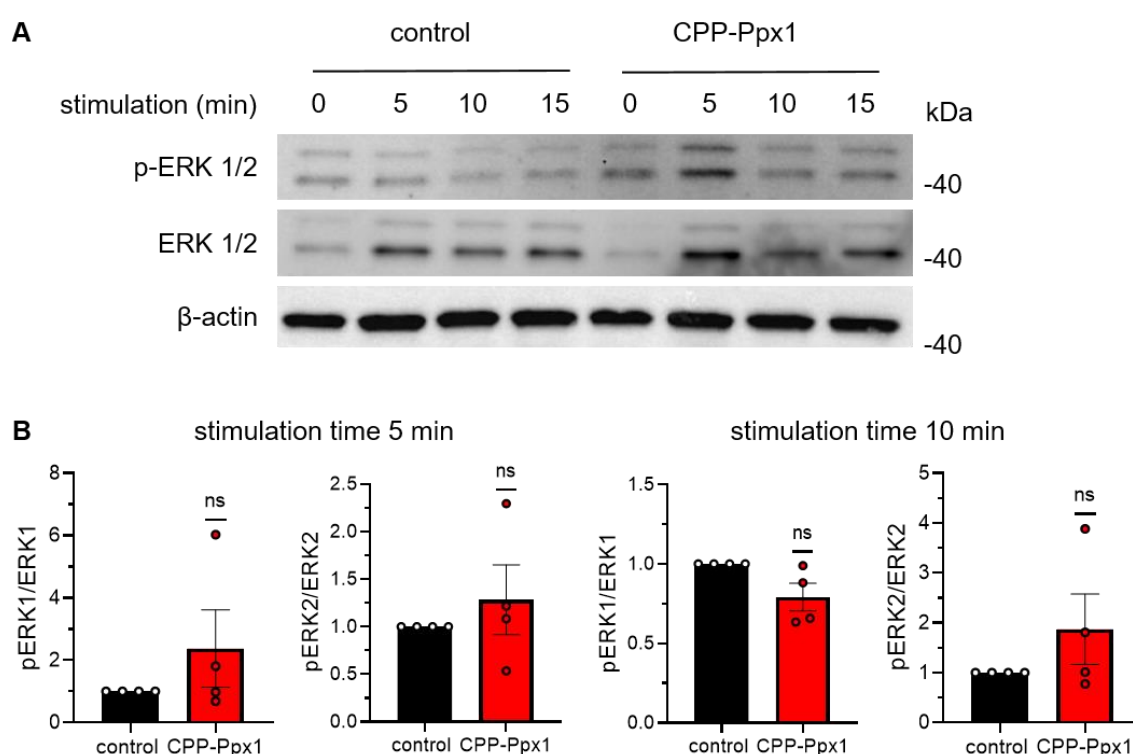
Figure 16. Ca^{2+} mobilisation by polyP degradation induces phosphorylation of ERK. Isolated murine CD4+ T cells were treated with buffer control or CPP-Ppx1 (80 µg/mL) for 15 min at 37 °C to enable cell penetration of phosphatase. Following incubation for up to 15 min at 37 °C in fresh medium ERK phosphorylation was analysed by immunoblotting. (**A**) Representative immunoblots of cells lysed after indicated incubation times analysed with α-phospho ERK1/2-antibodies (44/42 kDA) and α-ERK1/2-antibodies (44/42 kDA). β-actin immunoblotting was performed as loading control. (**B**) Quantification of ERK phosphorylation at 5 and 10 min in cells treated with buffer control or CPP-Ppx1. Data represent mean ± SEM, *p*-value by one sample t-test, ns=non-significant, represented as n=4 independent experiments.

Next, we performed flow cytometry analysis for T-cell activation markers CD69 and CD25 16 hours after incubation with CPP-Ppx1. While unstimulated T cells showed no expression of either of the markers, a stimulation with α-CD3/α-CD28 resulted in the formation of a CD25+ and a CD69+ population (**Figure 17A)**. Treating the cells with buffer control or denatured CPP-Ppx1 resulted in similar expression of CD25 and CD69 (**Figure 17B** and **C**) Even though the CD25+ population size was rather decreased in CPP-Ppx1 treated samples (**Figure 17A**) the treatment with CPP-Ppx1 significantly increased MFI of both CD25 and CD69 compared to controls (**Figure 17B** and **C**).
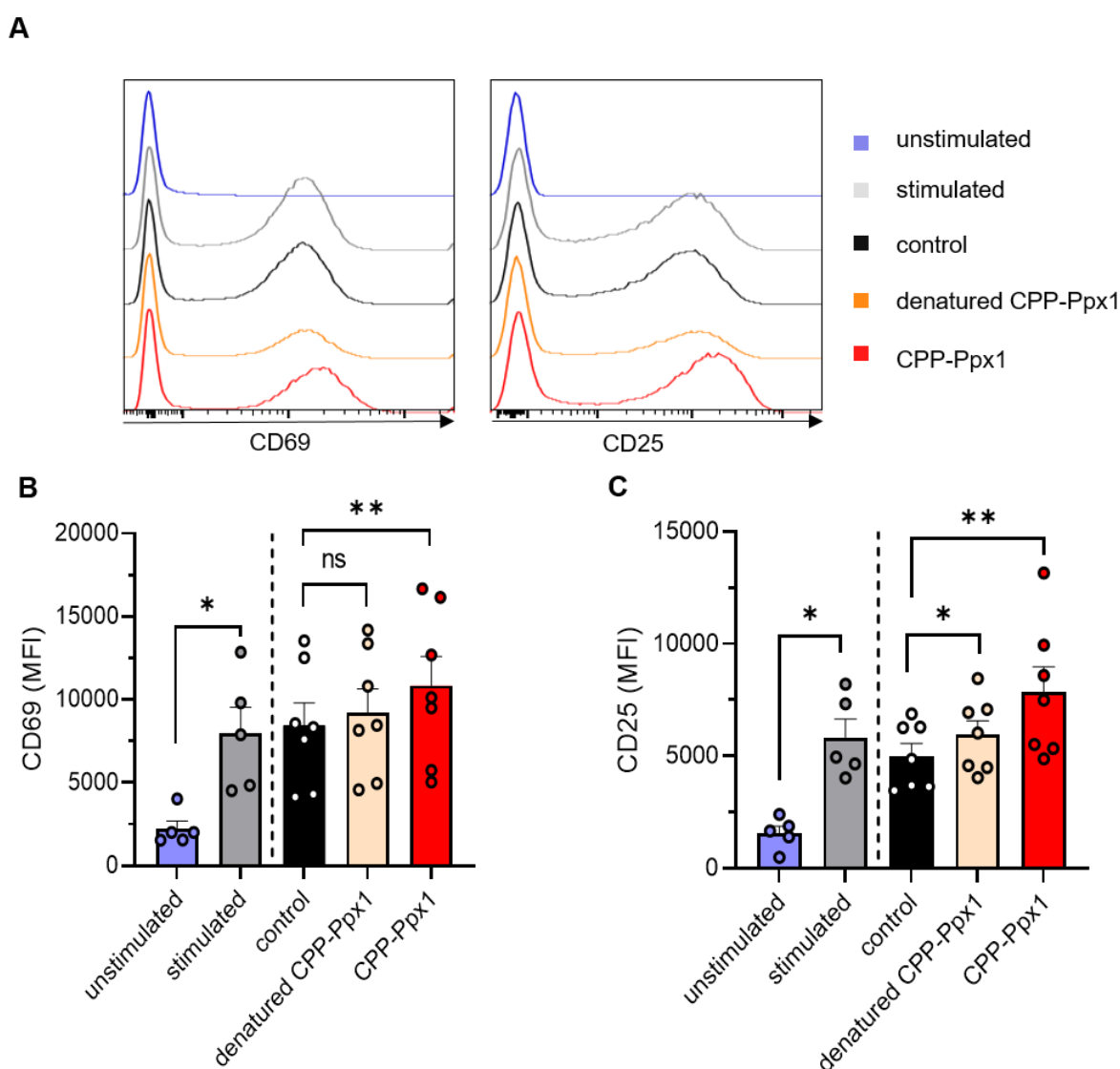
Figure 17. CPP-Ppx1 mediated polyP degradation increases CD69 and CD25 expression. CD4+ T cells were treated with buffer control, denatured or native CPP-Ppx1 (80µg/mL, twice for 15 min at 37 °C) and stimulated on α-CD3/α-CD28 (2 µg/mL / 0.5 µg/mL) coated plates for 16 hours. Activation markers CD69 and CD25 were analysed in flow cytometry. (**A**) Representative flow cytometry histograms of all tested conditions. (**B**) Statistical analysis of CD69 MFI expression levels. (**C**) Statistical

analysis of CD25 MFI expression levels. (**B** and **C**) Data represent mean ± SEM, *p*-value by paired Student's t-test, *p < 0.05, **p < 0.01 and ns=non-significant, unstimulated and stimulated represented in n=5 independent experiments; control, denatured and native CPP-Ppx1 represented as n=7 independent experiments.

Another commonly used signature cytokine for CD4+ T-cell activation is IL-2. T cells express IL-2 after stimulation and release this vital cytokine for autocrine consumption. We therefore compared the IL-2 production and its secretion to the cell-culture supernatant of unstimulated, stimulated, buffer control, denatured CPP-Ppx1 or CPP-Ppx1 treated cells 16 hours after treatment. All cells except for the unstimulated control were cultured on α-CD3/α-CD28 coated wells in order to achieve a measurable basal level of IL-2 production. The stimulation itself resulted in the production of approximately 50 ng/mL IL-2. Treatment with the buffer control did not alter these IL-2 levels. Denatured CPP-Ppx1 raised the IL-2 production only slightly, while CPP-Ppx1 treatment increased the IL-2 levels in the medium by 2-fold (**Figure 18A**). Increased IL-2 production as a consequence of CPP-Ppx1 treatment in CD4+ T cells was further validated by RT-qPCR analysis that showed a 2.5-fold increase in *Il2* mRNA levels in comparison to control samples (**Figure 18B**).
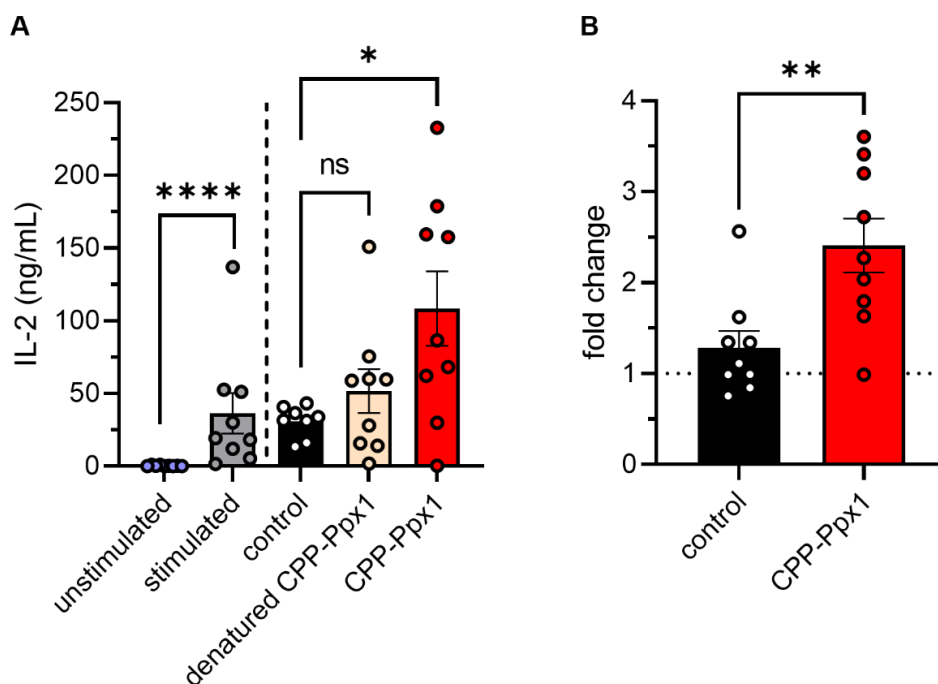
Figure 18. CPP-Ppx1 induced polyP degradation elevates IL-2 production. CD4+ T cells were treated with buffer control, denatured or native CPP-Ppx1 (80 μg/mL, twice for 15 min at 37 °C) and

stimulated on α-CD3/α-CD28 (2 µg/mL / 0.5 µg/mL) coated plates for 16 hours. (**A**) IL-2 in supernatants was quantified by ELISA. Data represent mean ± SEM, outliers were identified using the ROUT method, *p*-value by Kruskal-Wallis test, *$p < 0.05$, ****$p < 0.0001$ and ns=non-significant, represented as n=9 independent experiments. (**B**) *Il2* mRNA expression was analysed by RT-qPCR analysis, normalised to the house-keeping gene *Hprt* and the α-CD3/α-CD28-stimulated control group (set to 1, indicated as a dashed line). Data represent mean ± SEM, *p*-value by one sample t-test, **$p < 0.01$, represented as n=9 independent experiments.

Moreover, this heightened activation status of CD4+ T cells due to polyP degradation was also observed when proliferation was monitored by staining for Ki67 and staining with eFluor proliferation dye. CPP-Ppx1 treated T cells expressed more Ki67 compared to buffer treated T cells after 16 hours, indicating a larger population of proliferating cells (**Figure 19A**). To analyse the proliferation more closely, CD4+ T cells treated with buffer control or CPP-Ppx1 were stained with eFluor proliferation dye and stimulated on α-CD3/α-CD28 coated plates for three days, which allows the tracking of cell divisions by flow cytometry. Proliferation increased in T cells treated with CPP-Ppx1 in comparison to buffer control and the T-cell population that underwent four or more divisions was significantly larger. (**Figure 19B**).
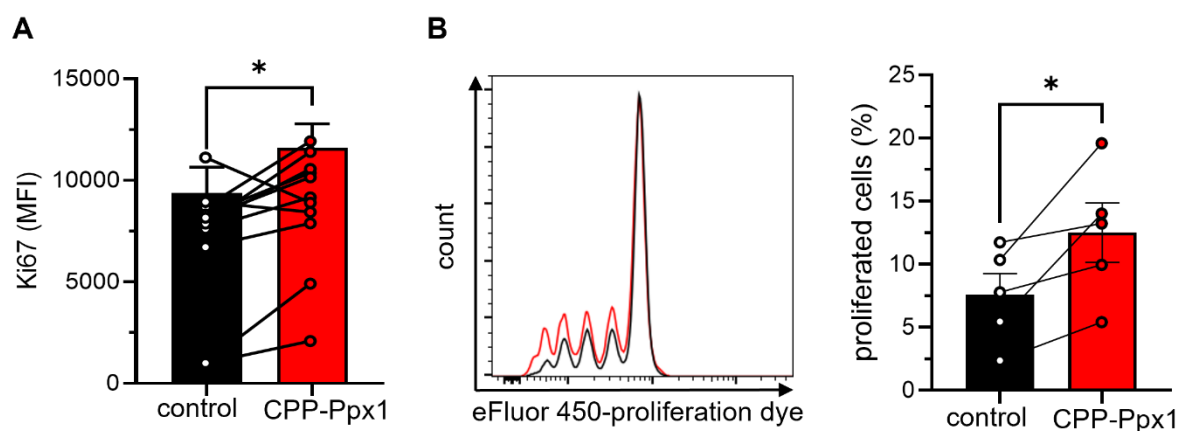
Figure 19. PolyP degradation induces a hyper-proliferative phenotype. (**A**) CD4+ T cells were treated with CPP-Ppx1 (80µg/mL, twice for 15 min at 37 °C) or buffer control and stimulated on α-CD3/α-CD28 (2 µg/mL / 0.5 µg/mL) coated plates for 16 hours. Ki67 expression was analysed in flow cytometry. (**B**) CD4+ T cells were stained with eFluor proliferation dye (2.5 µM), treated with CPP-Ppx1 (80µg/mL, twice for 15 min at 37 °C) or buffer control and stimulated on α-CD3/α-CD28 (2 µg/mL / 0.5 µg/mL) coated plates for 3 days. (left) Representative flow cytometry plot of proliferation dye dilution and (right) statistical analysis of population size with at least four proliferation cycles. Data represent mean ± SEM, *p*-value by Student's paired t-test *$p < 0.05$, represented as (**A**) n=11, (**B**) n=5 independent experiments.

Taken together these data indicate that the degradation of polyP by CPP-Ppx1 in CD4+ T cells results in a higher activation status, as a result of Ca^{2+} mobilisation and ERK signalling, which induces the expression of activation markers like CD69, CD25 and production of IL-2. Furthermore, polyP depleted CD4+ T cells have an increased proliferative capacity.

4.3.3 PolyP degradation affects the metabolic status of T cells

As stated before, T-cell activation goes hand in hand with a pronounced metabolic reprogramming [69] and intracellular polyP levels have been shown to be tightly linked to cellular metabolism [102]. We therefore hypothesised that in addition to T-cell activation also the T-cell metabolism might be affected by polyP degradation through CPP-Ppx1.

To test this hypothesis, CD4+ T cells were isolated from murine splenocytes treated with CPP-Ppx1, stimulated for 16 hours on α-CD3/α-CD28 coated plates and an array of genes related to metabolic pathways or the metabolic remodelling of T cells after activation was analysed by RT-qPCR.

We chose to analyse mRNA levels of myelocytomatosis oncogene (Myc, gene: *Myc*) and hypoxia-inducible factor 1α (Hif1α, gene: *Hif1α*) as two transcription factors previously shown to be involved in metabolic reprogramming and preceding the upregulation of glycolysis [120]. Glucose transporter 1 (Glut1, gene: *Slc2a1*), hexokinase 2 (Hk2, gene: *Hk2*) and triosephosphate isomerase 1 (Tpi1, gene: *Tpi1*) were analysed as genes involved in glycolysis. To identify alternative energy sources, we further validated mRNA levels of glutaminase 2 (Gls2, gene *Gls2*), which is relevant for hydrolysis of glutamine to glutamate, and the lactate exporting enzyme monocarboxylate-transporter 4 (Mtc4 gene: *Slc16a3*).

While the mRNA levels for the transcription factors Myc and Hif1α did not show any differences between T cells treated with CPP-Ppx1 or buffer control (**Figure 20A** and **B**), significantly more *Slc2a1* mRNA was observed in T cells with reduced polyP levels (**Figure 20C**). A tendency for higher glycolytic capacity was further seen in slightly elevated levels of *Hk2* and *Tpi1* (**Figure 20D** and **E**). While the mRNA levels for the *Gls2* gene remained unchanged upon treatment (**Figure 20F**), the amounts of *Slc16a3* had a tendency to be upregulated (**Figure 20G**). The upregulation of *Glut1* and the slightly elevated levels of *Hk2* and *Tpi1* suggest an upregulation of glycolysis

while the tendency towards more *Slc16a3* might indicate the metabolic switch from oxidative phosphorylation towards aerobic fermentation, which is characteristic for CD4+ T-cell activation.
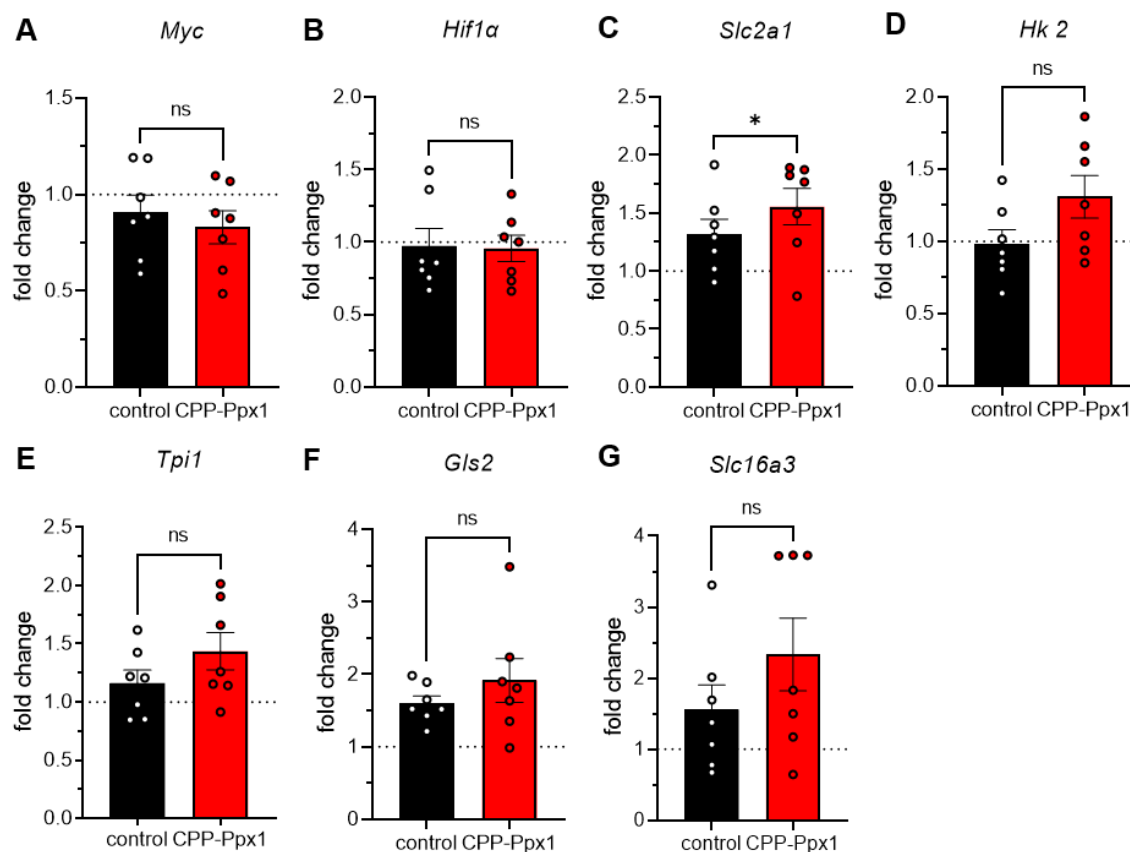
Figure 20. RT-qPCR analysis of metabolic markers in response to polyP degradation. CD4+ T cells were treated with CPP-Ppx1 (80µg/mL, twice for 15 min at 37 °C) or buffer control and stimulated on α-CD3/α-CD28 (2 µg/mL / 0.5 µg/mL) coated plates for 16 hours. ΔΔCt values were normalised to the house-keeping gene *Hprt* and the α-CD3/α-CD28 stimulated control group (set to 1, indicated as a dashed line). The mRNA expression of (**A**) *Myc*, (**B**) *Hif1α*, (**C**) *Slc2a1*, (**D**) *Hk2*, (**E**) *Tpi1*, (**F**) *Gls2* and *(G) Slc16a3* was analysed. Data represent mean ± SEM, *p*-value by paired t-test, *$p < 0.05$, ns=non-significant, represented as n=7 independent experiments.

To elucidate the metabolic changes in more detail, we performed Seahorse metabolic flux assays that measure the oxidative consumption rate (OCR) as quantification for oxidative phosphorylation and the extracellular acidification rate (ECAR) due to lactic acid release by cells into the medium, which serves as a measurement for glycolysis.

In Seahorse Real Time ATP Rate Assays cells are subjected to oligomycin treatment that inhibits the ATP-synthase, followed by simultaneous rotenone and antimycin A treatment that inhibits complexes I and III of the respiratory chain, respectively.

Oligomycin blocks all ATP production during oxidative phosphorylation and the difference between the two phases before and after oligomycin treatment represents the total ATP production. By addition of rotenone and antimycin A the metabolism of the cell is reduced to an OCR representing the non-mitochondrial respiration.

Consistent with other analyses before, CD4+ T cells were isolated from murine splenocytes, incubated with CPP-Ppx1 or buffer control and stimulated for 16 hours on α-CD3/α-CD28 coated plates. CPP-Ppx1 treatment elicited higher OCR and ECAR compared to buffer control treated T cells (**Figure 21A** and **B**). The differences between the basal rates and rates measured after oligomycin treatment showed that the general ATP production, both from glycolysis and oxidative phosphorylation, was elevated in the CPP-Ppx1 treated group compared to the control group (**Figure 21C** and **D**). Accordingly, the overall ATP production was also significantly increased (**Figure 21E**).
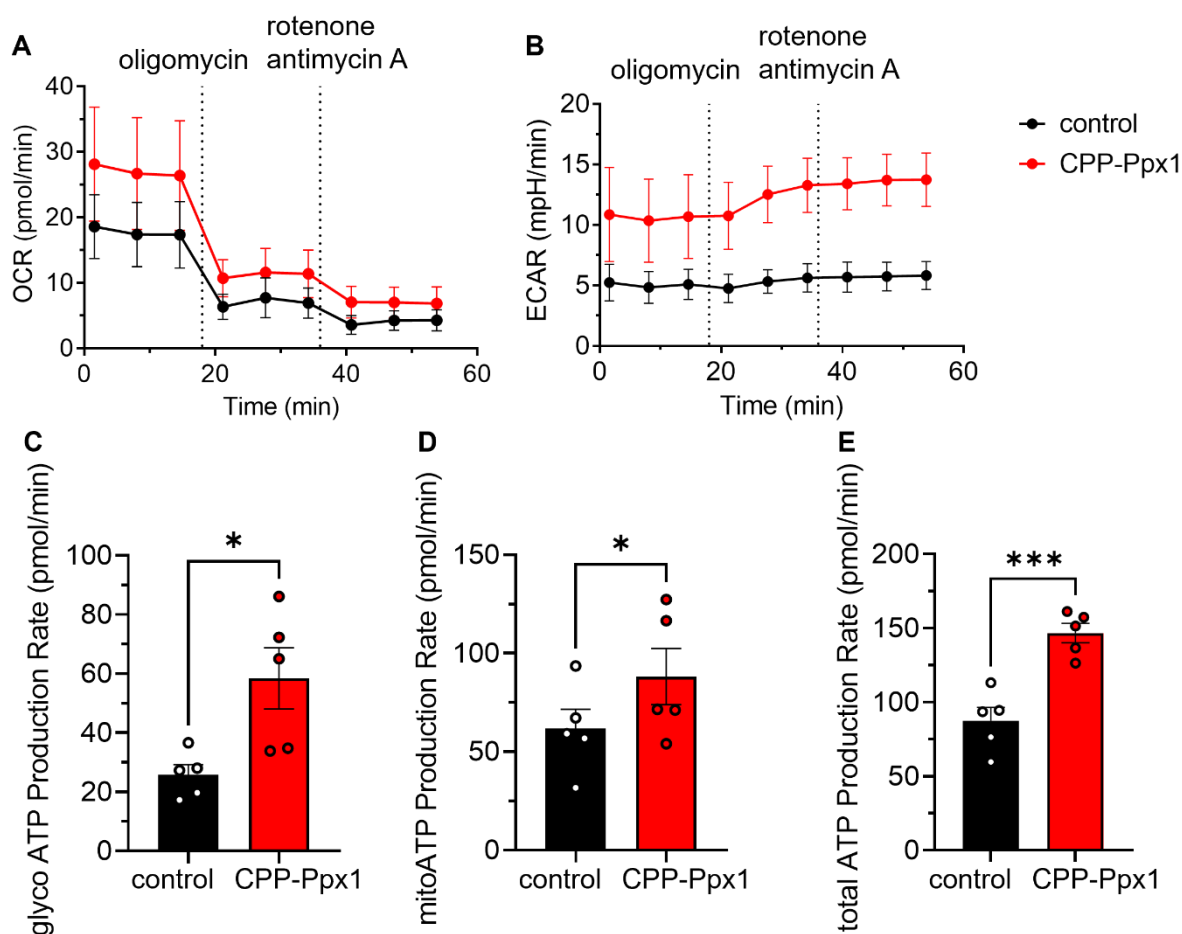
Figure 21. PolyP degradation stimulates the metabolic activity of T cells. Seahorse ATP Rate Assay was performed with murine CD4+ T cells treated with CPP-Ppx1 (80 μg/mL, twice for 15 min, 37 °C) or buffer control and stimulated on α-CD3/α-CD28 (2 μg/mL / 0.5 μg/mL) coated plates for 16 hours.

(**A**) Oxygen consumption rate and (**B**) extracellular acidification rate were monitored. (**C**) ATP production rate of glycolysis, (**D**) oxidative phosphorylation and (**E**) total ATP production were calculated. (**C-E**) Analysis of data was carried out with Seahorse Wave Pro 10.1.0 software. Data represent mean ± SEM, *p*-value by paired Student's t-test, *$p < 0.05$, ***$p < 0.001$, represented as n=5 independent experiments.

To further examine the mitochondrial metabolism, we used Seahorse T Cell Metabolic Profiling Kit. This kit is characterised by the injection of BAM 15 after oligomycin addition. BAM 15 uncouples the oxidative phosphorylation by annulling the proton gradient across the inner mitochondrial membrane. In order to compensate for the loss of the proton gradient, cells maximise the respiration. The difference measured between the basal respiration before oligomycin treatment and the maximal respiration after uncoupling of the respiratory chain is defined as the spare respiratory capacity.

CPP-Ppx1 treated CD4+ T cells displayed elevated OCR and ECAR levels compared to the control group (**Figure 22A** and **B**). Even though a tendency towards a higher spare respiratory capacity is recognisable (**Figure 22A**), no statistically significant increase could be observed (**Figure 22C**). These experiments show that a degradation of polyP increases the metabolic activity of both glycolysis and oxidative phosphorylation in CD4+ T cells.
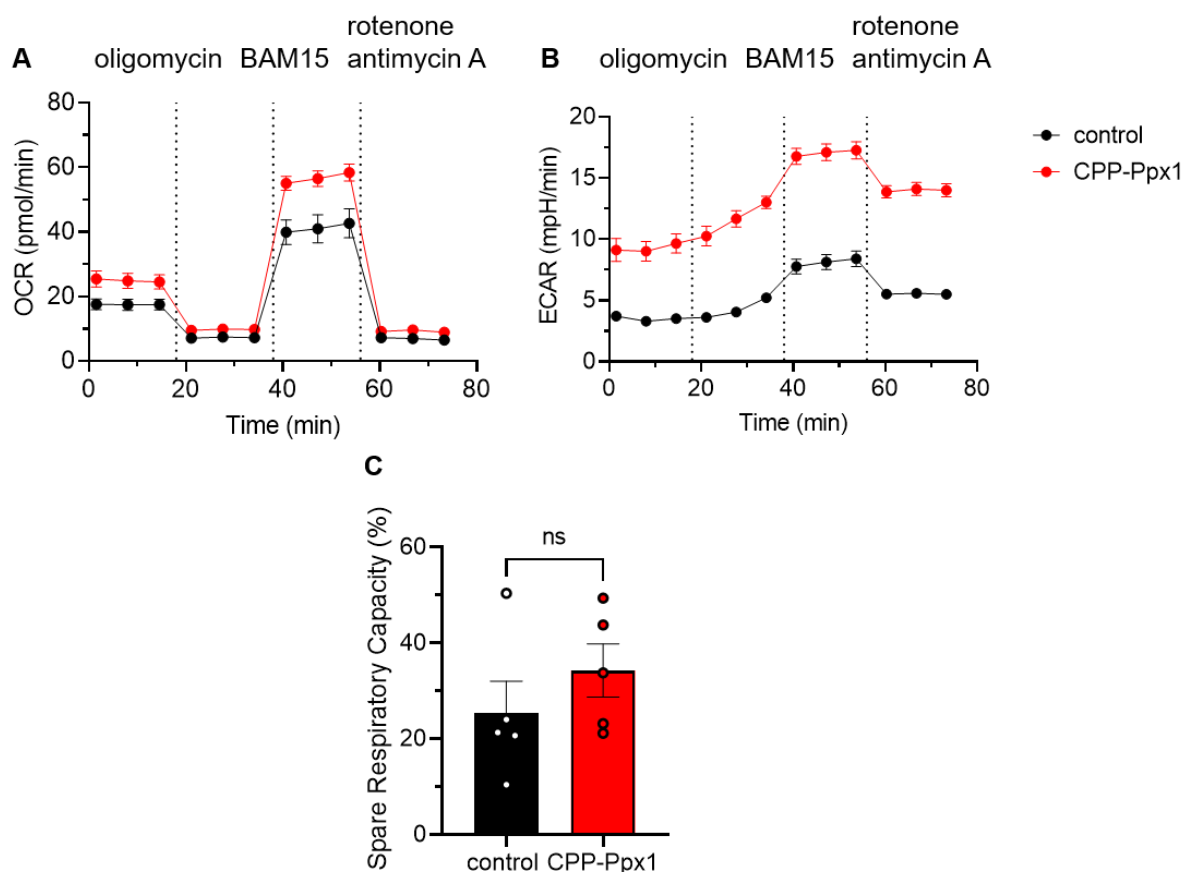
Figure 22. PolyP reduction tends to increase the spare respiratory capacity in T cells. Seahorse T-cell metabolic profiling Kit was performed with murine CD4+ T cells treated with CPP-Ppx1 (80 µg/mL, twice for 15 min, 37 °C) or buffer control and stimulated on α-CD3/α-CD28 (2 µg/mL / 0.5 µg/mL) coated plates for 16 hours. (**A**) Oxygen consumption rate and (**B**) extracellular acidification rate were monitored. (**C**) Spare respiratory capacity was calculated; analysis of data was carried out with Seahorse Wave Pro 10.1.0 software. Data represent mean ± SEM, *p*-value by paired Student's t-test, ns=non-significant, represented as n=5 independent experiments.

Increased oxidative phosphorylation has been reported to results in increased generation of reactive oxygen species (ROS) due to the natural proton leak [64, 73]. ROS are therefore used as a measurement for cellular stress. We analysed the amounts of superoxide and ROS in cells treated with buffer control or CPP-Ppx1, using the ROS/Superoxide Detection Assay Kit, which has two fluorescent reporters and includes a negative and a positive control. For the negative control, three days stimulated T cells were treated with the ROS inhibitor N-acetyl-L-cystein for 30 min prior to addition of the ROS inducer pyocyanin. As a positive control, cells were only treated with pyocyanin. The pyocyanin treated positive control showed a definite shift in both oxidative stress and superoxide stainings compared to the additionally treated N-acetyl-L-cystein treated negative control (**Figure 23A**). In order to normalise multiple

experiments, MFI ratios for each sample and each reporter were calculated in relation to the respective MFI of unstained, untreated controls.

Compared to buffer control treatment, CPP-Ppx1 treated CD4+ T cells showed a reduced MFI ratio for both superoxide and oxidative stress (**Figure 23B** and **C**). These results were surprising, as we expected that due to the metabolic enhancement - especially of the oxidative phosphorylation upon CPP-Ppx1 treatment - more reactive oxygen species would be produced.
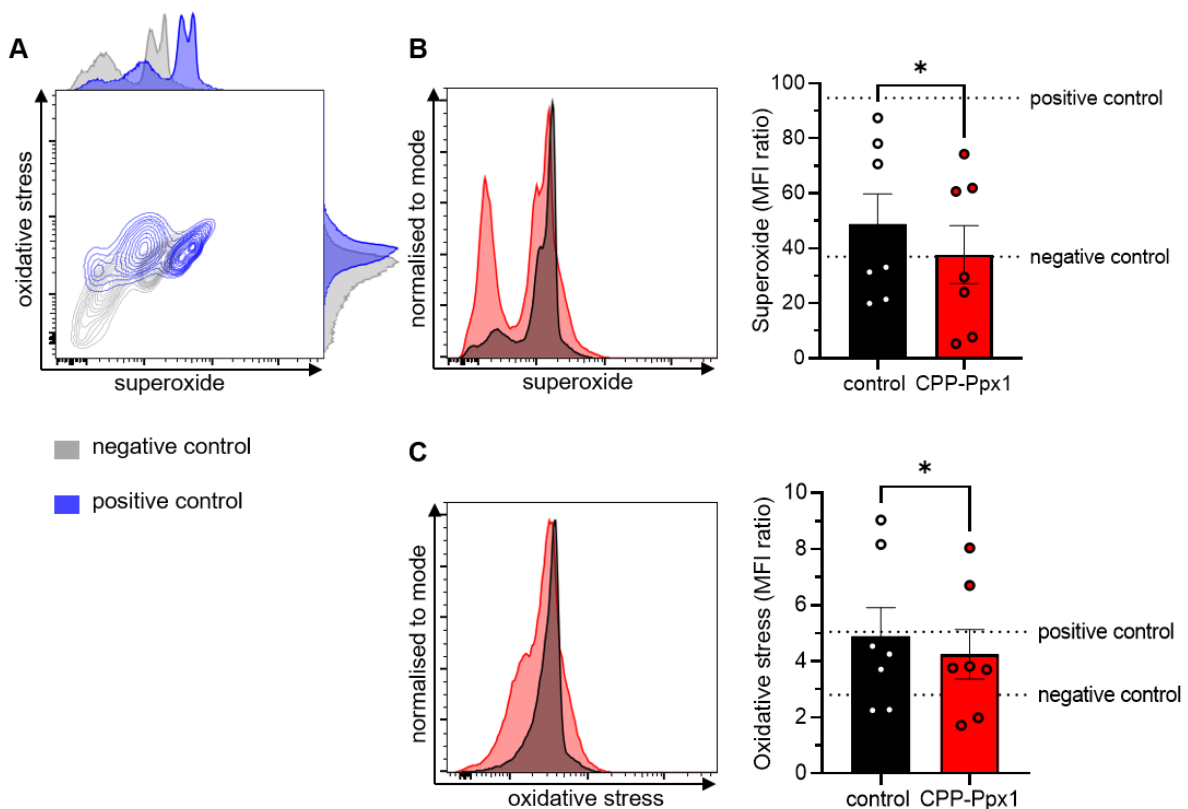
Figure 23. CPP-Ppx1 treatment significantly reduces production of superoxide and oxidative stress. (**A**) Representative flow cytometry plot of positive and negative controls for superoxide and oxidative stress reporter stainings. Analysis of (**B**) superoxide and (**C**) oxidative stress three days after CPP-Ppx1 (80 µg/mL, twice for 15 min, 37°C) or buffer control treatment and stimulation on α-CD3/α-CD28 (2 µg/mL / 0.5 µg/mL) coated plates; independent experiments were normalised to MFI of unstained controls. Data represent mean ± SEM, positive and negative control of one representative experiment indicated as dashed line, *p*-value by paired Student's t-test, *$p < 0.05$, represented as n=7 independent experiments.

In addition, we analysed mitochondrial mass and function by MitoTracker staining in CD4+ T cells with or without reduced polyP levels. MitoTracker Green (MG) permeates all mitochondria and is therefore used as a marker for overall mitochondrial mass. MitoTracker DeepRed (MDR) permeates only those mitochondria displaying an active

membrane potential and can be used to determine the mitochondrial function. Both parameters were analysed three days after CPP-Ppx1 or buffer control treatment in stimulated T cells. MitoTracker staining showed similar ratios of functional (MG high, MDR high) and dysfunctional (MG high, MDR low) mitochondria in both groups (**Figure 24A**). The average ratio of approximately 70% functional and 15% dysfunctional mitochondria did not change upon CPP-Ppx1 treatment (**Figure 24B** and **C**).

Overall, these results indicate that polyP depletion in CD4+ T cells results in a hyperactive phenotype with increased metabolism, but with a reduced oxidative stress level and no significant alterations in mitochondrial mass or function.
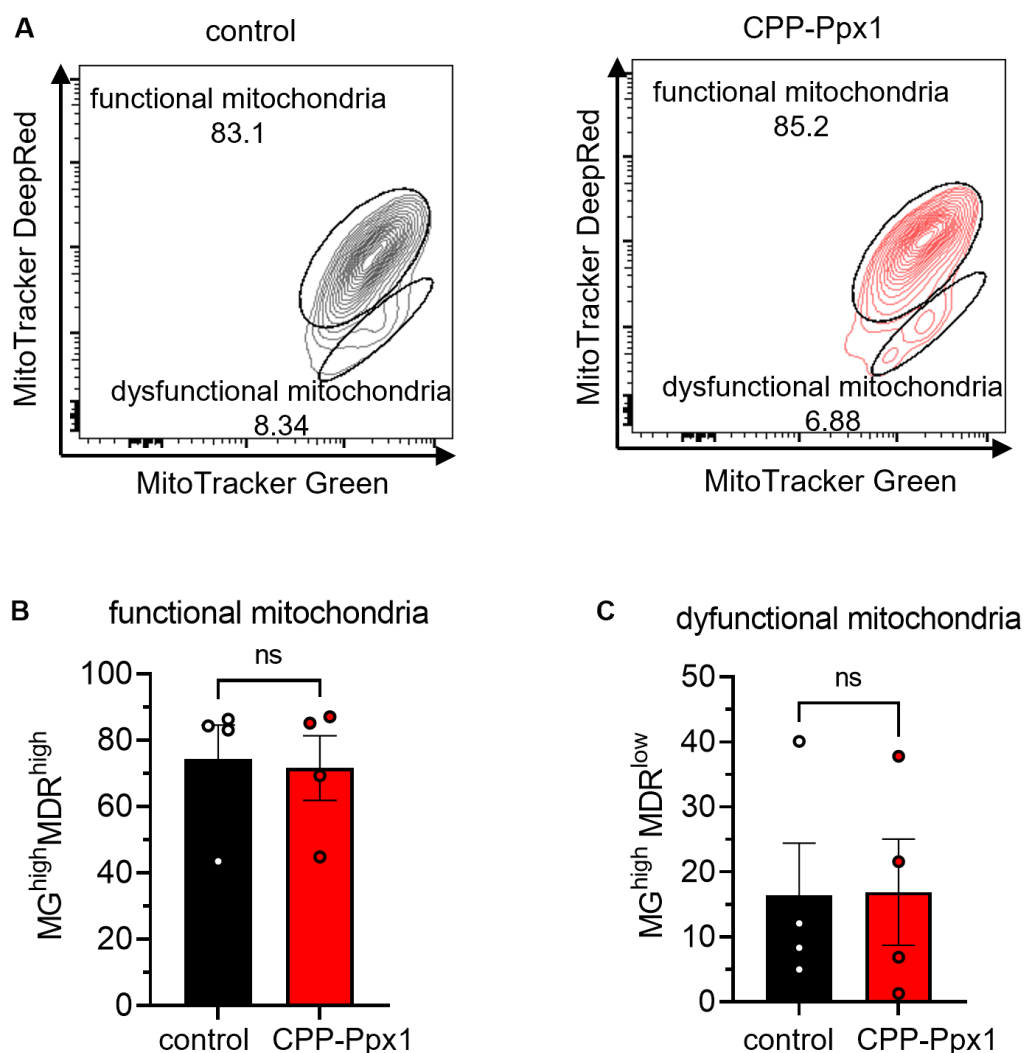
Figure 24. PolyP degradation does not alter mitochondrial mass or function in murine CD4+ T cells. Murine CD4+ T cells were treated with CPP-Ppx1 (80 µg/mL, twice for 15 min, 37 °C) and stimulated on α-CD3/α-CD28 (2 µg/mL / 0.5 µg/mL) coated plates for three days. (**A**) Representative flow cytometry plots of MitoTracker stainings. Statistical analysis of (**B**) functional and (**C**) dysfunctional

mitochondria. Data represent mean ± SEM, *p*-value by (**B**) Wilcoxon test or (**C**) paired Student's t-test, ns=non-significant, represented as n=4 independent experiments.

4.3.4 PolyP degradation induces a non-suppressive Foxp3 expression

To gain a comprehensive understanding of the changes caused by polyP degradation in CD4+ T cells we performed assay for transposase-accessible chromatin sequencing (ATAC-seq.). For this, freshly isolated naïve CD4+ T cells treated with CPP-Ppx1 or buffer control were stimulated on α-CD3/α-CD28 coated plates for 16 hours and sent to Active Motif Inc. for chromatin accessibility analysis. Two biological replicates were analysed and approximately 80.000 differentially accessible genomic regions (DAR) were detected. Due to the high overlap in PC1 variance between control and one of the CPP-Ppx1 treated samples (**Figure 25A**), no statistically significant differences in gene accessibility could be detected, based on the adjusted *p*-value (Padj). We therefore cautiously analysed our data on the basis of the unadjusted *p*-value, and results were visualised in a heat map representing the correlation of samples (**Figure 25B**). Correlation of the DARs with Gene ontology (GO) terms by GREAT v4.0.4 platform allowed us to gain an overview of the cellular processes related to the identified DAR (**Figure 25C**). Most hits were found upon GO terms related to T-cell adhesion, activation or differentiation, confirming our previous experiments that polyP depletion promotes CD4+ T-cell activation. We focused on the first 1000 DARs based on the smallest unadjusted *p*-value for respective associations with T-cell functions. Among them we found 50 genes reported to affect T-cell activation and T-cell differentiation, 53 genes associated with a regulatory T-cell phenotype and 23 genes related with signalling pathways activated after T-cell activation (Appendix 9.1, Table 6 - 8).
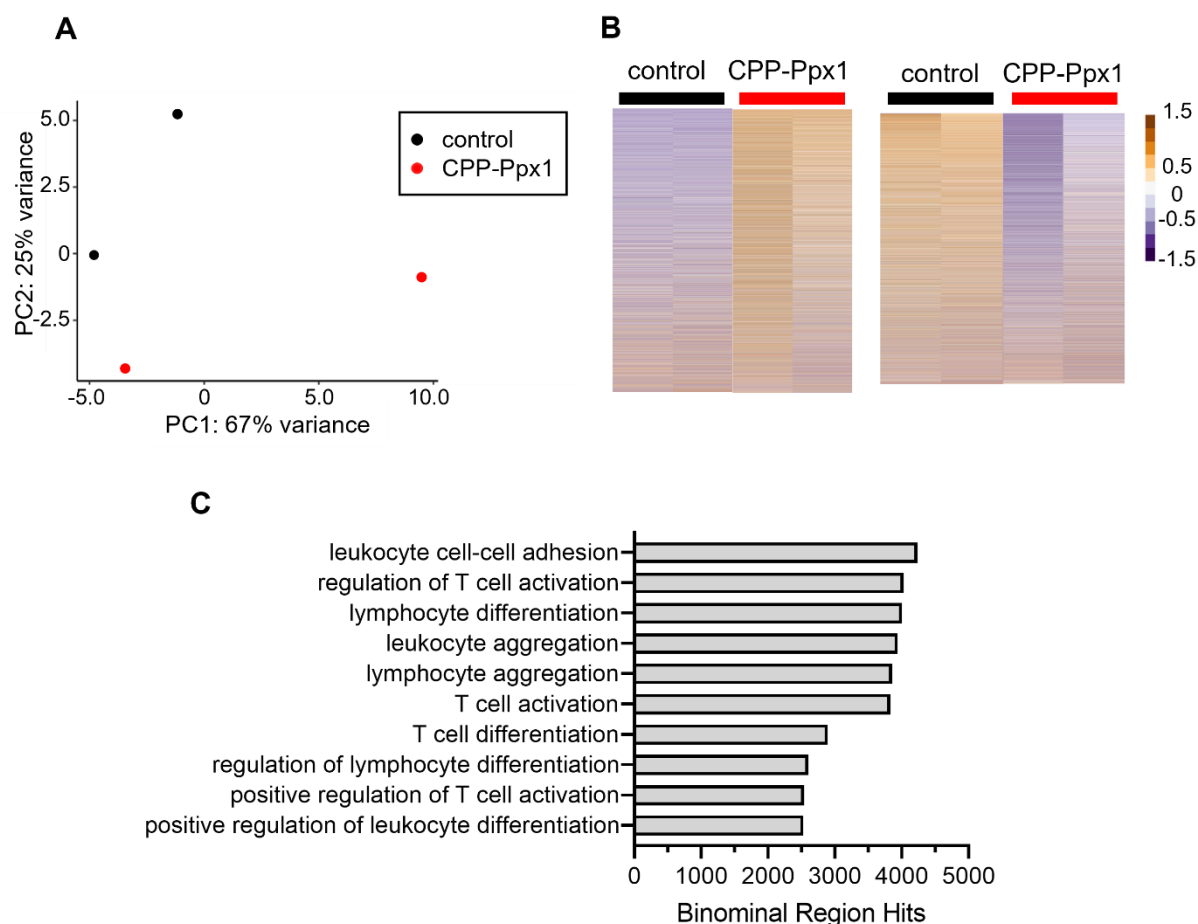
Figure 25. ATAC-seq. analysis of CPP-Ppx1 treated CD4+ T cells. CD4+ T cells were treated with CPP-Ppx1 (80 µg/mL, twice for 15 min, 37 °C) or buffer control and stimulated on α-CD3/α-CD28 (2 µg/mL / 0.5 µg/mL) coated plates for 16 hours. ATAC-seq. (Active Motif Inc., Belgium) was performed on samples from n=2 independent experiments. (**A**) Principle Component (PC) analysis and (**B**) heatmap of all annotated peaks were provided by Active Motif Inc. (**C**) Gene Ontology (GO) analysis performed with GREAT version 4.0.4 of all annotated peaks, top ten GO terms based on highest number of binominal region hits are shown.

Based on these findings, we characterised the impact of polyP reduction on CD4+ T-cell differentiation *in vitro*. CPP-Ppx1 or buffer control treated cells were stimulated on α-CD3/α-CD28 coated plates in IL-2 supplemented medium (Th0 condition) or skewing conditions for different T-cell subsets. In comparison to control samples, CPP-Ppx1 treatment did not change the expression of TNFα in Th0 or Th1 cells significantly (**Figure 26A**). Similarly, production of IL-4 was not altered by CPP-Ppx1 treatment in Th0 or Th2 cells (**Figure 26B**). Since relative polyP levels peaked upon Th17 cell-skewing conditions (**Figure 9B**) CPP-Ppx1 treatment was expected to decrease IL-17A production. Nevertheless, in comparison to control samples CPP-Ppx1 treatment displayed a trend towards an increased

58

IL-17A-expressing population under Th17 cell-skewing conditions, possibly representing the enhanced T-cell activation by polyP degradation (**Figure 26C**).
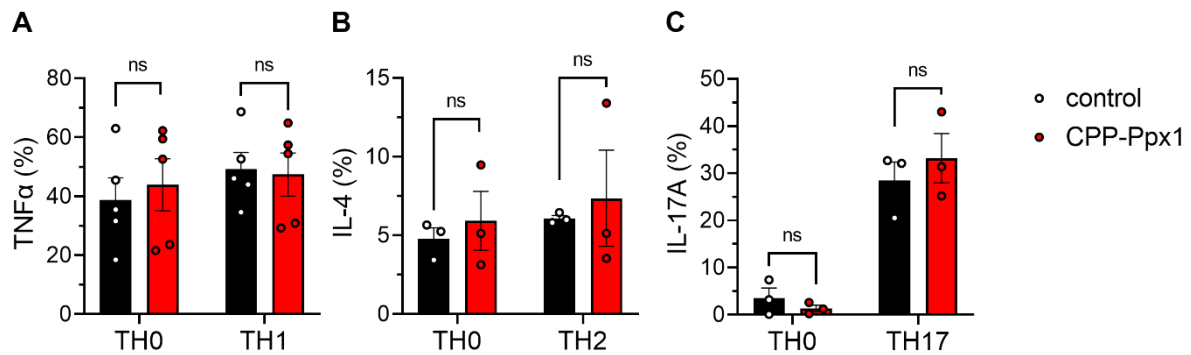
Figure 26. PolyP depletion does not affect the expression of pro-inflammatory cytokines. Production of (**A**) TNFα (**B**) IL-4 and (**C**) IL-17A in CD4+ T cells treated with CPP-Ppx1 (80 µg/mL, twice for 15 min, 37 °C) or buffer control, stimulated on α-CD3/α-CD28 (2 µg/mL / 0.5 µg/mL) coated plates for three days (**A** and **B**) or 5 days (**C**) in respective skewing conditions for T-cell subsets. Production of T-cell subset specific cytokines was analysed in flow cytometry following restimulation with PMA (50 ng/mL) and ionomycin (1 µg/mL) for two hours and protein transport inhibition for four hours. Data represent mean ± SEM from (**A**) n=5, (**B**) n=3, (**C**) n=3 independent experiments, *p*-value by paired Student's t-test, ns=non-significant.

Furthermore, we investigated the role of polyP degradation for the induction of anti-inflammatory phenotype in CD4+ T cells. We noticed a peak in the promotor region of the *Ctla4* locus among the top 1000 DARs in ATAC-seq. (**Figure 27A**). To verify differential CTLA4 expression in CD4+ T cells upon CPP-Ppx1 treatment, intra- and extracellular CTLA4 was compared in CPP-Ppx1 and buffer control treated T cells after stimulation with α-CD3/α-CD28 coated plates for 16 hours. We observed a significant increase in extra- and intracellular CTLA4 within the CD25+ T-cell population (**Figure 27B** and **C**), suggesting the induction of a Treg-like phenotype.
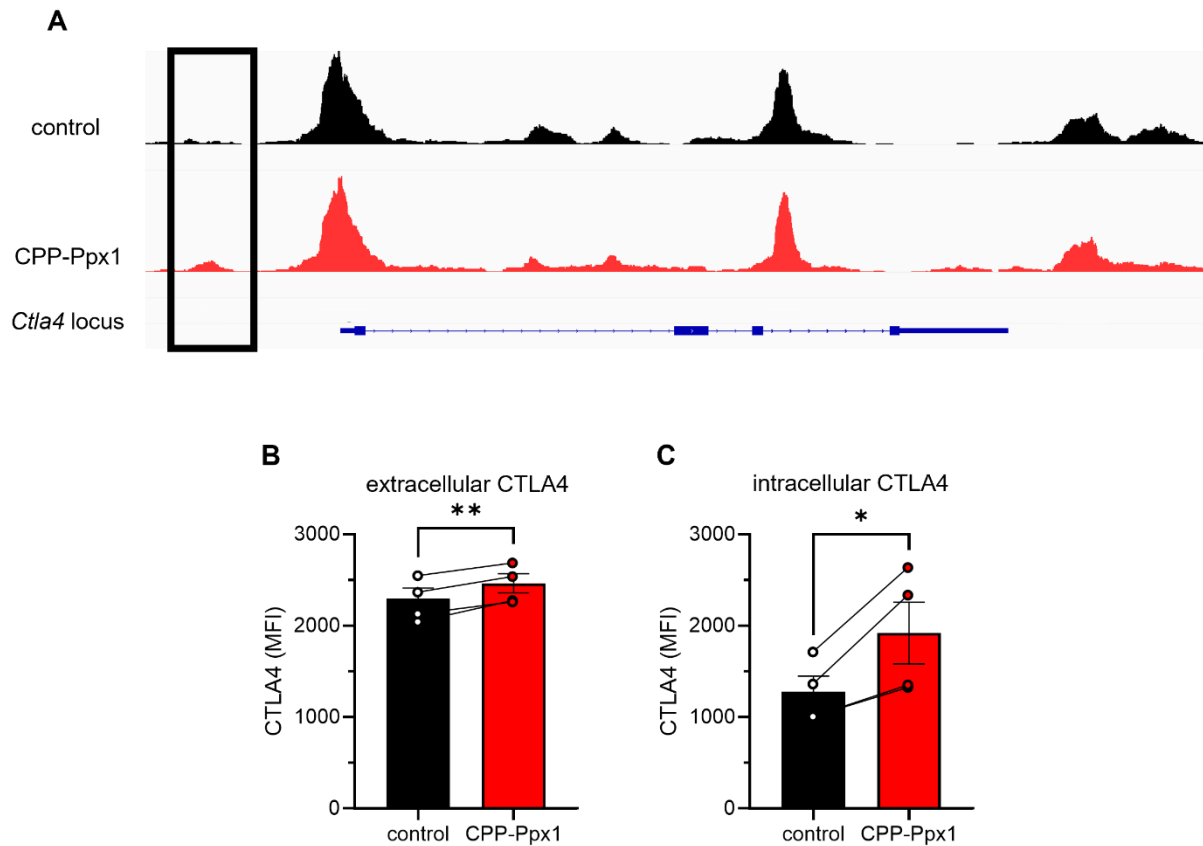
Figure 27. PolyP degradation induces CTLA4 expression. (**A**) Chromatin accessibility of the *Ctla4* locus visualised using the Integrative Genomic Viewer (IGV) version 2.18.4 and (**B**) extracellular and (**C**) intracellular CTLA4 expression levels of CD25+ T cells following the treatment of murine CD4+ T cells with CPP-Ppx1 (80 μg/mL, twice for 15 min, 37 °C) or buffer control and stimulation with α-CD3/α-CD28 (2 μg/mL / 0.5 μg/mL) coated plates for 16 hours. Data represent mean ± SEM, *p*-value by paired Student's t-test, *$p < 0.05$, **$p < 0.01$, represented as n=4 independent experiments.

To further validate this Treg-associated phenotype, we analysed the induction of Foxp3 in Th0 and iTreg cells with or without CPP-Ppx1 treatment *in vitro*. For this, isolated CD4+ T cells were incubated with CPP-Ppx1 or buffer control in respective skewing conditions on α-CD3/α-CD28 coated plates for three days. CPP-Ppx1 treatment increases Foxp3 expression in Th0 cells more than 2-fold in comparison to the buffer control group (**Figure 28A**), which corresponds to a small increase in band-intensity for CPP-Ppx1 treated Th0 cells in Foxp3 immunoblot analysis (**Figure 28B)**. Moreover, Foxp3 expression in iTreg cells was further enhanced by CPP-Ppx1 treatment compared to buffer control treatment as shown by elevated Foxp3 detection in flow cytometry (**Figure 28C**) and immunoblot analysis (**Figure 28D**).
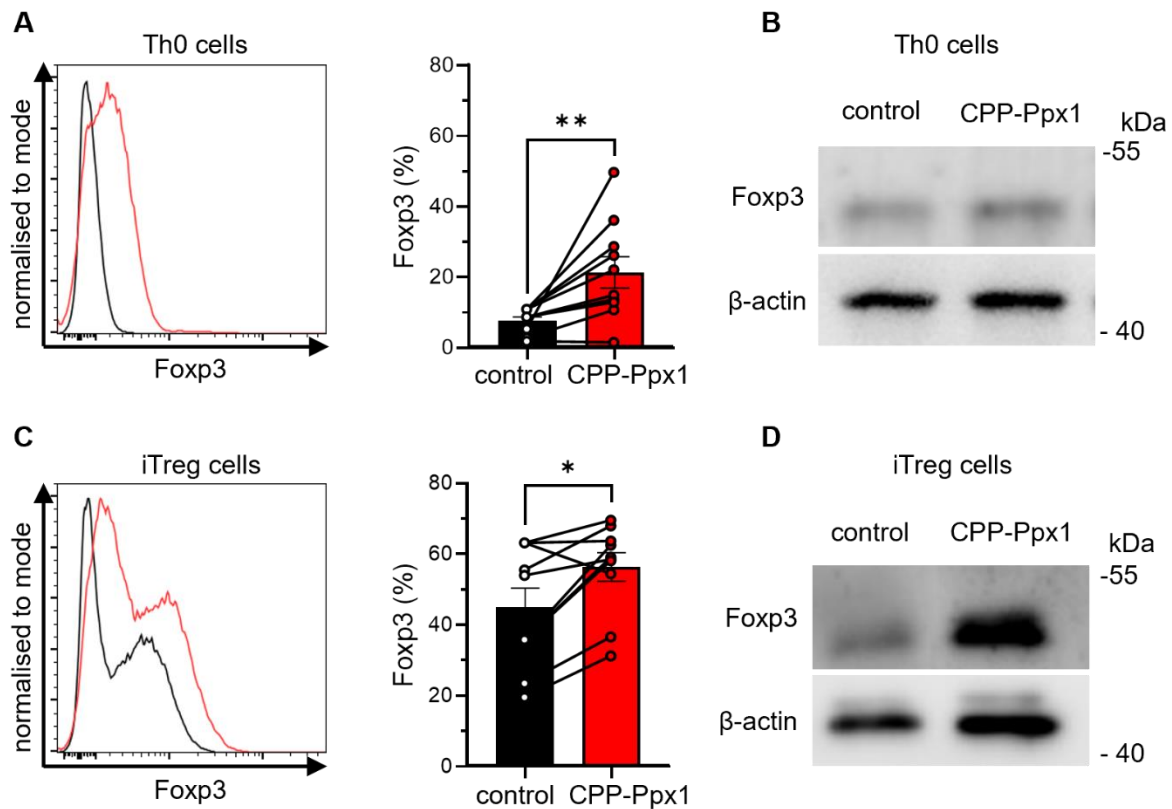
Figure 28. CPP-Ppx1 mediated polyP depletion increases Foxp3 expression. Foxp3 expression in CD4+ T cells treated with CPP-Ppx1 (80 µg/mL, twice for 15 min, 37°C) or buffer control and stimulated on α-CD3/α-CD28 (2 µg/mL / 0.5 µg/mL) coated plates for three days under Th0-skewing conditions (**A** and **B**) or iTreg-skewing conditions (**C** and **D**). Representative histograms (left), statistical flow cytometry analysis (middle) and representative Foxp3 immunoblots (**B** and **D**) are shown. β-actin immunoblotting was performed as loading control, respective protein ladder is indicated on the right. Data represent mean ± SEM, *p*-value by Wilcoxon test *$p < 0.05$, **$p < 0.01$, represented as (**A** and **C**) n=10 and (**B** and **D**) n=3 independent experiments.

Since the observed Foxp3 increase in response to CPP-Ppx1 treatment was analysed in CD4+ T cell populations, we next wanted to determine whether polyP degradation by CPP-Ppx1 increased the expansion of the naturally occurring Foxp3+ nTreg cells or whether *de novo* Foxp3 expression was induced in naïve T cells.

For this, naïve CD4+ T cells were isolated from mouse splenocytes and the CD4+CD25+ nTreg population was separated by magnetic cell separation. While nTreg cells were stained with eFluor670 proliferation dye, CD4+CD25- conventional T (Tcon) cells were stained with eFluor450 proliferation dye. After labelling, both populations were mixed at a physiological nTreg:Tcon ratio (1:10). Consistent with the experiments before, treatment with CPP-Ppx1 or buffer control was followed by stimulation on α-CD3/α-CD28 coated plates for three days. By gating on Foxp3

expressing cells, the contribution of nTreg and Tcon cells to this population could be monitored (**Figure 29A**). This analysis revealed that the proportion of Foxp3+ cells arising from Tcon cells significantly increased from 40% to 50% after polyP depletion by CPP-Ppx1 compared to control treatment, while the population of nTreg cells remained almost the same in both groups with approximately 40% (**Figure 29B**). These data suggest that polyP depletion induces *de novo* Foxp3 expression in stimulated CD4+ T cells rather than promoting the expansion of the nTreg cell pool.
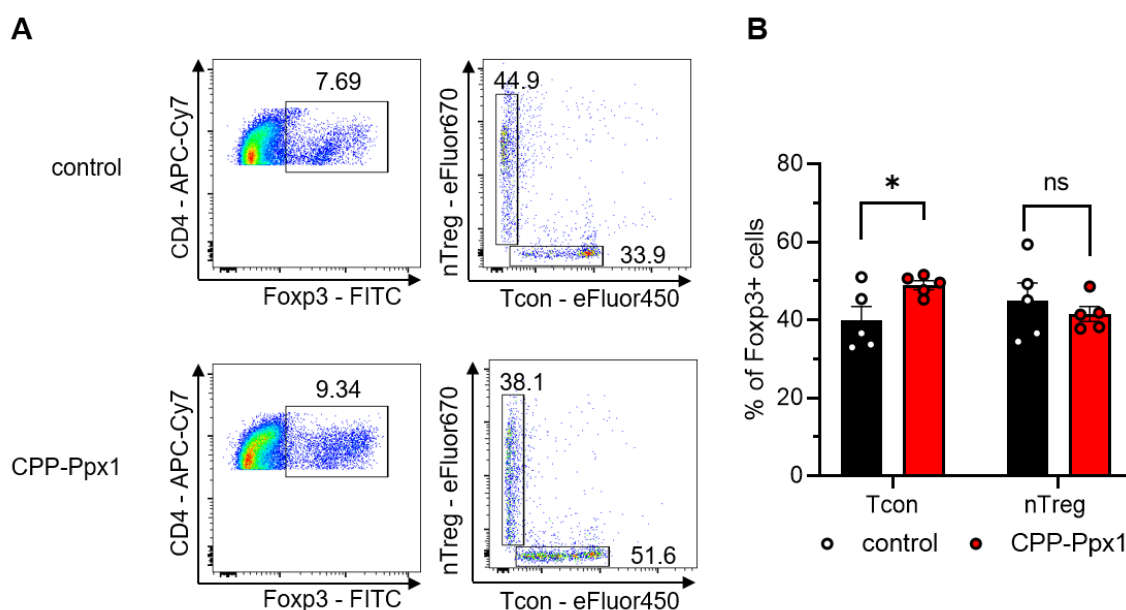
Figure 29. CPP-Ppx1 mediated polyP degradation induces *de novo* Foxp3 expression. Isolated CD4+CD25+ nTreg and CD4+CD25- conventional T (Tcon) cells were stained with eFluor670 and eFluor450 proliferation dye, respectively. Labelled population were mixed in a 1:10 ratio (Treg:Tcon), treated with CPP-Ppx1 (80 µg/mL, twice for 15 min, 37 °C) or buffer control and stimulated on α-CD3/α-CD28 (2 µg/mL / 0.5 µg/mL) coated plates for three days. (**A**) Representative flow cytometry plots of CD4+Foxp3+ T cells that were further tracked for respective origin from Tcon and nTreg population. (**B**) Statistical analysis of nTreg and Tcon cells contributing to the Foxp3+ population after CPP-Ppx1 and buffer control treatment. Gating strategy outlined in 7.2.31.2. Data represent mean ± SEM, *p*-value by paired Student's t-test, $*p < 0.05$; represented as n=5 independent experiments.

Considering that polyP degradation by CPP-Ppx1 results in the induction of Foxp3 and CTLA4 that sustain suppressive capacity in Treg cells [35, 121], we investigated the potential of CPP-Ppx1 treated CD4+ T cells to inhibit T-cell proliferation in suppression assays *in vitro*. In these experiments, the proliferation of TCR-stimulated CD4+ T cells (responder T cells) supported by APCs is analysed in the presence of variable amounts

of certain suppressor T cells to assess the potential suppressive capacity of this population.

Suppressor T-cell population were obtained from isolated CD4+ T cells that were incubated with CPP-Ppx1 or buffer control and stimulated on α-CD3/α-CD28 coated plates for three days under Th0 or iTreg cell-skewing conditions. On the third day of the stimulation, cells were then harvested and used next to freshly isolated CD4+CD25+ nTreg cells as positive control. Responder T cells were stained with proliferation dye to monitor proliferation after three days of co-culture with either nTreg cells, buffer control or CPP-Ppx1 treated Th0 and iTreg cells in 2-fold dilutions from 1:1 to 1:32 in flow cytometry. As expected, the highest concentration of freshly isolated nTreg cells suppressed the proliferation of responder T cells almost completely (**Figure 30A, G** and **H)** and dilution of the nTreg population increased the proliferation proportionally (**Figure 30A**) almost to the level of control samples without suppressor cells (**Figure 30B**). Th0 cells that were treated with buffer control did not suppress (**Figure 30C and G**), but also CPP-Ppx1 treated Th0 cells failed to inhibit the proliferation of responder T cells (**Figure 30D** and **G**). In contrast, *in vitro* differentiated iTreg cells incubated with the buffer control significantly reduced the proliferation of responder T cells in a concentration-dependent manner (**Figure 30E** and **H**). However, CPP-Ppx1 treated iTreg cells were unable to suppress the proliferation of responder T cells (**Figure 30F** and **H**). Surprisingly, both the CPP-Ppx1 treated Th0 and iTreg cells were not only unable to reduce proliferation but increased proliferation of responder T cells in comparison to controls without suppressor cells (**Figure 30B, G** and **H**).
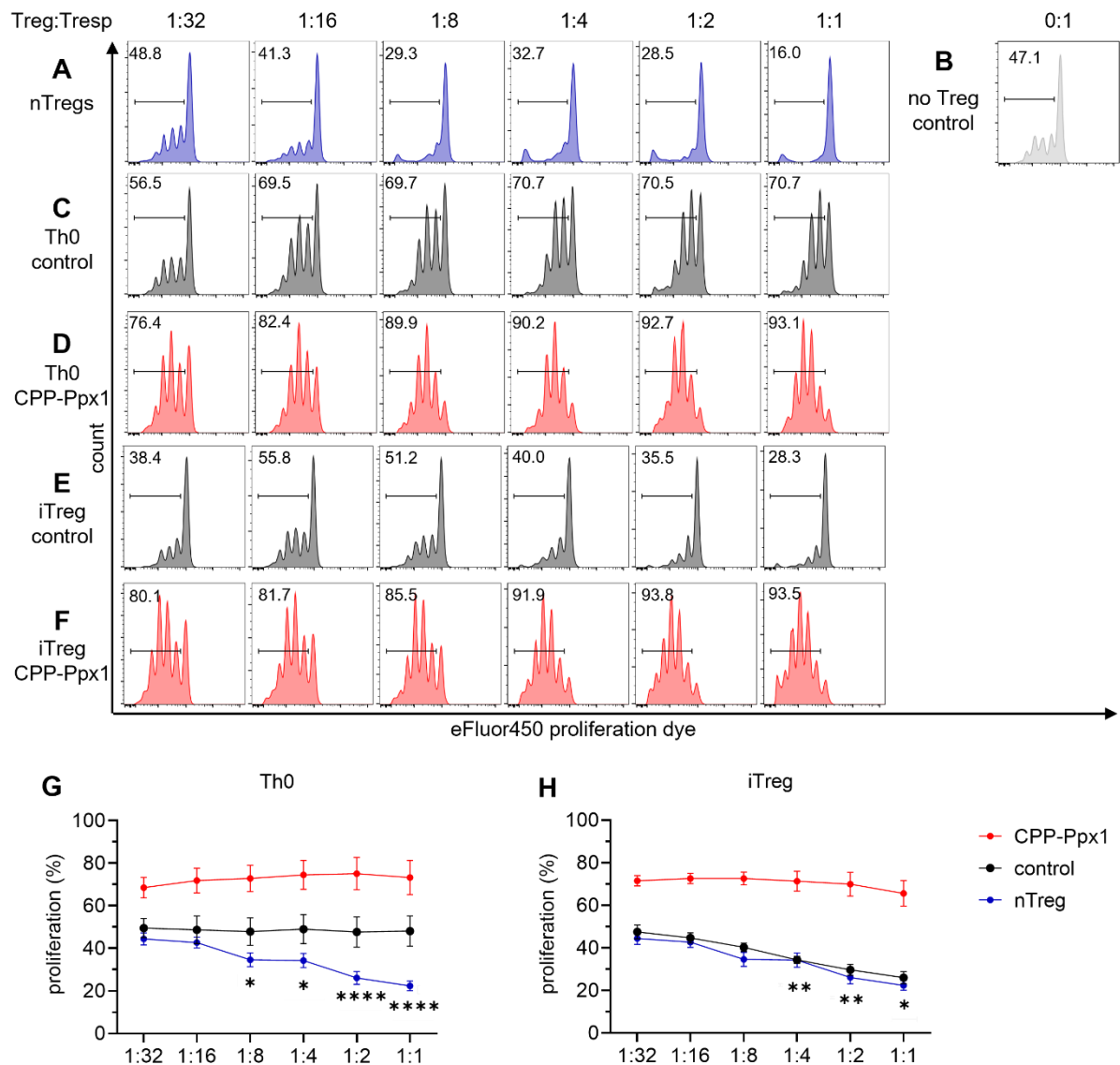
Figure 30. CPP-Ppx1 treatment of CD4+ T cells induces a non-suppressive Foxp3+ phenotype. Proliferation of responder T (Tresp) cells labelled with eFluor450 proliferation dye in the presence of irradiated APCs and soluble α-CD3 (1 µg/mL) for three days when cocultured (**A**) with or (**B**) without freshly isolated nTreg cells, with (**C**) buffer control or (**D**) CPP-Ppx1 treated Th0 cells, with (**E**) buffer control or (**F**) CPP-Ppx1 treated iTreg cells at indicated ratios. The suppressive capacity of tested populations was assessed by inhibition of eFluor450 proliferation dye dilution via flow cytometric analysis. Gating strategy provided in 7.2.31.3. (**G** and **H**) Line graphs summarising Tresp proliferation at indicated Treg/Tresp ratios from n=4 independent experiments with three technical replicates each. Data represent mean ± SEM, *p*-value by Two-way ANOVA *$p < 0.05$, **$p < 0.01$ and ****$p < 0.0001$, not statistically significant differences not indicated. Asterisks represent difference of indicated dilution of (**G**) nTreg cells and (**H**) control treated iTreg cells in comparison to respective 1:32 dilution.

To identify the reason for the lack of suppressive function we analysed the phenotype of CPP-Ppx1 or buffer control treated T cells after six days of stimulation, since these suppressor T cells were first stimulated for three days and then used in co-culture of the suppression assay for another three days. Interestingly, Foxp3 levels induced by CPP-Ppx1 treatment were not maintained, as both Th0 and *in vitro* differentiated iTreg cells treated with CPP-Ppx1 displayed similar Foxp3 expression six days after treatment in comparison to respective buffer control sample (**Figure 31A**). In contrast, IL-2 production was still significantly increased six days after CPP-Ppx1 treatment in comparison to buffer control treatment in Th0 cells (**Figure 31B**). A tendency towards higher IL-2 production in CPP-Ppx1 treated iTreg cells than in buffer control treated iTreg cells was also observed (**Figure 31B**). The transient induction of Foxp3 and the prolonged increase of IL-2 secretion could be one of the reasons why responder cells displayed an increased proliferation in co-cultures with CPP-Ppx1 treated T cells in suppression assays.
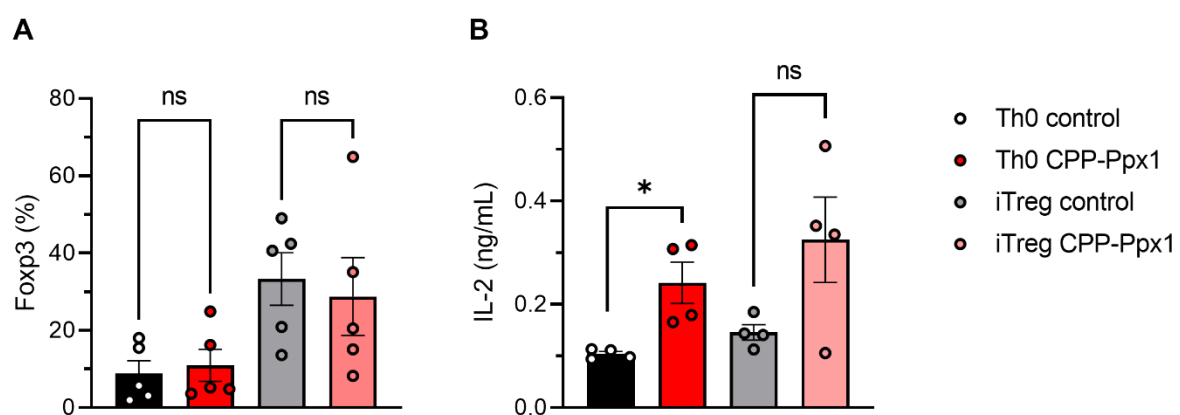
Figure 31. PolyP degradation induces unstable Foxp3 expression but sustained IL-2 production. (**A**) Expression of Foxp3 analysed by flow cytometry and (**B**) IL-2 production analysed by ELISA in supernatants of Th0 or iTreg cells treated with CPP-Ppx1 (80 µg/mL, twice for 15 min, 37 °C) or buffer control following stimulation on α-CD3/α-CD28 (2 µg/mL / 0.5 µg/mL) coated plates for three days and additional three days after medium exchange and soluble α-CD3 (1 µg/mL) supplementation to mimic conditions of the suppression assay. Data represent mean ± SEM, *p*-value by paired Student's t-test, *$p < 0.05$, represented as (**A**) n=5 and (**B**) n=4 independent experiments.

These data indicated a non-stable induction of Foxp3 by polyP degradation, which was then tested by analysis of the *Foxp3* demethylation status. Stable Foxp3 expression is characterised by demethylation of CpG islands within the *Foxp3* promotor region [58]. As before, murine CD4+ T cells were incubated with CPP-Ppx1 or buffer control and stimulated on α-CD3/α-CD28 coated plates for three days in IL-2 supplemented

medium (Th0 condition). On the third day cells were harvested, counted and snap frozen in liquid nitrogen. Samples were then sent to EpigenDx (Boston, USA) for targeted Next-generation bisulfide sequencing. The methylation status of 17 Treg-specific CpG islands including not only *Foxp3*, but also other known differentially methylated target genes (*Cd274*, *Cdkn1c*, *Ctla4*, *Ikzf2*, *Ikzf4*, *Il2*, *IL2ra*, *IL4*, *Tnf and Tnfrsf*), were analysed. The relative methylation data was normalised to the average value of the buffer control and is depicted as % methylation (**Figure 32**). Among the analysed Foxp3-regulatory genes, most CpG islands did not show any differences in methylation status between buffer or CPP-Ppx1 treated samples. However, three CpG islands of the *Ctla4* locus and both CpG islands of the *Il2* locus were significantly more methylated (**Figure 32B**). On the one hand, within the distal promotor region of the *Foxp3* locus some CpG islands had a tendency to being de-methylated (**Figure 32C**). On the other hand, within the proximal promotor region all CpG islands were significantly more methylated (**Figure 32D**). The majority of CpG islands of the intron 1 within the F*oxp3* locus also showed significantly higher methylation (**Figure 32E**).

Overall, we could not observe a demethylation of the *Foxp3* locus which indicates that polyP degradation by CPP-Ppx1 treatment induces a non-stable Foxp3 expression which results in a lack of suppressive capacity.
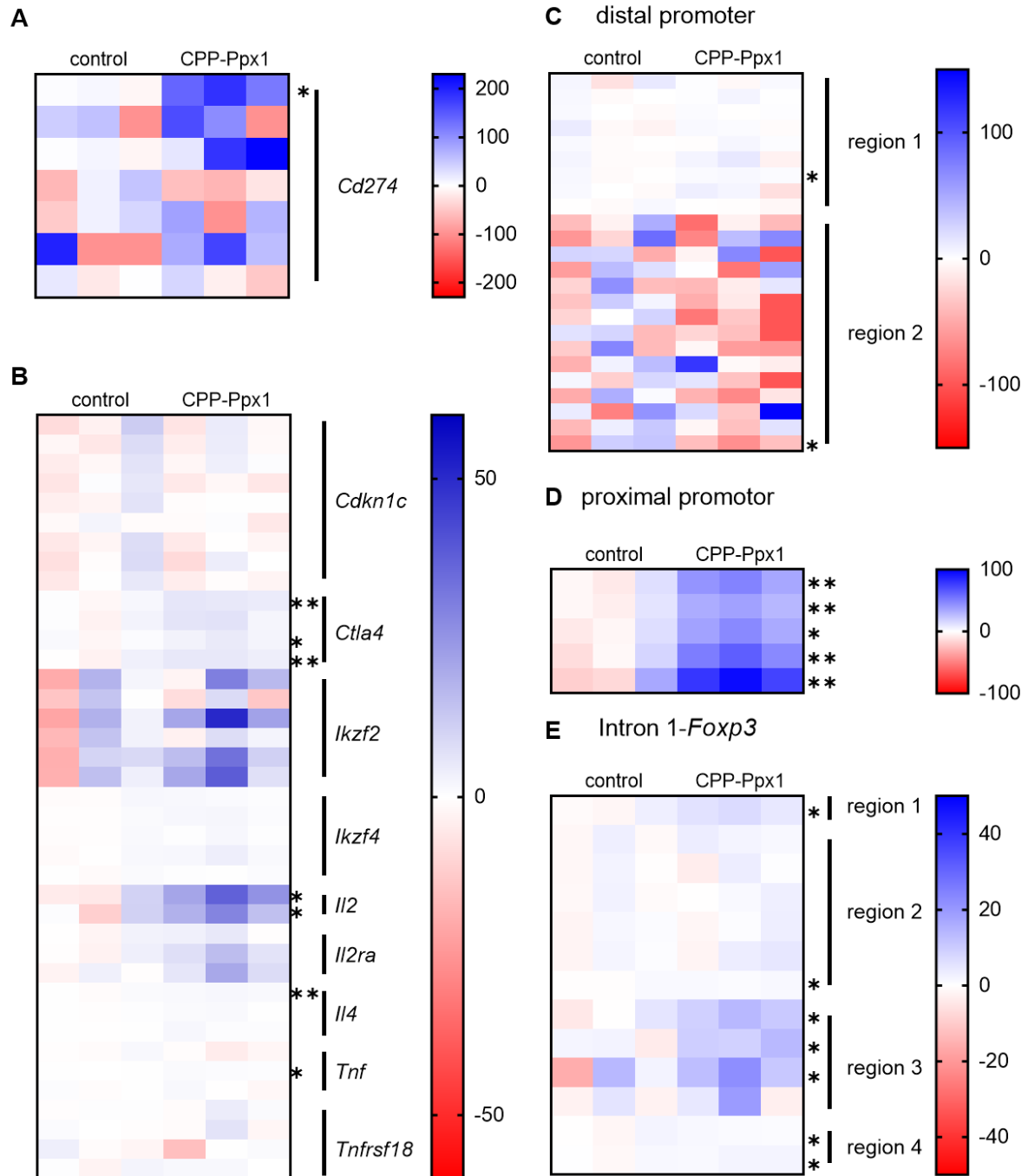
Figure 32. Targeted next-generation bisulfide sequencing of CPP-Ppx1 treated CD4+ T cells. CD4+ T cells were incubated with CPP-Ppx1 (80 µg/mL, twice for 15 min, 37 °C) or buffer control and stimulated on α-CD3/α-CD28 (2 µg/mL / 0.5 µg/mL) coated plates for three days. Targeted next-generation bisulfide sequencing was performed by EpigenDX in Boston Massachusetts, USA. Heatmaps represent methylation status relative to mean methylation of control samples for CpG islands of (**A**) *Cd274*, (**B**) *Cdkn1c*, *Ctla4*, *Ikzf2*, *Ikzf4*, *Il2*, *Il2ra*, *Il4*, *Tnf*,*Tnfrsf18*, (**C**) the distal *Foxp3* promotor (**D**) the proximal *Foxp3* promotor and (**E**) the *Foxp3* Intron 1. *p*-value by Student's t-test, *p < 0.05, **p < 0.01, represented as n=3 independent experiments.

5 Discussion

5.1 The role of polyP in immunity

PolyP is an ancient polymer that has been identified in every mammalian cell type, analysed to date [91], but its function remained elusive for a long time and is still poorly understood today [108]. In mammalian cells, little is known about the synthesis or degradation of this polymer, preventing strategies to target polyP by genetic modifications of endogenous enzymes. Recently, research interest into polyP functions has been intensified. In 2004 Ruiz *et al.* discovered that platelets store polyP in dense granules [113]. In a further study, polyP derived from platelets was shown to play an important role in the activation of the kallikrein-kinin system, whereby the first link of polyP to inflammation was found [122]. Platelet-released polyP was shown to activate coagulation factor XII (FXII) that proteolytically activates plasma kallikrein, which in turn cleaves high molecular weight kininogen to liberate bradykinin. The study also showed an increase in vasculature leakage upon intravenous polyP injection and even demonstrated that polyP administration leads to pulmonary embolism in mice due to activation of FXII and subsequently the kallikrein-kinin system in blood [122].

Here, we aimed to characterise polyP in CD4+ T-cell subsets and identify its role in T-cell responses. Both pro- and anti-inflammatory effects of polyP have been discovered for various tissues, albeit limited to signalling events elicited by extracellular polyP. In vasculature, polyP was found to promote pro-inflammatory effects by signalling through P2Y receptor and receptor for advanced glycation endproducts. As a consequence, adhesion molecules, such as E-selectin, vascular adhesion molecule-1 and intracellular adhesion molecule were found to be upregulated in an NFκB-dependent manner that allows for a better adhesion of leukocytes to the endothelium. [109, 110]. *In vivo* studies revealed that the secreted polyP has chemoattractive functions on neutrophils [123]. Neutrophils are part of the innate immune system and play an important role in the clearance of bacterial and fungal infections mainly through phagocytosis [124]. However, neutrophils also release pro-inflammatory cytokines and condensed DNA to form neutrophil extracellular traps [125]. These processes are supported by the interaction with platelets and largely facilitated by platelet-derived polyP release [126, 127].

Several studies showed that the addition of synthetic or bacterial-derived polyP affects the production of cytokines. On the one hand, addition of polyP to peripheral blood mononuclear cells produced more pro-inflammatory cytokines *in vitro* [128], on the other hand, uptake of bacterial polyP by macrophages reduced the type 1 interferon response [129]. Contrary to the latter observation, the treatment of macrophages with polyP and LPS was reported to induce IL-6, TNFα and IL-1β production in another study [130].

Also, anti-inflammatory functions of extracellular polyP have been discussed, predominantly in a pro-biotic context. Segawa *et al.* showed that probiotic bacteria secrete polyP which interacts through integrin β1 and β3 with enterocytes to inhibit the production of TNFα [131]. Contrary to the increased vascular leakage upon polyP treatment, as mentioned above [122], polyP lowered the mucosal permeability of *ex vivo* intestinal loops. In a dextran sulphate sodium-induced colitis model, mice treated with intrarectal application of polyP did not show a significant shrinkage of the colon or production of pro-inflammatory cytokines [131, 132].

While current studies show discrepancies in pro- and anti-inflammatory effects attributed to synthetic, bacterial or platelet-derived polyP in extracellular space, investigations of intracellular polyP functions for immune cell responses are lacking. We therefore analysed polyP endogenously produced and intracellularly stored in CD4+ T cells and were able to show that T-cell stimulation accumulates polyP both in a time- and concentration-dependent manner (**Figure 5**). PolyP has been found in dense granules and acidocalcisomes in platelets and mast cells, respectively [113, 133]. Nevertheless, we were unable to find equivalent membrane vesicles with polyP in stimulated murine CD4+ T cells via TEM (**Figure 6**). Cell fractionation experiments revealed that polyP is mainly present in the cytosol (**Figure 6**), suggesting that molecular mobility within the matrix may prevent TEM analysis of polyP. Noteworthy, electron dense structures were reported in autolysosomes of stimulated human CD4+ T cells [134], indicating that detection of polyP-rich structures may also depend on TEM sample preparation. However, also EDX analysis could not detect specific phosphorus-rich regions (data not shown). Thus, the subcellular localisation of accumulated polyP in the cytosol of stimulated CD4+ T cells, but not its molecular localisation could be resolved.

Importantly, we showed that T-cell subsets acquire different polyP levels (**Figure 9A** and **B**). *In vitro* differentiated pro-inflammatory T cells, e.g. Th17 cells and to some extent Th1 and Th2 cells, store more polyP in comparison to anti-inflammatory Treg cells. This could be validated in experiments using varying concentrations of TGF-β during the differentiation of iTreg cells. While a dose-dependent decrease of polyP accumulation was shown for TGF-β, the Th17-skewing cytokines IL-6 and IL-23 had a moderately positive and no effect on polyP levels, respectively (**Figure 9C** and **D**). Since we used R&D's CellXVivo Mouse Th17 Cell Differentiation Kit with proprietary cytokine combination for *in vitro* differentiation of Th17 cells, it might be possible that the cytokine concentrations differed in each experimental condition, necessitating the testing of even higher concentrations in order to identify an optimum for polyP accumulation.

Unfortunately, little is known about the mechanism of polyP accumulation in mammalian cells. While some assume that the F_0F_1 ATPase of the respiratory chain may be able to both hydrolyse and synthesise polyP [97], no specific polyP kinases have been identified so far. However, it is widely recognised that the accumulation of polyP is tightly linked to the metabolic status of a cell. For one, bacteria acquire polyP in a state of stress [92]; for another, mitochondrial polyP depletion leads to a decrease in mitochondrial membrane potential, followed by a reduced OXPHOS [102, 103, 135]. During T-cell activation, the activity of metabolic pathways is upregulated to meet the energy demands for expansion, proliferation and differentiation. It is therefore feasible that the stimulation-dependent accumulation of T-cell polyP (**Figure 5**) is related to this increased metabolic status**.** We could further show that in CD4+ T cells, polyP accumulation is sensitive to glycolysis inhibition (**Figure 7**), while blockade of the F_0F_1 ATPase with oligomycin or uncoupling of the electron chain did not impair the accumulation of polyP. From this, we conclude that CD4+ T cells synthesise polyP independent of the F_0F_1 ATPase but rely on glycolysis instead. However, it might also be the case that polyP is actively consumed as an energy storage molecule to produce ATP when glycolysis is inhibited, as Boyineni *et al.* proposed for tumour cells [95].

The differentiation of T cells is accompanied by a pronounced metabolic shift that is in part determined by cytokine signalling. While pro-inflammatory T cells shift their metabolism to aerobic fermentation, anti-inflammatory T cells utilise fatty acid oxidisation and oxidative phosphorylation for energy production [65, 70]. Our data

indicate that the cytokine environment leads to an accumulation of polyP in pro-inflammatory T cells by metabolic pathways, extending on previous findings that polyP exerts pro-inflammatory functions.

5.1.1 Methods for polyP detection

During all our experiments, we need to take into account that the methods for polyP detection remain challenging due to its structural similarity to other negatively charged biopolymers [111]. The most commonly used methods for polyP isolation are phenol-chloroform extraction and the retention of polyP on silica membranes [111]. Especially in regard to the chain lengths of purified polyP these methods differ greatly. A broad range of polyP chain lengths can be isolated with phenol-chloroform extraction, while only long chain polyP is retained on silica membranes [136]. We therefore used a method of polyP isolation based on phenol-chloroform extraction, which is analogous to the commonly used method for the isolation of nucleic acids from cell lysates. To avoid the co-isolation of nucleic acids, a wide variety of enzymatic digestions with DNases, RNases and proteinase K have been implemented [136]. In our protocol we use the QIAprep DNA extraction Kit for ablation of DNA and proteins. In a first step, proteins are precipitated and separated by centrifugation. Next, the supernatant is applied to a DNA extraction column, in which a silica membrane retains DNA, whereas the flow-through contains polyP, which is further isolated by phenol-chloroform extraction and precipitation.

As demonstrated in **Figure 4** our protocol successfully extracted polyP from T cells. Isolated DNA or RNA produced a white smear on urea PAGE, in contrast to the synthetic polyP standard and isolated T-cell polyP that was detected as a black smear in negative DAPI stainings. Nonetheless, some residual white staining remained in samples with isolated polyP, which might result from DNA or RNA contaminations in this specific experiment due to an exceeded binding capacity of the DNA extractions column (20 ng DNA as specified by the manufacturer). Furthermore, we observed that isolated T-cell polyP sometimes resulted in a continuous black smear (e.g. **Figure 7**, **Figure 9B**) or a banded pattern (e.g. **Figure 5A** and **B** and **Figure 11C**) in negative DAPI stainings. This could be due to the tertiary structures of polyP or associated proteins that impact the mobility of polyP in urea gels, but the reason for the different appearance is unknown.

Notably, we used different protocols for the analysis of T-cell polyP in urea PAGE and malachite green assays but obtained comparable results for polyP levels, in *in vitro* differentiated CD4+ T-cell subsets with both methods (**Figure 9A** and **B**). The latter protocol, modified from the method described by Christ and Blank [137], had the advantage that polyP was not precipitated but remained in solution after phenol-chloroform extraction.

Overall, we think that our methods for polyP extraction resulted in reproducible and valid information about the accumulation and distribution of polyP in CD4+ T cells, even though different techniques may have an effect on the prevalent polyP chain length distributions.

5.2 Protein transduction of CPP-Ppx1 into CD4+ T cells

To modify the polyP content in CD4+ T cells we applied recombinant Ppx1 fused to a cell-penetrating peptide tandem repeat (**Figure 10**). This approach allowed the exogenous expression of an intracellular enzyme without compromising the viability of the targeted CD4+ T cells (**Figure 13**).

The generation of CPP-Ppx1 presented us with some obstacles. For one, transformed DH5α *E. coli* appeared to express a reduced amount of CPP-Ppx1 which was stored in inclusion bodies, suggesting that polyP degradation by overexpression of CPP-Ppx1 is detrimental for bacteria. For another, the yield of protein was relatively low using standard affinity chromatography protocols, which could be improved with the addition of the chaotropic agent urea. On top of that the utilisation of CPP-Ppx1 in cell culture was challenging, as the storage buffer had to prevent precipitation and simultaneously be well tolerated by T cells. We managed to keep CPP-Ppx1 in solution and enable a long-term storage at -80°C in a buffer containing 300 mM NaCl, 50 mM TRIS and 10% glycerol. Since this buffer changes the osmotic pressure in cell-culture greatly, we included buffer treated samples as a control in every experiment and exchanged the medium after every 15 min incubation step with CPP-Ppx1.

It is likely that the yield of recombinant CPP-Ppx1 purification can still be optimised, as only approximately 3 mg protein were typically obtained from 500 mL of bacterial culture. The current setup uses competent DH5α *E. coli* transformed with constructs of the pTrcHisB vector that is optimised not only for plasmid production, but also for

expression of the recombinant proteins in DH5α *E. coli*. To increase the yield, we tried an alternative expression system with BL21 Star *E. coli*, designed specifically for the high-yield production of non-toxic recombinant proteins. However, the yield in CPP-Ppx1 production did not improve (data not shown). Optimisation of the expression systems prospectively could start with a redesign of the vector. The addition of tags with solubilising properties, like MBP or different promoter systems could be used to reduce the formation of inclusion bodies (e.g. *cspA*), or even enable a secretion of the protein to the culture medium (e.g. *PhoA*) [138]. Changes in the expression system might also be beneficial in regard to the notion that a bacterial system is reliant on polyP for its metabolism and growth and will show a reduced survival in the stationary phase when polyP cannot be accumulated due to its degradation by CPP-Ppx1 [139]. As an alternative, insect or mammalian cells could be used for the overexpression of CPP-Ppx1, though the culture is more complex, takes a longer time and is more costly, which is why a secreting promotor system in *E. coli* might be most suitable.

Taken together, many different strategies to optimise the protein production can be taken into consideration, to use CPP-Ppx1 in future large-scale experiments. For our protein transduction into primary CD4+ T cells however, a sufficient yield of recombinant CPP-Ppx1 could be obtained for the performance of cell culture experiments.

CPP-Ppx1 is a fusion protein designed from yeast Ppx1 and a cell-penetrating peptide sequence, enabling the transfer of the enzyme through plasma membranes of target cells. CPPs are a wide class of peptides with a plethora of different characteristics. Classification into specific groups is therefore a challenging task and has been tried with many different attributes like physicochemical structure, mode of entry or structural characteristics [140]. This classification is no less complex considering that the cargo carried by CPPs [141] and the concentration of the peptide [142] affect the mode of entry. CPPs are hypothesised to enter the cell in two distinctive pathways, either via direct translocation (through pore formation, charge or inverted micelles) or via endocytic pathways like clathrin or calveolin dependent endocytosis or micropinocytosis [140]. The CPP sequence that we used is derived from the human transcription factor HPH-1 (YARVRRRGPRRG). Due to this arginine-rich structure we assume a similar mode of action like other arginine-rich CPPs, such as Tat, which facilitates an endocytic mode of entry [141]. This is supported by data from fractionation

experiments (**Figure 12**), in which CPP-Ppx1 could be detected in the membrane and cytoskeletal fraction of target cells. In line with this, Futaki *et al.* proposed that arginine-rich CPPs interact with proteoglycans on the cell surface and evoke an actin-remodelling to form lamellipodia for pinocytotic uptake [143]. Thus, it could be possible to analyse the mode of entry and CPP-Ppx1 distribution in target cells in further studies using fluorescent microscopy or live cell imaging, although laser illumination and fixation might change the localisation of CPPs, as previously reported [144, 145].

5.3 Activation of CD4+ T cells through polyP depletion

In our experiments we could show that the digestion of polyP in CD4+ T cells leads to a mobilisation of Ca^{2+} even above the levels obtained with the Ca^{2+} ionophore ionomycin and also prevents the return to baseline Ca^{2+} levels (**Figure 15**). Ca^{2+} signalling is a key process in the activation of T cells in the wake of TCR stimulation [5], with several downstream signalling pathways depending on elevated intracellular Ca^{2+} concentrations [146]. Hereby, both the initial spike and the subsequent plateau of the Ca^{2+} level bears information for downstream signals in T-cell stimulation [118]. Our results indicate not only a higher spike in Ca^{2+} mobilisation, but also a higher Ca^{2+} plateau, which implicates polyP as a negative regulator for Ca^{2+} signalling.

The duration of Ca^{2+} signals is controlled by active export of Ca^{2+} into the extracellular space by Ca^{2+} pumps in the plasma membrane and the sarcoplasmic reticulum Ca^{2+}-ATPase that pumps Ca^{2+} into the ER. In addition, the storage of Ca^{2+} within mitochondria has been recognised as another pathway for Ca^{2+} clearance [118, 146]. Multiple Ca^{2+} sensitive carriers and uniporters transport Ca^{2+} into mitochondria to match the demand for mitochondrial metabolism upon stimulation [147], and secondly to buffer increasing concentrations of Ca^{2+}, which will then be slowly released back into the cytosol [148]. Notably, mitochondria rely on phosphate for this buffering capacity as Chalmers and Nicholls were able to show that phosphate depleted mitochondria were unable to maintain a Ca^{2+} uptake [149]. A role of polyP for the buffering of Ca^{2+} has also been reported, as mitochondrial depletion of polyP leads to a reduction of free Ca^{2+} within the mitochondria [150].

In respect of these studies in mitochondria and our findings in CD4+ T cells, we propose that polyP is accumulated in stimulated CD4+ T cells as a buffering agent for cytosolic free Ca^{2+} and that polyP digestion by CPP-Ppx1, releases polyP-bound Ca^{2+}. Fractionation experiments showed that CPP-Ppx1 does not seem to localise preferentially to mitochondria, but from the analysis of the fractionation purity we cannot exclude the transfer of CPP-Ppx1 to mitochondria either (**Figure 12**). Further studies will need to pinpoint CPP-Ppx1 localisation and the subcellular hotspot for polyP degradation, as already mentioned above. Assuming, however, that CPP-Ppx1 could enter mitochondria and exert comparable effects like the MitoPPX system (overexpression of mitochondrial-targeted Ppx1 in a human embryonic kidney cell line by Solesio *et al.* [151]), the elevated Ca^{2+} plateau in T cells observed after the initial spike of free Ca^{2+} could be explained with reduced Ca^{2+} clearance from cytosol to mitochondria due to an imbalanced buffering capacity within the mitochondria.

Considering that CPPs may disrupt the membrane integrity, we included ionomycin as a control to assess the contribution of extracellular Ca^{2+} influx to our signal in Ca^{2+} mobilisation experiments. In comparison to ionomycin, CPP-Ppx1 treatment resulted in higher Ca^{2+} levels, suggesting that no less than the observed surplus of free Ca^{2+} originates from polyP digestion. Although arginine-rich CPPs have previously been reported not to affect Ca^{2+} flux through endocytosis in Jurkat cells [152], addition of a Tat-Cre fusion protein led to intracellular Ca^{2+} concentrations comparable to ionomycin treatment (data not shown), indicating that the elevated and prolonged Ca^{2+} signal upon CPP-Ppx1 treatment is not caused by the CPP-mediated protein transduction but the degradation and Ca^{2+} release of polyP.

As mentioned above, Ca^{2+} mobilisation is a strong activation signal for the cell. PolyP degradation and liberation of bound Ca^{2+} is therefore to be expected to activate downstream signalling pathways like the ERK pathway that results in enhanced expression of CD69 and IL-2 production [153]. We found a tendency towards higher ERK phosphorylation in CD4+ T cells treated with CPP-Ppx1 compared to buffer controls (**Figure 16**). Consistently, T-cell stimulation after CPP-Ppx1 treatment increased the expression of activation markers CD69 and CD25 (**Figure 17**) and IL-2 (**Figure 18**) significantly above buffer control levels. CD4+ T cells with reduced polyP levels also proliferated more (**Figure 19**), supporting the findings by Suess *et al.* who described that *Dictyostelium discoideum* was inhibited in its growth by polyP [154].

Overall, these findings support the notion that polyP is accumulated upon stimulation to bind free cytosolic Ca^{2+} and to act as a further mechanism to terminate Ca^{2+}-mediated activation processes.

To further investigate the role of intracellular polyP for Ca^{2+} neutralisation, follow-up studies that include cell-penetrating PpxΔ12 that protects polyP from degradation [155] or cell-penetrating Ppk that enforces polyP synthesis could be suitable to observe an opposing effect in the future. Also, different cell types and other unrelated CPP-enzymes in addition to our buffer control and denatured CPP-Ppx1 treatment, which might penetrate the cell but is degraded rapidly (**Figure 12**), could be envisioned.

The digestion of polyP in mitochondria has not only been shown to affect the amount of Ca^{2+} stored within the mitochondrial matrix, but also to affect the mitochondrial membrane potential [135]. The function of complex IV of the respiratory chain was impaired upon polyP depletion [135] which lead to a shift from OXPHOS to glycolysis accompanied by a decrease in ATP production [102]. In line with this, we discovered increased Glut1 expression in polyP-deprived CD4+ T cells (**Figure 20C**), and slightly increased Hk2 levels (**Figure 20D**). Contrary to findings from overexpression experiments with mitochondria-targeted Ppx1 in human embryonic kidney cells [102], we show that polyP reduction by CPP-Ppx1 treatment increased overall ATP production in primary mouse T cells. Also, rather than shifting the metabolism from OXPHOS to glycolysis, an increase in both metabolic pathways could be observed (**Figure 21**). Furthermore, polyP-deprived CD4+ T cells also had a tendency towards a higher spare respiratory capacity (**Figure 22**). In line with the increased expression of activation markers, the heightened T-cell activation status was therefore validated again in these metabolic analyses, indicating that polyP digestion upregulates the metabolic activity and increases ATP production in CD4+ T cells.

Increased OXPHOS is accompanied by enhanced ROS production due to a proton leak of complexes I-III in the respiratory chain [64]. ROS can cause DNA damage and protein misfolding, but are also an important second messenger for T-cell activation [74, 156]. In bacteria, oxidative stress leads to increased polyP levels. This is thought to be due to: 1) PolyP preventing the aggregation of misfolded proteins through chaperone-like functions, 2) polyP binding Mn^{2+} which is needed in bacteria as a scavenging agent for ROS, and 3) polyP preventing the production of hydroxyl radicals [157, 158]. In a study by Hambardikar *et al.*, polyP reduction in mitochondria led to

dysregulation of OXPHOS and an accumulation of per- and superoxides [101]. While all these publications propose a protective function of polyP Samper-Martín *et al.* showed that oxidative stress in human embryonic kidney cells increases Zn^{2+} levels which activate the polyphosphatase Nudt3. They further suggest that polyP is digested in order to provide energy for the DNA repair machinery, as a phosphate source for the production of new dNTPs, and to release polyP-bound proteins which are needed for DNA repair [100]. Our experiments showed that the ROS and superoxide levels of CPP-Ppx1 treated samples were significantly reduced (**Figure 23**), while we observed no differences in the mitochondrial mass or function (**Figure 24**). This supports the notion that polyP indeed binds other metal ions or other ROS scavenging agents that protect the cell from damage. Those agents might be released upon polyP digestion and reduce the ROS burden of the cell.

ROS as a second messenger also impacts the stimulation and differentiation of T cells. Production of ROS increases rapidly after TCR stimulation as a response to Ca^{2+} influx to the mitochondria [73]. On the one hand, treatment of T cells with antioxidants inhibited the proliferation and activation [75]. On the other hand, deficiency in the ROS producing enzyme NADPH oxidase promoted Th1 and Th17 cells, while Treg cells lost their suppressive capacity [159-161]. These findings were supported by the study of Efimova *et al.* who showed a loss of Treg suppressive capacity upon treatment with antioxidants or NADPH oxidase inhibitors [162]. Moreover, iTreg cells were shown to have lower basal levels of ROS in general [163], supposedly due to an increased amount of glutathione as a cell intrinsic antioxidant. Accordingly, the inhibition of glutathione production reduced the suppressive capacity of Treg cells, but increased their activation status and metabolic activity [163]. In our study the degradation of polyP by CPP-Ppx1 treatment resulted in a T-cell phenotype characterised by increased IL-2 expression and reduced ROS production, in opposition to a publication from Kaminski *et al.*, in which they found thar ROS is required for IL-2 production [164]. However, in respect to the characterisation of iTreg cells as a population with reduced ROS production we found several Treg-associated genes that were differentially expressed in ATAC-seq. experiments upon CPP-Ppx1 treatment (Appendix 9.1, Table 7). Although ATAC-seq. data did not reach statistical significance for group analysis due to a relative similarity and the limited number of samples, gene ontology analysis and evaluation of the top 1000 DARs confirmed that polyP reduction has an impact on CD4+ T-cell activation and differentiation (**Figure 25C**). Moreover, the induction of a

Treg-like phenotype in response to CPP-Ppx1 treatment could be demonstrated by the enhanced accessibility of the *Ctla4* promotor (**Figure 27**). Consistently, flow cytometry analysis confirmed an increased expression of CTLA4 both intra- and extracellularly in CPP-Ppx1 treated CD4+ T cells compared to buffer controls within 16 hours. The skewing towards a Treg-like phenotype after CPP-Ppx1 treatment persisted also in differentiation assays for three days *in vitro*, in which we revealed an increased expression of Foxp3 in Th0 and iTreg cells (**Figure 28**). In contrast, CPP-Ppx1 treatment showed no significant inhibition of the cytokine production for *in vitro* differentiated Th1, Th2 or Th17 cells (**Figure 26**), suggesting that polyP degradation rather enforces CD4+ T-cell activation than induction of a stable T-cell subset.

5.4 Development of a non-suppressive Foxp3+ phenotype in CD4+ T cells through polyP depletion

Induced expression of Foxp3 was validated in another experiment that aimed to identify whether polyP degradation expands the pool of Foxp3+ nTreg cells or results in *de novo* Foxp3 expression in Tcon cells (**Figure 29**). We found that CPP-Ppx1 treatment induced *de novo* Foxp3 production in murine CD4+ T cells. In humans, the distinction between Treg cells and activated Tcon cells is less clear, because FOXP3 and CTLA4 are transiently expressed as markers of T-cell activation independent of a suppressive function [31, 165]. Indeed, Miyara *et al.* characterised three types of FOXP3+ T cells: 1) resting Treg cells (FOXP3^{lo} CD45RA$^+$) 2) activated Treg cells (FOXP3^{hi} CD45RA$^-$) and 3) non-Treg cells (FOXP3^{lo} CD45RA$^-$) [166]. However, a population of non-suppressive Foxp3+ T cells has not yet been described in mouse, where Foxp3 expression is sufficient to confer suppressive activity and remains to be a definite marker for Treg cells [27, 28, 33]. Therefore, it seems unlikely that Foxp3 and CTLA4 expression just illustrates the heightened activation status in polyP-deprived murine CD4+ T cells. To investigate this further, we performed suppression assays with CD4+ T cells that express Foxp3 after CPP-Ppx1 treatment as suppressor cells. We surprisingly found that responder T cells proliferated not less but more upon CPP-Ppx1 treated T cells (**Figure 30**), suggesting that the suppressive capacity conferred by Foxp3 and CTLA4 induction has been compensated for. To delineate why CPP-Ppx1 treated T cells fail to suppress, we reanalysed the phenotype at a later time point. We

found that the Foxp3 expression induced by polyP degradation is unstable and that Foxp3 expression decreased after six days, whereas the elevated production of IL-2 was sustained (**Figure 31**). This loss in Foxp3 expression over time might be the reason for the lack in suppressive capacity of polyP-deprived T cells, while their increased production of IL-2 could explain the increased proliferation of responder T cells. In line with this, next-generation bisulfide sequencing revealed that polyP reduction by CPP-Ppx1 treatment does not lead to a *bona fide* demethylation status of the Foxp3 locus that is characteristic for Treg cells [55, 167]. While some regions in the distal Foxp3 promotor had a tendency towards demethylation, all CpG regions of the proximal promotor were more methylated in CPP-Ppx1 treated CD4+ T cells compared to controls (**Figure 32 C** and **D**). Since demethylation of these regions has been shown to be important for the stability of Foxp3 expression in Treg cells and their suppressive capacity [56], polyP degradation by CPP-Ppx1 induces Foxp3 transiently without epigenetic determination and does not confer suppressive capacity in CD4+ T cells.

The observed Treg-like phenotype in polyP-deprived murine CD4+ T cells is reminiscent of non-Treg cells (FOXP3^{lo} CD45RA$^-$) described in humans [166]. These FOXP3+ T cells have been identified as cytokine secreting cells, since IL-2 and IFNγ production was found to be increased. Accordingly, in suppression assays the non-Treg population rather enhanced than inhibited the proliferation of responder T cells [166]. A similar Treg-cell population was found in mice with an overexpression of Glut1 [70]. Gerriets *et al.* identified Treg cells with a reduced ROS level, increased ECAR and OCR, reduced Foxp3 expression and suppressive capacity [70]. These studies display phenotype and function that correspond well with our non-suppressive Foxp3+ T cells induced by polyP degradation. No physiological role for non-suppressive T cells has been reported yet, but Miyara *et al.* proposed that these cells may be derived from a RORγt+-FOXP3+ double positive population [166]. Although not evident in Th17 differentiation assays *in vitro* (**Figure 26**), further studies to assess the plasticity of CPP-Ppx1 treated CD4+ T cells will elucidate whether the lack of suppressive capacity correlates with a skewing towards a pro-inflammatory T-cell subsets upon polyP digestion. Since many autoimmune diseases display a lack of suppressive function in Treg cells, accompanied by an increased production of pro-inflammatory cytokines [83, 168, 169], the role of CPP-Ppx1 treated Foxp3+ T cells should also be analysed in autoimmune disease models *in vivo*.

Taken together, we discovered that murine CD4+ T cells accumulate polyP upon stimulation in a glycolysis-dependent manner. Moreover, the differentiation into specific CD4+ T-cell subsets affects T-cell polyP levels, indicating that polyP plays a role in pro-inflammatory CD4+ T cells. We revealed that polyP accumulation acts as a sink for intracellular Ca^{2+} in stimulated CD4+ T cells and that polyP degradation releases Ca^{2+} which triggers the activation of CD4+ T cells evident by enhanced production of CD25, CD69, IL-2 and a higher proliferative capacity. Furthermore, CD4+ T cells respond to the polyP reduction with an increased ATP production, fuelled by both increased glycolysis and OXPHOS but a significant reduction in oxidative stress and superoxide production. As indicated by ATAC-seq. data, decreased polyP levels led to an activated Treg-like profile that was confirmed in ELISA, flow cytometry and immunoblot analyses. The induced expression of Foxp3 and CTLA4, however, did not enable polyP-deprived T cells to suppress lymphoproliferation. Thus, polyP plays an important role in the stimulation and differentiation of CD4+ T cells and presents a potential target to modulate CD4+ T-cell responses.

6 Outlook

The presented work is the first study that investigates polyP in CD4+ T cells and describes the role of polyP for T-cell differentiation and function through the modulation of intracellular polyP. The results show that polyP degradation triggers calcium-dependant activation and induces a non-suppressive Treg-like phenotype. Further experiments will have to elucidate the long-term effect of T cells with reduced polyP levels in *in vivo* experiments. For this, the adoptive transfer of CPP-Ppx1 treated CD4+ T cells in lymphopenic recipients is particularly suitable in a T-cell transfer colitis model. In humans, ulcerative colitis is an (auto-)immune disorder of the gastrointestinal tract with an accumulation of highly activated and phenotypically different CD4+ T cells in the inflamed mucosa [86], that include FOXP3+ T cells that are not capable to prevent tissue destruction *in situ* [170, 171]. In light of our presented results, a colitis model appears therefore promising to test insufficient immune regulation coupled with an altered pro-inflammatory capacity of CD4+ T cells with CPP-Ppx1 mediated polyP degradation *in vivo.*

Inflammatory processes in ulcerative colitis patients can be studied in a T-cell transfer colitis model in *Rag2* knockout mice, in which the homeostatic expansion of non-Treg cells (CD4+CD45RB^{high}) leads to a pathogenic immune reaction against commensals. Colitis induction is then monitored in the absence or presence of co-transfer Treg cells that prevent disease severity in relation to their immunosuppressive function [172]. Since CPP-Ppx1 treated CD4+ T cells are non-suppressive *in vivo* despite induction of Foxp3, which remains a definite marker for suppressive capacity in murine T cells, these experiments could elucidate the differentiation and pro- or anti-inflammatory functions of polyP-deprived T cells *in vivo.*

Plasticity of human CD4+ T-cell subsets can be observed in many autoimmune diseases [76, 169, 173]. *In vivo* mouse models would therefore also be beneficial to study the stability of the phenotype of CPP-Ppx1 treated CD4+ T cells and to determine pro-inflammatory cytokine production after T-cell stimulation by distinct self-antigens in different autoimmune diseases. Although an impaired response in autoimmunity is very well described, strategies to prevent tissue damage through the modification of metabolism, differentiation, proliferation and functional activity of CD4+ T cells is limited. Our findings suggest that T-cell polyP has implications in these processes and is therefore a potential target for further investigations in disease models.

In addition to intracellular polyP, the possible secretion of T-cell polyP to activate pro-thrombotic pathways in the extracellular space is another research focus, which demands further investigations. As thrombotic diseases are a common co-morbidity in autoimmune diseases, pro-inflammatory T-cell subsets may contribute to blood coagulation through the release of pro-coagulant polyP. In this respect, the analysis of polyP metabolism by endogenous enzymes, the release of polyP by stimulated CD4+ T cells and the subsequent activation of thrombin-mediated pathways for intra- and intercellular interactions represent important questions that remain to be answered in the future.

7 Material and Methods

7.1 <u>Materials</u>

7.1.1 Animals

Strain	Reference
C57BL/6J	Jax stock #000664
Marilyn mice	EMMA Strain #EM:00133

7.1.2 Antibodies used in flow cytometry

Antibody	Fluorophore	Supplier	Catalog #	Dilution
Foxp3	AF 488	invitrogen	53-5773-82	1:100
Foxp3	APC	invitrogen	1936921	1:100
IL-4	APC	BioLegend Inc.	504106	1:20
CD44	APC	BioLegend Inc.	103012	1:100
CD4	Biotin	BioLegend Inc.	100404	1:40
Rorγt	BV421	BD Pharminogen	562894	1:100
CD25	BV421	BioLegend Inc.	102043	1:160
TNFα	BV421	BioLegend Inc.	506327	1:20
Gata3	BV421	BioLegend Inc.	653814	1:20
IFNγ	BV421	BioLegend Inc.	505830	1:200
IL-17A	FITC	Miltenyi Biotec	130-102-262	1:10
CD25	FITC	eBioScience	11-0251-81	1:10
IFNγ	PE	invitrogen	12-7311-82	1:80
CD4	PE	BioLegend Inc.	100408	1:40
CD62L	PerCP	BioLegend Inc.	104429	1:80
IL-4	PerCP/Cy5.5	BioLegend Inc.	504124	1:80
T-bet	PerCP/Cy5.5	BioLegend Inc.	644805	1:20
IL-22	PerCP/Cy5.5	BioLegend Inc.	516411	1:20
CD69	PE-Vio770	Miltenyi Biotec	130-103-944	1:10
Ki67	Pe-Vio770	Miltenyi Biotec	130-120-559	1:50

(continued)

LIVE/DEAD™ Fixable Aqua Dead Cell Stain Kit, for 405 nm excitation	AmCyan	ThermoFischer scientific	L34957	1:400
MitoTracker Deep Red FM	APC	ThermoFischer scientific	M22426	1:10000
MitoTracker Green FM	FITC	ThermoFischer scientific	M7514	1:100000
Zombie Violet	Pacific Blue	BioLegend Inc.	423113	1:500
FITC Annexin V Apoptosis Detection Kit with 7-AAD	FITC/7-AAD	BioLegend Inc.	640922	1:20
eBioscience™ Cell proliferation Dye	eFluor450	ThermoFischer scientific	65-0840-85	1:4000
eBioscience™ Cell Proliferation Dye	eFluor670	ThermoFischer scientific	65-0842-90	1:4000

7.1.3 Antibodies and stimulating or blocking reagents for cell culture

Reagent	Supplier	Catalog #
α-CD3	Antibodies online	A86500
α-CD28	BioLegend Inc.	102102
CD16/CD32 (mouse BD Fc Block™)	BD Pharminogen	553142
H-Y peptide	ThermoFischer scientific	PKB102780.4
Ionomycin	Sigma Aldrich	I0634-1MG
PMA	Abcam	ab120297
Protein Transport Inhibitor Cocktail, 500x	ThermoFischer scientific	00-4980-03
recombinant human TGF-β	peprotech	AF100-21C
recombinant human IL-2	BioLegend Inc.	589102
recombinant mouse IL-12	BioLegend Inc.	577002

(continued)

recombinant mouse IL-4	BioLegend Inc.	574302
recombinant mouse IL-6	BioLegend Inc.	575702
recombinant mouse TGF-β-1	BioLegend Inc.	763102
Ultra-LEAF purified anti mouse IL-4	BioLegend Inc.	504121
Ultra-LEAF purified anti mouse IFNγ	BioLegend Inc.	505708

7.1.4 Antibodies for immunoblotting

Target	Host species	Supplier	Catalog #	Dilution
ATPase	rabbit	antibodies.com	A95104	1:1000
β-actin	Mouse	R&D systems	MAB8929	1: 20000
Calnexin	rabbit	invitrogen	PA534754	1:10000
COX IV	mouse	BioLegend Inc.	937801	1:2500
ERK 1/2 phospho (Thr202/Tyr204)	mouse	BioLegend Inc.	369501	1:500
ERK 1/2	rat	BioLegend Inc.	686901	1:1000
GAPDH (D16H11)	rabbit	Cell Signalling	5174	1:1000
His-tag	rabbit	Cell Signalling	2365S	1:1000
Histone H3	rabbit	Abcam	ab1791	1:2500
Vimentin	rabbit	antibodies.com	A85420	1:10000
α-rabbit-HRP	Goat	Jackson	111-055-045	1:10000
α-rat-HRP	Goat	ThermoFischer scientific	31460	1:10000
α-mouse-HRP	Goat	Santa Cruz	sc-2064	1:10000

7.1.5 Bacterial strains

Bacterial Strain	Purpose
DH5α	Competent cells and protein production

7.1.6 Buffers and solutions

Buffer	Composition	
Binding Buffer	TRIS	20 mM
	NaCl	0.5 M
	Imidazole	20 mM
Binding Buffer with Urea (8 M)	TRIS	20 mM
	NaCl	0.5 M
	Imidazole	20 mM
	Urea	8 M
Elution Buffer	TRIS	20 mM
	NaCl	0.5M
	Imidazole	0.5 M
Coomassie Brilliant Blue staining solution	Coomassie R-250	0,10%
	EtOH	40%
	acetic acid (glacial)	10%
Coomassie Brilliant Blue destaining solution	EtOH	10%
	acetic acid (glacial)	7,50%
SDS-Running Buffer (10x)	TRIS	0.5 M
	Glycine	2 M
	SDS 20%	1%
TBE (10x)	TRIS	1 M
	Boric acid	1 M
	EDTA 0.5 M pH8	0.02 M
TBS-T (10x)	TRIS	25 mM
	NaCl	0.15 M
	Tween 20	0,05%
Transfer Buffer (10x)	TRIS	0.5 M
	Glycin	2 M
RBC Lysis Buffer	NH_4Cl	155 mM
	EDTA	0.1 mM
	$NaHCO_3$	12 mM

(continued)

Isolation Buffer	Sucrose	880 mM
	HEPES	20 mM
	NaCl	50 mM
	$MgCl_2$	5 mM
	EGTA	5 mM
Hypotonic Buffer	HEPES	20 mM
	NaCl	10 mM
	$MgCl_2$	1,5 mM
	Triton-X	0,10%
Nuclear Lysis Buffer	HEPES	20 mM
	NaCl	500 mM
	Glycerol	20%
	$MgCl_2$	2 mM
	Triton-X	1%
TE-buffer	TRIS	10 mM
	EDTA	1 mM
ME-buffer	MOPS	25 mM
	EDTA	2.5 mM
HBSS staining solution	$CaCl_2$	10 mM
	$MgCl_2$	10 mM
	FCS	1%

7.1.7 Chemicals

Chemical	Supplier	Catalog #
2-Deoxy-D-glucose	Merck	D8375
2-Mercaptoethanol 50 mM	ThermoFischer scientific	3135-010
30% Acrylamide and bis acrylamide solution (29:1)	Bio-Rad Laboratories, Inc.	1610156
Acetic acid (glacial)	Merck	31.03.06
Ammonium chloride	Carl Roth	K298.2

(continued)

Ammonium hydrogen carbonate	Carl Roth	T871.1
Ammonium sulphate	Carl Roth	9212.1
Aqua ad injectabilia 20x10mL	B.Braun	2351744
Boric-Acid	Sigma-Aldrich	B0394
Calcium chloride	Merck	1.02378.500
Chloroform	J.T. Baker	7386
Coomassie Brilliant Blue R-250 Solution	Bio-Rad Laboratories, Inc.	1610436
DMSO	Sigma-Aldrich	D5879
Dulbecco's PBS	Gibco	14190-094
EDTA	Sigma-Aldrich	ED255-50g
Ethanol absolute	Chemsolute	2273.1000
Ethanol 70%	Chemsolute	2202.5000
Fetal Calf Serum (FCS)	Gibco	A5256801
Glucose	Gibco	A24940-01
Glycerol	Invitrogen	15514011
Glycine	Sigma-Aldrich	G712-1kg
Hanks Balanced Salt Solution (HBSS)	Gibco	14175-063
HEPES	Sigma-Aldrich	H3375-500
Hydrochloric acid (37%)	Chemsolute	836.10000
Hydrochloric acid (4N)	Chemsolute	824.1011
Imidazole	Merck	1.04712.0250
Isoflurane	sedana medical	3000-225-2109
IPTG	Sigma-Aldrich	I6758-10G
LB	Carl Roth	X968.2
L-Glutamine 200 mM	Gibco	25030-081
MACS Buffer	Miltenyi Biotec	130-091-221
Magnesium chloride hexahydrate	Sigma-Aldrich	13152-1kg
Minimum Essential Medium Non-Essential Amino Acids (MEM NEAA)	Gibco	11140-050
Methanol	J.T.Baker	8045
MOPS	Calbiochem	475898

(continued)

Oligomycin	Merck	O4876
Penicillin Streptomycin	ThermoFischer scientific	15140-122
Phenol TE	Sigma-Aldrich	77607
PhosCheck P30	BK Giulini	2840
Pluronic™ F127	ThermoFischer scientific	P6866
Rapamycin	Sigma-Aldrich	553210-100UG
ROTI®Phenol Chloroform/Isoamylalkohol	Carl Roth	A156.1
RPMI Medium 1640 + GlutaMax	Gibco	72400-021
SDS 20%	PanReac Applichem	A3942
Seahorse XF RPMI, 500 ml	Agilent Technologies™	103681-100
Sodium acetate	Carl Roth	X891.1
Sodium chloride	Sigma-Aldrich	59625-1Kg
Sodium hydroxide (4N)	Carl Roth	T198.1
Sodium iodoactate	Sigma-Aldrich	I2512-25g
Sodium pyruvate	Gibco	1136-070
Succrose	Sigma-Aldrich	S0389
Sulfuric acid (4N)	Carl Roth	X873.1
TBE urea sample buffer	ThermoFischer scientific	J60186.AC
N,N,N′,N′-Tetramethylethylendiamin (TEMED)	Sigma-Aldrich	T9281
Triton-X	Bio-Rad Laboratories, Inc.	161-0407
Trizma Base	Sigma-Aldrich	T15-03
Trypanblue solution (0.4%)	Gibco	15250-061
Tween-20	Sigma-Aldrich	P1379-500mL
Urea	Sigma-Aldrich	U6504
X-Vivo 15 Medium with Gentamicin Phenolred	Lonza	BE02-060F

7.1.8 Cell lines

Cell line	Supplier	Catalog #
Jurkat, clone E6-1	ATCC	TIB-152

7.1.9 Consumables

Consumable	Supplier	Catalog #
12% Mini-PROTEAN TGX PrecastPr. Gel 15µl	Bio-Rad Laboratories, Inc.	4561046
7.5% Mini-PROTEAN(R) TGX (TM) precast protein gels 15 well 15 µL	Bio-Rad Laboratories, Inc.	L006904 B
96 well multiply Fast PCR plate, 0,2 mL	Sarstedt	72.1981.010
Cell culture flask T-75	Sarstedt	93.3911.002
Cell culture flask T-25	Sarstedt	
Cell culture plate, 96 well, f-bottom sterile	Sarstedt	83.3924.005
Cell culture plate, 96 well v-bottom sterile	Sarstedt	82.1583.001
Cell culture plate, 96 well u-bottom sterile	ThermoFischer scientific	268200
Cell culture plate, 24 well f-bottom sterile	Falcon	353226
Cell strainer 100 µm	Sarstedt	93.3945.100
cOmplete ULTRA tablets, EDTA free protease inhibitor-cocktail	Roche	6538282001
Corning®falcon®Cell culture plate 48 wells f bottom	Falcon	353230
HisTrapFF 1 mL	Cytiva Europe GmbH	17531901
HisTrapFF 5 mL	Cytiva Europe GmbH	17525501

(continued)

LS column	Miltenyi Biotech	130-042-401
LD column	Miltenyi Biotech	130-042-901
Microtest-plate, 96 well unsterile	Sarstedt	82.1581
Microtest-plate, 96 well, v-bottom, unsterile	Sarstedt	82.1583
Parafilm® M	Merck	P6543
Pipette tips 10 µL	Sarstedt	70.3010.200
Pipette tips 200 µL	Sarstedt	70.3030.100
Pipette tips 200 µL Refill	Sarstedt	70.3030.100
Pipette tips 300 µL	Sarstedt	70.3040.355
Pipette tips 1000 µL	Sarstedt	70.3050.200
Seahorse XFp FluxPaks	Agilent Technologies™	103022100
Seahorse XFp Cell Culture Miniplates	Agilent Technologies™	103025100
Serological pipette 5mL	Sarstedt	86.1253.001
Serological pipette10mL	Sarstedt	86.1254.001
Serological pipette 25mL	Sarstedt	86.1685.001
Serological pipette 50mL	Sarstedt	86.1256.001
Scalpel No.10	Dahlhausen	11.000.00.710
Slide-A-Lyzer™ G3 dialysis cassettes 10K MWCO 15 mL	ThermoFisher Scientific	A52972
Sterile filter, Filtropur S, PES, 0.2 µm	Sarstedt	83.1826.001
sterile filter 0.2 µm	Sarstedt	83.1826.001
Syringe 30 mL PCA LuerLock	BD Plastipak	301229
Waste bags	TH Geyer	7696994

7.1.10 Flow cytometer

Device	Supplier
FACSCanto II flow cytometer	BD Biosciences
Novocyte Quanteon	Agilent Technologies™

7.1.11 Growth Media

Growth Medium	Composition	
T cell medium complete	RPMI 1640 + GlutaMax	500 mL
	FCS	10%
	HEPES	10 mM
	Sodium Pyruvate	1 mM
	ß-Mercaptoethanol	50 µM
	MEM NEAA	1 mM
	L-Glutamine	2 mM
	Penicillin/Streptomycin	1%
Jurkat cell culture medium	RPMI 1640 + GlutaMax	500 mL
	FCS	10%
	Penicillin/Streptomycin	1%

7.1.12 Kits

Kit	Supplier	Catalog #
Anti-PE MicroBeads Ultra Pure	Miltenyi Biotech	130-105-639
CD4+ T Cell Isolation Kit, mouse	Miltenyi Biotech	130-104-454
CD4+CD25+ Regulatory T Cell Isolation Kit	Miltenyi Biotech	130-091-041
CellXVivo Mouse Th17 Cell Differentiation Kit	R&D Systems	CDK017
ECL Prime Western Blotting Detection Reagent	Cytiva Europe GmbH	GERPN2232
ELISA MAX™ Standard Set Mouse IL-2	BioLegend Inc.	431001

(continued)

Halt protease and phosphatase Inhibitor Cocktail (100x)	ThermoFischer Scientific	78440
FITC Annexin V Apoptosis detection kit with 7-AAD	BioLegend Inc.	640922
Foxp3/Transcription Factor Staining Buffer Set	ThermoFischer Scientific	00-5523-00
Naïve CD4+ T cell isolation Kit, mouse	Miltenyi Biotech	130-104-453
Phosphate assay kit (colorimetric)	abcam	ab65622
Pierce BCA Protein Assay Kit	ThermoFischer Scientific	23225
QIaprep spin Miniprep Kit (250)	Qiagen	27106
RNeasy Mini Kit	Qiagen	74104
ROS/Superoxide Detection Assay Kit (Cell-based)	abcam	ab139476
Seahorse XF T Cell Metabolic Profiling Kit	Agilent Technologies™	103772-100
Seahorse XF Real-Time ATP Rate Assay Kit	Agilent Technologies™	103592-100
SuperSkript IV VILO Master Mix	invitrogen	11756050
TaqMan Universal Mastermix II, no UNG	applied Biosystems	4440040

7.1.13   Laboratory equipment

Device	Supplier
Äkta start	Cytiva
Accujet	Brand
BioPhotometer	Eppendorf
Certomat MV	B.Braun Biotech international
ChemiDoc Imager	Bio-Rad Laboratories, Inc.
CLARIOstar Plus	BMG Labtech
Electrophoresis chamber	Bio-Rad Laboratories, Inc.

(continued)

Heidolph Duomax x1000 Platform Shaker	Heidolph
Heraeus Megafuge 8	ThermoFischer Scientific
LLG-Micro-Pistil, F.1,5	TH Geyer
Microscope ECLIPSE Ts2R	Nikon
MIKRO 220R centrifuge	Hettrich
NanoDrop Spectrophotometer ND-1000	NanoDrop
PowerPac Basic	Bio-Rad Laboratories, Inc.
SIGMA 4-16K refrigerated centrifuge	Sigma
Sonoplus Sonicator	Bandelin
Sorvall LYNX 4000 Superspeed Centrifuge	ThermoFischer scientific
StepOnePlus Real Time PCR system	Applied Biosystems
Tecan Spark Multiplate Reader	Tecan
ThermoMixer C	eppendorf
ThermoStar	BMG Labtech
Tube Roller	Benchmark Scientific
Water bath	GFL

7.1.14　　TaqMan probes

Target Gene	Fluorophore	Supplier	Catalog #
Gls2	FAM-MGB	ThermoFisher scientific	Mm01164862_m1
Hif1a	FAM-MGB	ThermoFisher scientific	Mm00468869_m1
Hk2	FAM-MGB	ThermoFisher scientific	Mm00443385_m1
HPRT1	FAM-MGB	ThermoFisher scientific	Mm00446968_m1
Il2	FAM-MGB	ThermoFisher scientific	Mm00434256_m1
Myc	FAM-MGB	ThermoFisher scientific	Mm00487804_m1
Slc2a1	FAM-MGB	ThermoFisher scientific	Mm00441473_m1
Slc3a2	FAM-MGB	ThermoFisher scientific	Mm00500521_m1
Slc16a3	FAM-MGB	ThermoFisher scientific	Mm01246825_m1
Tpi1	FAM-MGB	ThermoFisher scientific	Mm00833691_m1

7.2 Methods

7.2.1 Animals

Marilyn mice were purchased from EMMA (Strain #EM:00133), mice with a C57BL/6J background were in-house bread. All animals were kept at the animal facility of the University Medical Center Hamburg Eppendorf under pathogen free conditions in ventilated cages.

7.2.2 Cell culture work

All cell culture work was performed under a laminar air flow workbench. Cells were cultured in flasks (T25, T75) or plates (24-, 48- or 96-well) at 37 °C, 5% CO_2 saturation and approximately 90% humidity. The human lymphoblastic T-cell line Jurkat E6-1 (ATCC, TIB-152) was cultured in RPMI GlutMax™ Medium supplemented with 10% FCS and 1% penicillin-streptomycin. Murine CD4+ T cells were cultured in RPMI GlutMax™ Medium supplemented with 10% FCS, 10 mM HEPES, 1 mM pyruvate, 50 µM β-mercaptoethanol, 1% MEM NEAA, 1% L-glutamine and 1% penicillin and streptomycin.

7.2.3 CD4+ T-cell isolation

Secondary lymphoid organs were isolated from mice and pressed through a 100 µm cell strainer to ensure a single cell suspension. Red blood cell lysis was performed for 3 min 30 s at RT with red blood cell lysis buffer. The lysis was stopped by adding 25 mL PBS and subsequent centrifugation at 500 *g* for 5 min. The pellet was re-suspended in 2 mL of PBS and the CD4+ T cells were isolated following Miltenyi's CD4+ T cell isolation Kit instructions. In brief, cell suspension was incubated with PE or biotin labelled α-CD4 antibody for 15 min at 4 °C. Unbound antibody was removed by centrifugation and magnetic α-PE or streptavidin beads were added to the mixture and incubated for another 15 min at 4 °C. A LS column was placed in a magnetic field and conditioned with MACS buffer. The cells were washed with MACS buffer and applied to the column, the flow-through contained the CD4 negative cell population. CD4+ cells were collected from the column by elution with MACS buffer outside of the magnetic

field. Cells were pelleted, resuspended in complete T-cell medium and cell numbers assessed.

7.2.4 H-Y antigen stimulation

For antigen specific CD4+ T cell stimulation CD4+ T cells from *Marilyn* mice that express only one transgenic TCR recognizing male H-Y antigen on a *Rag2* knockout background were used. The *Rag2* gene deficiency prevents recombination of endogenous TCR chains and allows only T cells reactive against male H-Y antigen to egress from the thymus. The spleen of *Marilyn* mice were pressed through a 100 µm cell strainer to obtain a single cell suspension. Red blood cells were lysed for 3 min 30 s at RT with Red Blood Cell Lysis buffer and the lysis stopped by adding 25 mL PBS. Splenocytes were washed and plated. 0.6 or 10 µg/mL H-Y antigen were added to the cell culture and the cells were stimulated for three days. After stimulation CD4+ T cells were isolated from splenocytes following the instruction of section 7.2.3.

7.2.5 In vitro T-cell differentiation

Differentiation of murine CD4+ T cells *in vitro* was performed on freshly isolated CD4+ T cells incubated in 24 well plates coated with αCD3/αCD28 (2 µg/mL / 0.5 µg/mL) at a cell density of $1x10^6$ cells per well for TH0, Th1, Th2 and iTreg cells. Th17 cells were differentiated using R&D's CellXVivo Mouse Th17 Cell Differentiation Kit. Cytokines were prepared according to manufacturer's instructions in X-Vivo Medium, cells were seeded at $5x10^5$ cells per well and stimulated on αCD3/αCD28 (2 µg/mL / 0.5 µg/mL) coated plates for three days after which an equal amount of differentiation medium was added and cells were cultured for two more days.

For Th1, Th2 and iTreg-cell differentiation 2x differentiation media were prepared according to Table 1 and mixed with an equal volume of cell suspension. Cells were then cultured for three days.

Table 1: Composition of 2x differentiation media for T-helper cells

Reagent	Th0	Th1	Th2	iTreg
Recombinant IL-2	2 µg/mL	2 µg/mL	2 µg/mL	4 µg/mL
Recombinant IL-12		10 ng/mL		
Recombinant IL-4			8 ng/mL	

(continued)

Recombinant TGF-β				20 ng/mL
α-IFNγ			20 µg/mL	2 µg/mL
α-IL-4		20 µg/mL		2 µg/mL

7.2.6 Transmission electron microscopy (TEM)

PolyP is a negatively charged polymer that can be visualised in electron microscopy as electron dense structures as previously shown in platelets [174]. To identify possible polyP storage compartments CD4+ T cells were stimulated for three days, washed in PBS (500 g, 5 min, 4 °C), pelleted and fixated in 4% paraformaldehyde and 1% high grade EM glutaraldehyde in PBS. The fixative was kindly provided by Michaela Schweizer from the Center for Molecular Neurobiology Hamburg (ZMNH), who also performed further sample preparation and imaging in electron microscopy. Furthermore, the Schweizer Group uses an energy dispersive X-ray spectroscopy (EDX) to identify the element composition of the image detail in view.

7.2.7 Subcellular fractionation

For subcellular fractionation cells were harvested and washed twice in 50 mM TRIS buffer. The composition of buffers and the protocol for the assay was modified from Dias *et al.* [175]. All following steps were either performed on ice or at 4 °C. The cells were re-suspended in 250 µL isolation buffer supplemented with protease inhibitors and homogenised with a micropistill. Centrifugation at 720 g for 7 min separated the pelleted nuclear and cytoskeleton fraction from cytosol, membrane and mitochondrial fraction in the supernatant. The pellet was washed twice in hypotonic buffer by repetitive re-suspension and centrifugation at 100 g for 10 min. The resulting pellet was lysed in nuclear lysis buffer for one hour and the lysate cleared at 20,000 g for 20 min. The fraction containing cytosol, membrane and mitochondria was centrifuged at 1,000 g for 10 min. The resulting pellet contained parts of the membrane fraction while the supernatant was processed in another centrifugation at 20,000 g for 45 min. The generated pellet contained the mitochondria and was washed twice with isolation buffer. Cytosol and remaining membranes were further separated by two centrifugations at 20,000 g for each 25 min, whereby the resulting supernatant

presents the cytosolic fraction, and generated pellets were combined in isolation buffer as the membrane fraction.

Proper fractionation was validated by immunoblotting according to section 7.2.36 using GAPDH as a cytosolic marker, calnexin as a membrane marker, COX IV as a mitochondrial marker and histone H3 as a nuclear marker.

7.2.8 PolyP extraction for urea PAGE separation

For isolation of polyP, cells were harvested and washed twice in 50 mM TRIS buffer, then lysed using SDS-lysis buffer at RT for 10 min. DNA was extracted using QIAprep2.0 spin columns and associated buffers. In brief, SDS and cellular debris were removed from cell lysates by addition of N3 buffer and centrifugation at 13,000 g for 10 min. Supernatant was collected and applied to DNA extraction columns. The flow-through, containing polyP, was collected and applied to phenol-chloroform extraction. The spin columns with bound DNA were discarded. The flow-through was mixed with one volume of phenol-chloroform isoamylalcohol and centrifuged at 10,000 g for 5 min. The aqueous phase containing polyP was collected, the organic phase washed with 20 mM TRIS and the hereby generated aqueous phase was united with the first. This step was repeated, and the polyP fraction was mixed with one volume of chloroform. The extracted polyP was precipitated with 20 mM ammonium sulphate, 0.3 M sodium acetate and 100% ice cold EtOH, pelleted and air dried overnight.

7.2.9 Urea PAGE

8 M, 7.5% urea PAGE gels were cast between 1.5 mm spacer plates in the Bio-Rad Laboratories, Inc. system using the following composition.

Table 2: Composition of 8 M, 7.5% urea gel

Component	Amounts
Urea	9.45 g
10x TBE	2.25 mL
30% Acrylamide and bis acrylamide solution (1:29)	6 mL

(continued)

ddH$_2$O	6.5 mL
TEMED	9 µL
10% APS	225 µL

PolyP pellets were dissolved in 50 mM TRIS and supplemented with 2x TBE Urea sample buffer. Before loading, the gel was run for 30 min at 100 V for equal heat distribution and removal of any undissolved urea. The pockets were then washed with running buffer and samples were loaded. After separation at 120 V the gel was stained in 2.5 µg/mL DAPI for 30 min and washed in negative DAPI solution for one hour. Photobleaching and imaging was performed on a ChemiDoc™ Imager (Bio-Rad Laboratories, Inc.).

Prior to phenol-chloroform extraction the protein concentration of each sample was measured as described in section 7.2.33 and the amount of sample loaded to the urea gel adjusted accordingly. β-actin immunoblot was performed according to section 7.2.36 as loading control.

7.2.10   PolyP extraction for malachite green assay

For polyP quantification, polyP was isolated following the protocol established by Christ and Blank [137]. In summary, cells were harvested and washed twice in 50 mM TRIS buffer, re-suspended in ME buffer and phenol-saturated TE buffer. Lysis was performed at 45 °C for 10 min followed by 2 min on ice. The polyP containing aqueous phase was mixed with chloroform and TE buffer and centrifuged at 12,000 g for 5 min at 4 °C. The aqueous phase was directly processed in Abcam's colorimetric phosphate assay kit.

7.2.11   Malachite green assay

For colorimetric measurement of phosphate levels Abcam's colorimetric phosphate assay kit was used. For this, the polyP-containing sample volume was split in half. One part was processed in acidic hydrolysis by adding 1N HCl and heating the sample to 95 °C for 10 min to determine maximal phosphate levels whereas an equal volume of ddH$_2$O was given to the other half before the colorimetric measurement of phosphate

concentration was performed. 30 µL of malachite green reagent were mixed with 200 µL of the sample in a flat bottom 96-well plate. Light absorbance of green malachite complexes formed in the samples was determined in duplicates in a microplate reader (Tecan Spark) at 650 nm wavelength. Phosphate concentrations were calculated in relation to freshly prepared phosphate standards. PolyP amounts were estimated by subtraction of the polyP content of the untreated sample from those of the fully hydrolysed sample.

7.2.12   CPP-Ppx1 overexpression

For overexpression of CPP-Ppx1 the pTrc-HisB vector encoding a His-tagged cell-penetrating peptide domain from Choi *et al.* [33] fused to the polyphosphatase 1 (Ppx1) from *S. cerevisiae* [176] was used. The cloning of this construct was performed by B.Sc Banafsheh Afshar as part of her bachelor work.

The vector was transformed to DH5α competent *E.coli* via heat shock (thawing on ice, 42 °C for 45 s, 2 min on ice). Transformed bacteria were then plated on ampicillin agar and grown overnight in a bacteria incubator at 37 °C. One ampicillin resistant clone was picked and grown further in ampicillin LB medium. For long term storage 500 µL of this overnight culture were mixed with 500 µL glycerol and frozen at -80 °C. This glycerol stock was prepared during the Master thesis of M.Sc Lydia Zhan.

For high scale production of CPP-Ppx1 expressing bacteria small aliquots of the glycerol stock were inoculated in 200 µL of LB medium and incubated overnight at 37 °C with gentle agitation. The overnight culture was added to 1,8 L of fresh ampicillin containing LB medium and cultured until the bacterial growth reached the lag phase. Bacterial growth was monitored by regular measurements of optical density at 600 nm. Once the lag phase was reached, CPP-Ppx1 production was induced for 4 hours with 1 mM IPTG. CPP-Ppx1 containing bacteria were then pelleted at 4 °C 4,000 *g* for 20 min. Bacteria pellets were stored at -20 °C until protein purification.

7.2.13   His-tag purification of CPP-Ppx1

The cell pellets were re-suspended in Äkta Binding Buffer containing 8 M Urea and EDTA free protease inhibitors. The suspension was sonicated and, in order to fully

dissolve microbodies, incubated for one hour at 4 °C with constant agitation. The lysate was clarified by centrifugation at 12,000 g, 4 °C for 20 min and loaded onto two connected 5 mL HisTrap columns connected to the Äkta start system. The bound protein was washed with a urea gradient from 8 to 0 M Urea to ensure on-column refolding of the protein. Elution was performed with imidazole containing Äkta Elution buffer. Proper purification was assessed by separating fraction aliquots in SDS-PAGE followed by Coomassie Brilliant Blue staining.

To remove the imidazole from the elution buffer, the protein containing fraction was dialyzed against 300 mM NaCl, 50 mM TRIS (pH 7.4) at 4 °C in a Slide-A-Lyzer™ cassette (ThermoFischer scientific) with a 10 kDa molecular weight cut-off. The dialyzed protein was then supplemented with the frost-free freezer glycerol (10%) and stored in aliquots at -80°C.

7.2.14   CPP-Ppx1 activity assay

Every batch of CPP-Ppx1 was tested for activity in urea PAGE analysis. For this, 20 ng of synthetic polyP (P30) were incubated with increasing concentrations of CPP-Ppx1 for 30 min at 37 °C. Reaction mixtures were then mixed with TBE loading dye and applied to urea PAGE for sample separation. DAPI staining with subsequent UV-photobleaching using the ChemiDoc system (Bio-Rad Laboratories, Inc.) was applied for visualisation of polyP digestion.

For determining the enzymatic activity of CPP-Ppx1 in T cells, murine CD4+ T cells were stimulated with 50 ng/mL PMA and 1 µg/mL ionomycin for three days to accumulate maximal amounts of polyP. Stimulated T cells were incubated hourly with 80 µg/mL CPP-Ppx1 three times at 37 °C and washed twice in PBS afterwards. Extracellular staining with α-CD4-PE, FITC-Annexin V and 7-AAD was carried out for 20 min at 4 °C. Staining for polyP was carried out after fixation and permeabilization with 100 µg/mL of polyP binding probe derived from the first two exons of the bacterial polyphosphatase (PpxΔ12) labelled with AlexaFluor 647. The samples were analysed by flow cytometry on the Canto II (BD Biosciences)

7.2.15   CPP-Ppx1 treatment of CD4+ T cells

Freshly isolated T cells were incubated with 80 µg/mL CPP-Ppx1 for 15 min at 37 °C. Cells were spun down and the medium exchanged. After 45 min of resting at 37 °C another 80 µg/mL of CPP-Ppx1 were added to the cells for 15 min. The cell were spun down, re-suspended in fresh T-cell medium and stimulated on α-CD3/α-CD28 coated plates for 16 hours to three days.

7.2.16   Calcium flux measurement

For calcium flux measurement the ratiometric dye Fura-2 was used. Fura-2 bound to calcium ions (Ca^{2+}) has an excitation maximum at 340 nm and an emission maximum at 520 nm, while in the absence of Ca^{2+} Fura-2 has an excitation maximum at 380 nm and an emission wavelength at 520 nm. Jurkat cells were stained with 2 µM Fura-2 AM in HBSS staining buffer supplemented with 0.2% pluronic acid at 37 °C for 30 min. Cells were washed in HBSS twice and adhered on fibronectin coated 96-well plate (black with transparent bottom) at 37 °C for one hour while also allowing intracellular ester conversion. Fura-2 fluorescence was measured in the ClarioStar Plus plate reader (BMG Labtech) using its on board injection system to measure the cellular reaction to an injection of 80 µg/mL CPP-Ppx1 or equal amounts of controls. The injection was carried out after 11 s of baseline measurement, followed by double orbital shaking of the plate to properly disperse the experimental substance and another 480 s of measurement. For analysis the fluorescent data was blank corrected and the excitation quotient for Fura-2 (340/380) was calculated.

7.2.17   Enzyme-linked Immunosorbent Assay

For quantification of IL-2 released by T-cell cultures supernatants were collected and frozen until analysis via with ELISA-MAX mouse IL-2 set (BioLegend). In summary, a high affinity binding 96-well plate was coated with the diluted capture antibody and incubated at 4 °C overnight. The plate was washed, and unspecific binding sites were blocked by incubation of the plate with assay diluent for one hour at RT. The plate was washed again, and cell culture supernatant was added for IL-2 binding to the capture antibody at RT for two hours. The plate was washed in three subsequent washing steps

and the cytokine specific biotinylated detection antibody added. After incubation for one hour at RT the plate was washed three times and incubated with avidin-horseradish peroxidase for 30 min at RT. The HRP substrate tetramethylbenzidine (TMB) was added and colour reaction was stopped with 2 N sulfuric acid after 30 min. Absorbance was measured at 450 and 512 nm in a microplate reader (Tecan Spark).

7.2.18   Proliferation assay

Murine CD4+ T cells were isolated according to section 7.2.3 and stained with eFluor450 or eFluor 670 proliferation dye (eBioscience™). The fluorescent proliferation dye binds to primary amines and will be divided evenly during cell-divisions which allows for the tracking of cell proliferation in flow cytometry analysis.

Proliferation dye was prepared by dissolving the lyophilised dye in DMSO according to manufacturer's instructions and was further diluted in PBS to obtain a 2x working solution (5 µM). Cells were resuspended in PBS at a concentration of $2x10^6$ cells /mL and an equal volume of proliferation dye working solution was added. The mixture was immediately mixed by vortexing, to achieve an evenly distributed 1x staining solution at a cell number of $1x10^6$ cells/mL. Cells were stained at 37 °C for 20 min and staining was stopped by addition of 500 mL FCS per mL cell-suspension and incubated for 5 min at 37 °C. Stained T cells were treated with CPP-Ppx1 or buffer control according to section 7.2.15 and stimulated on α-CD3/α-CD28 coated plates for three days.

7.2.19   RNA isolation

RNA of murine CD4+ T cells was extracted using RNeasy Mini Kit (Quiagen). In brief, up to $1x10^7$ cells were harvested, washed in PBS and stored in 350 µL RLT buffer supplemented with β-mercaptoethanol at -20 °C until further processing. For RNA isolation, one volume of 70% EtOH was added and the sample transferred to a spin column. The column was washed with RW1 and RPE buffer and then dried by centrifugation on full speed for 1 min. Elution of RNA was performed in RNase free water. RNA concentration was determined by measurement of the UV-absorption at

260 nm using the NanoDrop system. RNA was stored at -20 °C or -80 °C for short-term or long-term storage, respectively.

7.2.20   Reverse transcription

For reverse transcription SuperScript™ IV Vilo™ Master Mix (invitrogen) was mixed with RNA at a one to five ratio (4 µL SuperScript™ IV Vilo™ Master Mix with 16 µL RNA) and incubated for 10 min at 25 °C for primer annealing. Reverse transcription was performed at 50 °C for 10 min, followed by a 5 min incubation at 85 °C to inactivate the enzyme.

7.2.21   Real-time quantitative polymerase chain reaction (RT-qPCR)

The cDNA was processed in RT-qPCR measurement using the respective TaqMan (ThermoFischer scientific) probes. Master-mixes were prepared to a multiple of the following composition:

Table 3: Composition of RT-qPCR mastermix

Component	Volume (µL)
cDNA	0.5
TaqMan Universaler Mastermix II, no UNG	10
ddH$_2$O	8.5

Of each mix 19 µL were filled into a PCR multiwell plate and 1 µL respective TaqMan probe was added. Each sample was measured in triplicates. For the RT-qPCR the StepOnePlus System (ThermoFisher scientific) was used with the following settings:

Table 4: RT-qPCR program

Step	Temperature (°C)	Time (min:sec)	Cycle description
1	50	2:00	
2	95	10:00	Initial denaturation
3	95	00:15	Denaturation
Repeated for 40	60	01:00	Annealing
cycles	60	00:01	Extension
4	60	00:15	Final extension

7.2.22   Seahorse metabolic flux analysis

Metabolic status was measured using the Seahorse XF HS Mini analyser. CD4+ T cells were isolated and incubated with CPP-Ppx1 according to sections 7.2.3 and 7.2.15 and stimulated on α-CD3/α-CD28 coated plates for 16 hours. On the day of the assay, cells were harvested, counted and seeded in complete Seahorse XF RPMI Medium at $1,5x10^5$ cells per well in a Seahorse cell culture plate. Oxygen consumption rate (OCR) and extracellular acidification rate (ECAR) were determined. Seahorse Flux cartridges were prepared according to manufacturer's instructions and loaded with the experimental compounds as stated in the respective kit. All measurements were carried out in triplicates. Seahorse Wave Pro 10.1.0 software was used for data analysis.

7.2.23   Measurement of reactive oxygen species (ROS)

For detection of reactive oxygen species, the ROS/Superoxide Detection Assay Kit (Abcam) was used. To ensure proper controls each experiment was carried out with a negative and a positive control. In brief, $1x10^5$ murine CD4+ T cells were resuspended in 250 µL complete T-cell medium. The negative control was incubated with 5 mM of the supplied ROS inhibitor (N-Acetyl-L-cystein) for 30 min prior to staining. The 2xROS/Superoxide detection mix was prepared by diluting the oxidative stress detection reagent (5 mM) and the superoxide detection reagent (5 mM) at a 1:2500 ratio in culture medium. For positive control a 2x dilution (40 µM) of the ROS inducer Pyocyanin was prepared and added to the positive control at the same time as the 2x ROS/Superoxide detection mix. After incubation at 37 °C for 30 min at gentle agitation

the samples were immediately analysed by flow cytometry using the NovoCyte Quanteon (Agilent Technologies™).

7.2.24 Analysis of mitochondrial mass and function

For analysis of the mitochondrial function murine CD4+ T cells were stained with MitoTracker DeepRed and MitoTracker Green. While MitoTracker Green can access any mitochondria and is thereby used as a marker for the overall mitochondrial mass, MitoTracker DeepRed only passes the membranes of polarised mitochondria and gives information about the functionality of the mitochondrium. $5x10^5$ cells were resuspended in PBS supplemented with 10 nM MitoTracker Green, 100 nM MitoTracker DeepRed, ZombieViolet for Live-Dead discrimination and α-CD4-PE. After 30 min of incubation at 37 °C with gentle agitation the cells were washed once in PBS and analysed by flow cytometry using the NovoCyte Quanteon (Agilent Technologies™).

7.2.25 Naïve CD4+ T-cell isolation

Singel cell suspension were obtained as described in section 7.2.3. Naïve CD4+ T cells were isolated following Miltenyi's naive CD4+ T cell isolation Kit. In essence, splenocytes were incubated with the biotin-anitbody cocktail for 5 min on ice. Next, MACS buffer, biotin-binding microbeads and αCD44 microbeads were added and incubated for another 10 min on ice. For higher recovery, cells were washed in 2 mL of MACS buffer and then added onto an LS column, placed in a magnetic field. The flow-through containing the naïve CD4+ T cells was collected and centrifuged at 300 *g* for 10 min. T cells were resuspended in complete T-cell medium and cell numbers were assessed.

7.2.26 Assay for transposase-accessible chromatin sequencing (ATAC-seq.)

ATAC-seq. was performed on naïve mouse CD4+ T cells isolated following the instruction of section 7.2.25 and treated as described in section 7.2.15. Subsequently,

cells were stimulated on α-CD3 and α-CD28 coated cell culture plates in complete T-cell medium for 16 hours at 37 °C. After that, cells were counted and frozen in FCS containing 10% DMSO at a concentration of 1×10^6 cells per mL. Samples were sent to Active Motif Inc. Belgium on dry ice for further analysis. In brief, to determine CPP-Ppx1 mediated differences in chromatin accessibility, a hyperreactive transposase loaded with next generation sequencing adapters, fragments the chromatin and integrates these adapters at open chromatin sites. Adapter-tagged DNA fragments are then amplified and sequenced. Peaks were allocated to nearest gene localisation and annotated data files were processed with publicly available software program GREAT v4.0.4 to perform pathway prediction analysis [177] or Integrative Genomics Viewer v2.18.4 for visualization of gene loci.

7.2.27   CD4+CD25+ T-cell isolation

Single cell suspensions were obtained as described in section 7.2.3. CD4+CD25+ and CD4+CD25- T cells were isolated following Miltenyi's CD4+CD25+ Regulatory T Cell Isolation Kit. Briefly, non-CD4+ T cells were labelled with the biotin antibody cocktail for 5 min on ice. Next, MACS-buffer, CD25-PE and α-CD44 microbeads were added and incubated for another 15 min on ice. Non-CD4+ T cells were depleted through binding to an LD column placed in a magnetic field. The flow-through containing all CD4+ T cells was collected, centrifuged and labelled with α-PE Microbeads. CD4+CD25+ T cells were retained in the magnetic field of a MS column, washed and flushed out. For optimal purity the collected cells were applied to another MS column, washed and eluted. The flow-through of the MS columns contained the CD4+CD25- population. Cells were pelleted, resuspended in complete T-cell medium and cell numbers assessed.

7.2.28   T-cell population tracing

To test whether CPP-Ppx1 treatment induces Foxp3 expression *de novo* or stimulates Treg expansion, CD4+CD25- Tcon and CD4+CD25+ Treg cells, isolated from murine splenocytes according to section 7.2.27 were stained in eFluor450 and eFluor670 proliferation dye, respectively, according to section 7.2.18. After labelling, 1×10^5 Treg cells were mixed with 9×10^5 Tcon to obtain a physiological ratio and treated with

CPP-Ppx1 or buffer control according to section 7.2.15. Cell-mixtures were stimulated on α-CD3/α-CD28 coated plates for three days, stained for viability, CD4, CD25 and Foxp3 and analysed in flow cytometry on the NovoCyte Quanteon (Agilent Technologies™).

7.2.29   Treg suppression assay

To assess the suppressive capacity of T-cell populations, CD4+CD25+Treg cells were freshly isolated from murine splenocytes following the instructions of section 7.2.27. The CD4- population was irradiated at 30 Gy and used as antigen presenting cells (APCs) whereas CD4+CD25- T cells were stained with eFluor450 proliferation dye according to section 7.2.18 and used as responder T cells. The stained cells were pelleted and seeded at $5x10^4$ cells in a 96-well U-bottom plate. CD4+CD25+ T cells were added in twofold dilutions to responder T cells in the presence of $1x10^5$ irradiated APCs and 1 µg/mL α-CD3-antibody. Suppression of T-cell proliferation was analysed by flow cytometry after three days of co-culture on the NovoCyte Quanteon (Agilent Technologies™).

To compare the CPP-Ppx1 mediated induction of regulatory functions in T cells, murine CD4+ T cells were isolated as described in section 7.2.3, incubated with CPP-Ppx1 according to section 7.2.15 and stimulated on α-CD3/α-CD28 coated plates for three days under skewing conditions. The in-vitro differentiated T cells were then harvested, counted and used as a Treg fraction in suppression assay as described above.

7.2.30   Analysis of *Foxp3* methylation status

For determining the *Foxp3* methylation status, murine CD4+ T cells were isolated from secondary lymphoid organs and incubated as described in sections 7.2.3 and 7.2.15, respectively. After three days of cultivation, cells were harvested, counted and pellets of $1x10^5$ cells were snap frozen in liquid nitrogen for short term storage until transport on dry ice to Epigen-DX (Boston, USA) for further analysis (bisulfide sequencing Treg panel N4V1P15, P16 and P17).

Table 5: Next-generation bisulfide sequencing assay details

Gene	Number of CpG regions	Nucleotides from TSS
Cd276	7	-91 to -12
Cdkn1c	9	33 to 108
Ctla4	4	3448 to 3549
Ikzf2	6	28548 to 28625
Ikzf4	5	1738 to 1846
Il2	2	-255 to -210
Il2ra	3	2914 to 2947
Il4	3	249 to 293
Tnf	4	-839 to -743
Tnfrsr	4	2403 to 2485
Foxp3 distal promotor	24	-6229 to -6181
		-5493 to -5380
Foxp3 proximal promotor	5	-71 to -35
Foxp3 Intron 1	14	4125 to 4147
		4275 to 4393
		4442 to 4473
		4535 to 4605

7.2.31 Flow cytometry

7.2.31.1 Staining for flow cytometry

For expression analysis of fluorescently labelled proteins on the surface, cells were washed twice in cold PBS and stained with primary antibodies at 4 °C for 15 - 30 min. To reduce non-specific antibody binding every mixture of primary antibodies was supplemented with an Fc-blocking agent (CD16/CD32 (mouse BD Fc Block™)). Discrimination of dead cells was possible by staining with LIVE/DEAD™ Fixable Aqua Dead Cell Stain Kit, for 405 nm excitation (ThermoFischer scientific) which detects intracellular free amines only reachable when the cell membrane has become permeable.

After removal of unbound antibodies by two subsequent washing steps (500 *g*, 5 min, 4 °C) cells were fixed with FoxP3/Transcription factor staining buffer set

(ThermoFischer scientific) for 10 min at 4 °C. Permeabilization was performed using the kits reagents according to manufacturer's instructions. Subsequently, antibody staining solutions in permeabilization buffer were applied to permeabilized cell samples and incubated at 4 °C for 15 - 30 min to analyse the expression of intracellular proteins. Following two washing steps (500 g, 5 min, 4 °C) flow cytometry analysis was performed using the Canto II (BD Biosciences) or the NovoCyte Quanteon (Agilent Technologies™).

7.2.31.2 General gating strategy

The first gate in SSC-H/FSC-H plot was set according to lymphocyte's size and granularity (**Figure 33A**). Using FSC-A/FSC-H plots for doublet discrimination, only events within a diagonal gate were included for further analysis (**Figure 33B**). Finally, gating on CD4 expressing cells that were not stained by LIVE/DEAD™ Fixable Aqua Dead Cell Stain Kit, for 405 nm excitation (ThermoFischer scientific) resulted in the CD4+ living T-cell population used for further analysis (**Figure 33C**). Flow cytometry data were analysed using the Flowjo 10 software (FlowJo, LLC).
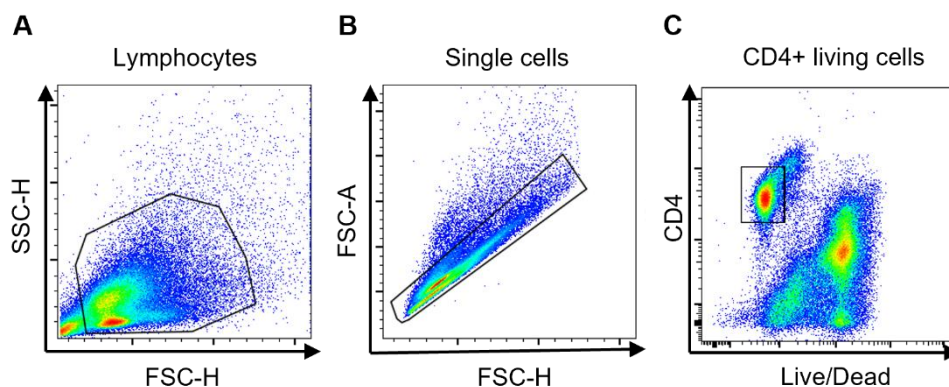
Figure 33. Gating strategy for flow cytometry analysis. (**A**) Lymphocytes were identified according to their size and granularity in the SSC-H/FSC-H plot. (**B**) Doublet discrimination was carried out by gating only those cells lying on a diagonal in the FSC-A/FSC-H plot. (**C**) Target cells were identified as CD4+live/dead- cells according to fluorescent staining of CD4 and a live/dead marker.

7.2.31.3 Gating strategy for Treg suppression assay

The first gate was set in the SSC-H/FSC-H plot according to lymphocyte's size and granularity (**Figure 34A**). Doublet discrimination was carried out on this gate in the

FSC-A/FSC-H plot by including only those events lying on a diagonal (**Figure 34B**). Finally, target cells were identified as eFluor450 positive cells that were not stained by LIVE/DEAD™ Fixable Aqua Dead Cell Stain Kit, for 405 nm excitation (ThermoFischer scientific) (**Figure 34C**). Proliferation was analysed by gating on cells that displayed eFluor450 dilutions, indicating one or more cell divisions (**Figure 34D**). Flow cytometry data were analysed using the Flowjo 10 software (FlowJo, LLC).
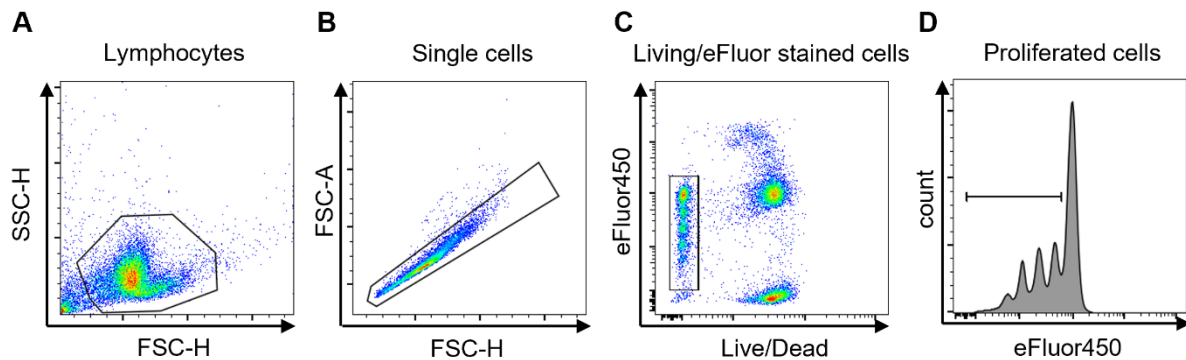
Figure 34. **Gating strategy for Treg suppression assay.** (**A**) Lymphocytes were identified according to their size and granularity in the SSC-H/FSC-H plot. (**B**) Doublet discrimination was carried out by gating only those cells lying on a diagonal in the FSC-A/FSC-H plot. (**C**) Target cells were gated as live/dead-eFluor450+ cells. (**D**) Cells that underwent one or more divisions were considered for the proliferation gate.

7.2.31.4   Gating strategy for T-cell population tracing

Living CD4+ T cells were identified as described in section 7.2.31.2 (**Figure 35A-C**). Gating on Foxp3+ T cells (**Figure 35D**) revealed the origin from eFluor670-labelled CD4+CD25+ Treg cells or eFluor450-labelled CD4+CD25- Tcon cells (**Figure 35E**).
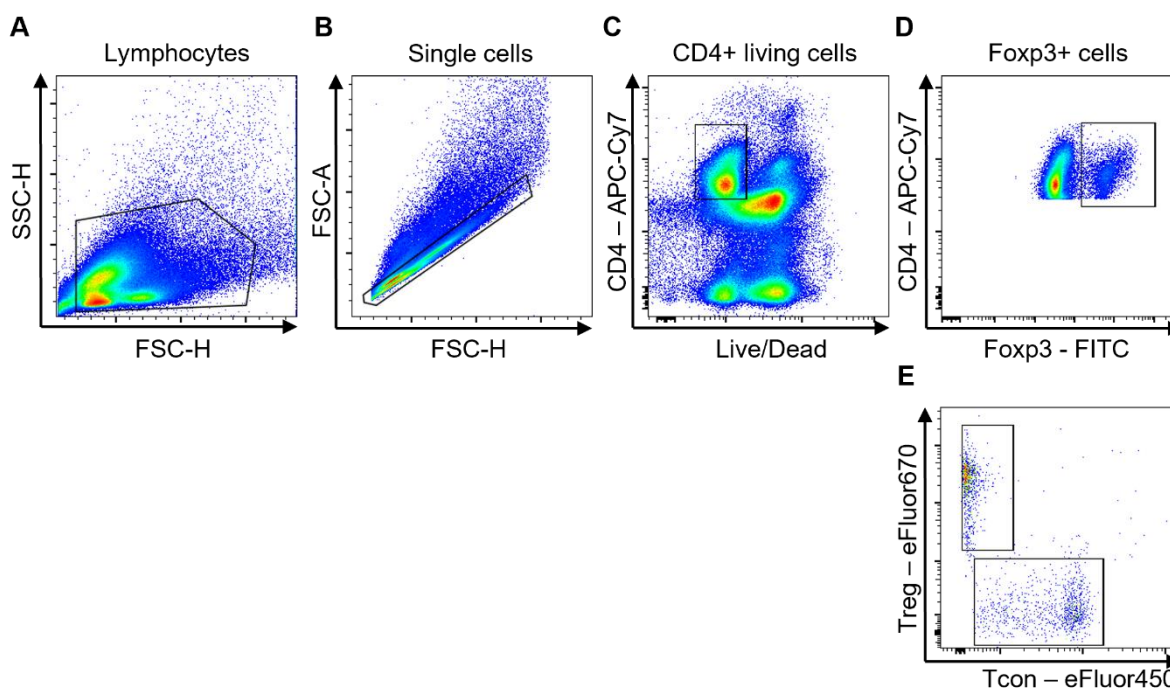
Figure 35. Gating strategy for T-cell population tracing. (**A**) Lymphocytes were gated according to their size and granularity in the SSC-H/FSC-H plot. (**B**) Single cell discrimination was carried out in the FSC-A/FSC-H plot and (**C**) living CD4 cells identified as the CD4+live/dead- population. (**D**) Foxp3+ cells were gated and (**E**) analysed for their origin from distinct T-cell populations labelled with eFluor450 or eFluor670 straining.

7.2.32   Sample preparation for SDS PAGE

Cells were harvested and washed twice in PBS. Lysis was performed in RIPA buffer supplemented with Halt™ protease and phosphatase inhibitors (ThermoFischer scientific) for at least 30 min on ice with occasional vortexing. After two sonication steps in an ultrasonic water bath for 5 min each with 5 min resting time on ice in between, the lysate was cleared by centrifugation at 20,000 g for 20 min at 4 °C. Supernatants were used for subsequent analysis.

7.2.33   Measurement of protein concentration

For measuring protein concentrations Pierce™ BCA Protein Assay Kit (ThermoFischer scientific) was used. Albumin standards were prepared according to manufacturer's instructions and stored at -20 °C for further use. 10 µL of standard and a defined volume of sample were mixed with 200 µL of the working reagent in a 96-well plate

and incubated at 37 °C for 30 min. in proportion to the protein content in samples, complexes between cuprous cation and bicinchoninic acid are formed and quantified by absorbance at 562 nm using a microplate reader (Tecan Spark).

7.2.34 SDS PAGE

To achieve an even protein concentration across samples, based on BCA assay results described in section 7.2.33, loaded sample volumes were adjusted with RIPA buffer, accordingly. The samples were mixed with 4x Lämmli buffer (Bio-Rad Laboratories, Inc.) to achieve a 1x solution and were boiled at 95 °C for 5 - 10 min. TGX stain-free gels (Bio-Rad Laboratories, Inc.) were used for protein separation of samples at 120 V in running buffer until desired separation was reached.

7.2.35 Coomassie staining

After SDS PAGE Coomassie Brilliant Blue solution was applied for 30 min at RT to stain proteins in the gel. Destaining was performed for up to 16 hours at RT in Coomassie destaining solution with gentle agitation. Bands were detected with the ChemiDoc™ system (Bio-Rad Laboratories, Inc.).

7.2.36 Immunoblot

After separation of samples by SDS PAGE the gel was blotted on a methanol activated polyvinylidene fluoride (PVDF) membrane at 100 V for 75 min in Transfer Buffer on ice. The membrane was blocked in 10% TBS-T milk for one hour and then incubated with the primary antibody in 2.5% TBS-T milk or 2.5% BSA in TBS-T solution overnight at 4 °C or for one hour at RT. After three washes in TBS-T for 5 - 10 min each, the membrane was incubated with the secondary HRP-coupled antibody for one hour at RT, followed again by three TBS-T washes. Protein detection was performed using ECL Western Blotting detection reagent (Cytiva) and imaging on the ChemiDoc™ system (Bio-Rad Laboratories, Inc.).

7.2.37 Statistical Analysis

Statistical analysis was performed using GraphPad Prism software (version 9). Gaussian distribution of data points was tested by Shapiro-Wilk normality test. If the normality test was passed, a paired or unpaired Student's t-test for two samples was carried out. One or Two Way ANOVA was performed for multiple comparisons. If normality criteria weren't matched, non-parametric Wilcoxon or Kruskal Wallis tests were carried out, respectively. For statistical analysis of normalised data one sample t-tests were applied. Values are expressed as mean ± SEM and differences were considered significant at p-values < 0.05 (*p < 0.05, **p < 0.01, ***p < 0.001 and ****p < 0.0001).

8 References

1.   Tang, D., et al., *PAMPs and DAMPs: signal 0s that spur autophagy and immunity.* Immunol Rev, 2012. **249**(1): p. 158-75.
2.   Rosati, E., et al., *Overview of methodologies for T-cell receptor repertoire analysis.* BMC Biotechnol, 2017. **17**(1): p. 61.
3.   Ciofani, M. and J.C. Zúñiga-Pflücker, *Determining γδ versus αβ T cell development.* Nature Reviews Immunology, 2010. **10**(9): p. 657-663.
4.   Luckheeram, R.V., et al., *CD4+T cells: differentiation and functions.* Clin Dev Immunol, 2012. **2012**: p. 925135.
5.   Shah, K., et al., *T cell receptor (TCR) signaling in health and disease.* Signal Transduction and Targeted Therapy, 2021. **6**(1): p. 412.
6.   McAdam, A.J., A.N. Schweitzer, and A.H. Sharpe, *The role of B7 co-stimulation in activation and differentiation of CD4+ and CD8+ T cells.* Immunol Rev, 1998. **165**: p. 231-47.
7.   Moser, M. and K.M. Murphy, *Dendritic cell regulation of TH1-TH2 development.* Nature Immunology, 2000. **1**(3): p. 199-205.
8.   Mosmann, T.R., et al., *Two types of murine helper T cell clone. I. Definition according to profiles of lymphokine activities and secreted proteins. 1986.* J Immunol, 2005. **175**(1): p. 5-14.
9.   Bluestone, J.A., et al., *The functional plasticity of T cell subsets.* Nat Rev Immunol, 2009. **9**(11): p. 811-6.
10.   Huber, S., et al., *CD4(+) T Helper Cell Plasticity in Infection, Inflammation, and Autoimmunity.* Mediators Inflamm, 2017. **2017**: p. 7083153.
11.   Koenen, H.J., et al., *Human CD25highFoxp3pos regulatory T cells differentiate into IL-17-producing cells.* Blood, 2008. **112**(6): p. 2340-52.
12.   Caza, T. and S. Landas, *Functional and Phenotypic Plasticity of CD4(+) T Cell Subsets.* Biomed Res Int, 2015. **2015**: p. 521957.
13.   Wilson, C.B., E. Rowell, and M. Sekimata, *Epigenetic control of T-helper-cell differentiation.* Nature Reviews Immunology, 2009. **9**(2): p. 91-105.
14.   Jäger, A. and V.K. Kuchroo, *Effector and regulatory T-cell subsets in autoimmunity and tissue inflammation.* Scand J Immunol, 2010. **72**(3): p. 173-84.
15.   Aarvak, T., et al., *IL-17 is produced by some proinflammatory Th1/Th0 cells but not by Th2 cells.* J Immunol, 1999. **162**(3): p. 1246-51.
16.   Shahrara, S., et al., *TH-17 cells in rheumatoid arthritis.* Arthritis Res Ther, 2008. **10**(4): p. R93.
17.   Kim, J., et al., *Elevated levels of T helper 17 cells are associated with disease activity in patients with rheumatoid arthritis.* Ann Lab Med, 2013. **33**(1): p. 52-9.
18.   Leppkes, M., et al., *RORgamma-expressing Th17 cells induce murine chronic intestinal inflammation via redundant effects of IL-17A and IL-17F.* Gastroenterology, 2009. **136**(1): p. 257-67.
19.   Fujino, S., et al., *Increased expression of interleukin 17 in inflammatory bowel disease.* Gut, 2003. **52**(1): p. 65-70.
20.   Annunziato, F., et al., *Phenotypic and functional features of human Th17 cells.* J Exp Med, 2007. **204**(8): p. 1849-61.
21.   Li, J., et al., *Profiles of Lamina Propria T Helper Cell Subsets Discriminate Between Ulcerative Colitis and Crohn's Disease.* Inflamm Bowel Dis, 2016. **22**(8): p. 1779-92.

22. Kaskow, B.J. and C. Baecher-Allan, *Effector T Cells in Multiple Sclerosis.* Cold Spring Harb Perspect Med, 2018. **8**(4).

23. Brucklacher-Waldert, V., et al., *Phenotypical and functional characterization of T helper 17 cells in multiple sclerosis.* Brain, 2009. **132**(Pt 12): p. 3329-41.

24. Murphy, A.C., et al., *Infiltration of Th1 and Th17 cells and activation of microglia in the CNS during the course of experimental autoimmune encephalomyelitis.* Brain Behav Immun, 2010. **24**(4): p. 641-51.

25. Codarri, L., et al., *RORγt drives production of the cytokine GM-CSF in helper T cells, which is essential for the effector phase of autoimmune neuroinflammation.* Nat Immunol, 2011. **12**(6): p. 560-7.

26. Sakaguchi, S., et al., *Immunologic self-tolerance maintained by activated T cells expressing IL-2 receptor alpha-chains (CD25). Breakdown of a single mechanism of self-tolerance causes various autoimmune diseases.* J Immunol, 1995. **155**(3): p. 1151-64.

27. Hori, S., T. Nomura, and S. Sakaguchi, *Control of regulatory T cell development by the transcription factor Foxp3.* Science, 2003. **299**(5609): p. 1057-61.

28. Fontenot, J.D., M.A. Gavin, and A.Y. Rudensky, *Foxp3 programs the development and function of CD4+CD25+ regulatory T cells.* Nat Immunol, 2003. **4**(4): p. 330-6.

29. Singh, K., et al., *Concomitant analysis of Helios and Neuropilin-1 as a marker to detect thymic derived regulatory T cells in naïve mice.* Sci Rep, 2015. **5**: p. 7767.

30. Weiss, J.M., et al., *Neuropilin 1 is expressed on thymus-derived natural regulatory T cells, but not mucosa-generated induced Foxp3+ T reg cells.* J Exp Med, 2012. **209**(10): p. 1723-42, s1.

31. Tran, D.Q., H. Ramsey, and E.M. Shevach, *Induction of FOXP3 expression in naive human CD4+FOXP3 T cells by T-cell receptor stimulation is transforming growth factor-beta dependent but does not confer a regulatory phenotype.* Blood, 2007. **110**(8): p. 2983-90.

32. Gavin, M.A., et al., *Single-cell analysis of normal and FOXP3-mutant human T cells: FOXP3 expression without regulatory T cell development.* Proc Natl Acad Sci U S A, 2006. **103**(17): p. 6659-64.

33. Choi, J.M., et al., *Cell-permeable Foxp3 protein alleviates autoimmune disease associated with inflammatory bowel disease and allergic airway inflammation.* Proc Natl Acad Sci U S A, 2010. **107**(43): p. 18575-80.

34. Kröger, B., et al., *Expression of full-length FOXP3 exceeds other isoforms in thymus and stimulated CD4 + T cells.* J Clin Immunol, 2024. **44**(5): p. 114.

35. Vignali, D.A., L.W. Collison, and C.J. Workman, *How regulatory T cells work.* Nat Rev Immunol, 2008. **8**(7): p. 523-32.

36. Itahashi, K., T. Irie, and H. Nishikawa, *Regulatory T-cell development in the tumor microenvironment.* European Journal of Immunology, 2022. **52**(8): p. 1216-1227.

37. Joetham, A., et al., *Naturally occurring lung CD4(+)CD25(+) T cell regulation of airway allergic responses depends on IL-10 induction of TGF-beta.* J Immunol, 2007. **178**(3): p. 1433-42.

38. Asseman, C., et al., *An essential role for interleukin 10 in the function of regulatory T cells that inhibit intestinal inflammation.* J Exp Med, 1999. **190**(7): p. 995-1004.

39. Amado, I.F., et al., *IL-2 coordinates IL-2-producing and regulatory T cell interplay.* J Exp Med, 2013. **210**(12): p. 2707-20.

40. Setoguchi, R., et al., *Homeostatic maintenance of natural Foxp3(+) CD25(+) CD4(+) regulatory T cells by interleukin (IL)-2 and induction of autoimmune disease by IL-2 neutralization.* J Exp Med, 2005. **201**(5): p. 723-35.

41. Caudy, A.A., et al., *CD25 deficiency causes an immune dysregulation, polyendocrinopathy, enteropathy, X-linked-like syndrome, and defective IL-10 expression from CD4 lymphocytes.* J Allergy Clin Immunol, 2007. **119**(2): p. 482-7.

42. Kofoed, E.M., et al., *Growth hormone insensitivity associated with a STAT5b mutation.* N Engl J Med, 2003. **349**(12): p. 1139-47.

43. Kuehn, H.S., et al., *Immune dysregulation in human subjects with heterozygous germline mutations in CTLA4.* Science, 2014. **345**(6204): p. 1623-1627.

44. Schubert, D., et al., *Autosomal dominant immune dysregulation syndrome in humans with CTLA4 mutations.* Nat Med, 2014. **20**(12): p. 1410-1416.

45. Lo, B., et al., *AUTOIMMUNE DISEASE. Patients with LRBA deficiency show CTLA4 loss and immune dysregulation responsive to abatacept therapy.* Science, 2015. **349**(6246): p. 436-40.

46. Allard, B., et al., *The ectonucleotidases CD39 and CD73: Novel checkpoint inhibitor targets.* Immunol Rev, 2017. **276**(1): p. 121-144.

47. Borsellino, G., et al., *Expression of ectonucleotidase CD39 by Foxp3+ Treg cells: hydrolysis of extracellular ATP and immune suppression.* Blood, 2007. **110**(4): p. 1225-32.

48. Cao, X., et al., *Granzyme B and perforin are important for regulatory T cell-mediated suppression of tumor clearance.* Immunity, 2007. **27**(4): p. 635-46.

49. Loebbermann, J., et al., *Regulatory T cells expressing granzyme B play a critical role in controlling lung inflammation during acute viral infection.* Mucosal Immunol, 2012. **5**(2): p. 161-72.

50. Yagi, H., et al., *Crucial role of FOXP3 in the development and function of human CD25+CD4+ regulatory T cells.* Int Immunol, 2004. **16**(11): p. 1643-56.

51. Brunkow, M.E., et al., *Disruption of a new forkhead/winged-helix protein, scurfin, results in the fatal lymphoproliferative disorder of the scurfy mouse.* Nat Genet, 2001. **27**(1): p. 68-73.

52. Bennett, C.L., et al., *The immune dysregulation, polyendocrinopathy, enteropathy, X-linked syndrome (IPEX) is caused by mutations of FOXP3.* Nat Genet, 2001. **27**(1): p. 20-1.

53. Marie, J.C., et al., *TGF-beta1 maintains suppressor function and Foxp3 expression in CD4+CD25+ regulatory T cells.* J Exp Med, 2005. **201**(7): p. 1061-7.

54. Williams, L.M. and A.Y. Rudensky, *Maintenance of the Foxp3-dependent developmental program in mature regulatory T cells requires continued expression of Foxp3.* Nat Immunol, 2007. **8**(3): p. 277-84.

55. Zheng, Y., et al., *Role of conserved non-coding DNA elements in the Foxp3 gene in regulatory T-cell fate.* Nature, 2010. **463**(7282): p. 808-12.

56. Li, X., et al., *Function of a Foxp3 cis-element in protecting regulatory T cell identity.* Cell, 2014. **158**(4): p. 734-748.

57. Alvarez Salazar, E.K., et al., *Methylation of FOXP3 TSDR Underlies the Impaired Suppressive Function of Tregs from Long-term Belatacept-Treated Kidney Transplant Patients.* Front Immunol, 2017. **8**: p. 219.

58. Baron, U., et al., *DNA demethylation in the human FOXP3 locus discriminates regulatory T cells from activated FOXP3(+) conventional T cells.* Eur J Immunol, 2007. **37**(9): p. 2378-89.

59. Floess, S., et al., *Epigenetic control of the foxp3 locus in regulatory T cells.* PLoS Biol, 2007. **5**(2): p. e38.

60. van Loosdregt, J., et al., *Regulation of Treg functionality by acetylation-mediated Foxp3 protein stabilization.* Blood, 2010. **115**(5): p. 965-74.

61. Kumar, S., et al., *CD4+CD25+ T regs with acetylated FoxP3 are associated with immune suppression in human leprosy.* Mol Immunol, 2013. **56**(4): p. 513-20.

62. Deng, G., et al., *Pim-2 Kinase Influences Regulatory T Cell Function and Stability by Mediating Foxp3 Protein N-terminal Phosphorylation.* J Biol Chem, 2015. **290**(33): p. 20211-20.

63. Wang, L., et al., *Ubiquitin-specific Protease-7 Inhibition Impairs Tip60-dependent Foxp3+ T-regulatory Cell Function and Promotes Antitumor Immunity.* EBioMedicine, 2016. **13**: p. 99-112.

64. Peng, H.Y., et al., *Metabolic Reprogramming and Reactive Oxygen Species in T Cell Immunity.* Front Immunol, 2021. **12**: p. 652687.

65. van der Windt, G.J. and E.L. Pearce, *Metabolic switching and fuel choice during T-cell differentiation and memory development.* Immunol Rev, 2012. **249**(1): p. 27-42.

66. Xu, S., et al., *Interleukin-6 classic and trans-signaling utilize glucose metabolism reprogramming to achieve anti- or pro-inflammatory effects.* Metabolism, 2024. **155**: p. 155832.

67. Düvel, K., et al., *Activation of a metabolic gene regulatory network downstream of mTOR complex 1.* Mol Cell, 2010. **39**(2): p. 171-83.

68. Macintyre, A.N., et al., *The glucose transporter Glut1 is selectively essential for CD4 T cell activation and effector function.* Cell Metab, 2014. **20**(1): p. 61-72.

69. Michalek, R.D., et al., *Cutting edge: distinct glycolytic and lipid oxidative metabolic programs are essential for effector and regulatory CD4+ T cell subsets.* J Immunol, 2011. **186**(6): p. 3299-303.

70. Gerriets, V.A., et al., *Foxp3 and Toll-like receptor signaling balance T(reg) cell anabolic metabolism for suppression.* Nat Immunol, 2016. **17**(12): p. 1459-1466.

71. Patsoukis, N., et al., *PD-1 alters T-cell metabolic reprogramming by inhibiting glycolysis and promoting lipolysis and fatty acid oxidation.* Nat Commun, 2015. **6**: p. 6692.

72. Ma, S., et al., *Cellular metabolism regulates the differentiation and function of T-cell subsets.* Cell Mol Immunol, 2024. **21**(5): p. 419-435.

73. Sena, Laura A., et al., *Mitochondria Are Required for Antigen-Specific T Cell Activation through Reactive Oxygen Species Signaling.* Immunity, 2013. **38**(2): p. 225-236.

74. Chávez, M.D. and H.M. Tse, *Targeting Mitochondrial-Derived Reactive Oxygen Species in T Cell-Mediated Autoimmune Diseases.* Front Immunol, 2021. **12**: p. 703972.

75. Yang, Y., et al., *Reactive oxygen species in the immune system.* Int Rev Immunol, 2013. **32**(3): p. 249-70.

76. Sun, L., et al., *T cells in health and disease.* Signal Transduction and Targeted Therapy, 2023. **8**(1): p. 235.

77. Seiringer, P., N. Garzorz-Stark, and K. Eyerich, *T-Cell–Mediated Autoimmunity: Mechanisms and Future Directions.* J Invest Dermatol, 2022. **142**(3 Pt B): p. 804-810.

78. So, M., et al., *Proinsulin C-peptide is an autoantigen in people with type 1 diabetes.* Proc Natl Acad Sci U S A, 2018. **115**(42): p. 10732-10737.

79. Plochg, B.F.J., et al., *Liver damage promotes pro-inflammatory T-cell responses against apolipoprotein B-100.* J Intern Med, 2022. **291**(5): p. 648-664.

80.   van Roon, J.A., et al., *Numbers of CD25+Foxp3+ T cells that lack the IL-7 receptor are increased intra-articularly and have impaired suppressive function in RA patients.* Rheumatology (Oxford), 2010. **49**(11): p. 2084-9.

81.   Hirota, K., et al., *Autoimmune Th17 Cells Induced Synovial Stromal and Innate Lymphoid Cell Secretion of the Cytokine GM-CSF to Initiate and Augment Autoimmune Arthritis.* Immunity, 2018. **48**(6): p. 1220-1232.e5.

82.   Viglietta, V., et al., *Loss of functional suppression by CD4+CD25+ regulatory T cells in patients with multiple sclerosis.* J Exp Med, 2004. **199**(7): p. 971-9.

83.   Venken, K., et al., *Compromised CD4+ CD25(high) regulatory T-cell function in patients with relapsing-remitting multiple sclerosis is correlated with a reduced frequency of FOXP3-positive cells and reduced FOXP3 expression at the single-cell level.* Immunology, 2008. **123**(1): p. 79-89.

84.   Bonelli, M., et al., *Quantitative and qualitative deficiencies of regulatory T cells in patients with systemic lupus erythematosus (SLE).* Int Immunol, 2008. **20**(7): p. 861-8.

85.   Crispín, J.C., et al., *Pathogenesis of human systemic lupus erythematosus: recent advances.* Trends Mol Med, 2010. **16**(2): p. 47-57.

86.   Müller, S., et al., *Activated CD4+ and CD8+ cytotoxic cells are present in increased numbers in the intestinal mucosa from patients with active inflammatory bowel disease.* Am J Pathol, 1998. **152**(1): p. 261-8.

87.   Pariente, B., et al., *Activation of the receptor NKG2D leads to production of Th17 cytokines in CD4+ T cells of patients with Crohn's disease.* Gastroenterology, 2011. **141**(1): p. 217-26, 226.e1-2.

88.   Jaeger, N., et al., *Single-cell analyses of Crohn's disease tissues reveal intestinal intraepithelial T cells heterogeneity and altered subset distributions.* Nat Commun, 2021. **12**(1): p. 1921.

89.   Ebert, O., et al., *Lymphocyte apoptosis: induction by gene transfer techniques.* Gene Ther, 1997. **4**(4): p. 296-302.

90.   Choi, J.M., et al., *Transduction of the cytoplasmic domain of CTLA-4 inhibits TcR-specific activation signals and prevents collagen-induced arthritis.* Proc Natl Acad Sci U S A, 2008. **105**(50): p. 19875-80.

91.   Kumble, K.D. and A. Kornberg, *Inorganic polyphosphate in mammalian cells and tissues.* J Biol Chem, 1995. **270**(11): p. 5818-22.

92.   Kornberg, A., N.N. Rao, and D. Ault-Riché, *Inorganic polyphosphate: a molecule of many functions.* Annu Rev Biochem, 1999. **68**: p. 89-125.

93.   Dunn, T., K. Gable, and T. Beeler, *Regulation of cellular Ca2+ by yeast vacuoles.* J Biol Chem, 1994. **269**(10): p. 7273-8.

94.   Archibald, F.S. and I. Fridovich, *Investigations of the state of the manganese in Lactobacillus plantarum.* Arch Biochem Biophys, 1982. **215**(2): p. 589-96.

95.   Boyineni, J., et al., *Inorganic polyphosphate as an energy source in tumorigenesis.* Oncotarget, 2020. **11**(50): p. 4613-4624.

96.   Mailer, R.K.W., et al., *Polyphosphate as a Target for Interference With Inflammation and Thrombosis.* Front Med (Lausanne), 2019. **6**: p. 76.

97.   Baev, A.Y., P.R. Angelova, and A.Y. Abramov, *Inorganic polyphosphate is produced and hydrolyzed in F0F1-ATP synthase of mammalian mitochondria.* Biochem J, 2020. **477**(8): p. 1515-1524.

98.   Lonetti, A., et al., *Identification of an evolutionarily conserved family of inorganic polyphosphate endopolyphosphatases.* J Biol Chem, 2011. **286**(37): p. 31966-74.

99.   Müller, W.E., et al., *Amorphous Ca^{2+} polyphosphate nanoparticles regulate the ATP level in bone-like SaOS-2 cells.* J Cell Sci, 2015. **128**(11): p. 2202-7.

100. Samper-Martín, B., et al., *Polyphosphate degradation by Nudt3-Zn(2+) mediates oxidative stress response.* Cell Rep, 2021. **37**(7): p. 110004.

101. Hambardikar, V., et al., *Enzymatic Depletion of Mitochondrial Inorganic Polyphosphate (polyP) Increases the Generation of Reactive Oxygen Species (ROS) and the Activity of the Pentose Phosphate Pathway (PPP) in Mammalian Cells.* Antioxidants (Basel), 2022. **11**(4).

102. Solesio, M.E., et al., *Depletion of mitochondrial inorganic polyphosphate (polyP) in mammalian cells causes metabolic shift from oxidative phosphorylation to glycolysis.* Biochemical Journal, 2021. **478**(8): p. 1631-1646.

103. Pavlov, E., et al., *Inorganic polyphosphate and energy metabolism in mammalian cells.* J Biol Chem, 2010. **285**(13): p. 9420-9428.

104. Mailer, R.K., et al., *Xenotropic and polytropic retrovirus receptor 1 regulates procoagulant platelet polyphosphate.* Blood, 2021. **137**(10): p. 1392-1405.

105. Morrissey, J.H., S.H. Choi, and S.A. Smith, *Polyphosphate: an ancient molecule that links platelets, coagulation, and inflammation.* Blood, 2012. **119**(25): p. 5972-9.

106. Hassanian, S.M., et al., *Inorganic polyphosphate elicits pro-inflammatory responses through activation of the mammalian target of rapamycin complexes 1 and 2 in vascular endothelial cells.* J Thromb Haemost, 2015. **13**(5): p. 860-71.

107. Arredondo, C., et al., *Excessive release of inorganic polyphosphate by ALS/FTD astrocytes causes non-cell-autonomous toxicity to motoneurons.* Neuron, 2022. **110**(10): p. 1656-1670 e12.

108. Angelova, Plamena R., et al., *Role of inorganic polyphosphate in mammalian cells: from signal transduction and mitochondrial metabolism to cell death.* Biochemical Society Transactions, 2016. **44**(1): p. 40-45.

109. Dinarvand, P., et al., *Polyphosphate amplifies proinflammatory responses of nuclear proteins through interaction with receptor for advanced glycation end products and P2Y1 purinergic receptor.* Blood, 2014. **123**(6): p. 935-45.

110. Bae, J.S., W. Lee, and A.R. Rezaie, *Polyphosphate elicits pro-inflammatory responses that are counteracted by activated protein C in both cellular and animal models.* J Thromb Haemost, 2012. **10**(6): p. 1145-51.

111. Kullik, G.A., M. Waldmann, and T. Renné, *Analysis of polyphosphate in mammalian cells and tissues: methods, functions and challenges.* Curr Opin Biotechnol, 2024. **90**: p. 103208.

112. Smith, S.A. and J.H. Morrissey, *Sensitive fluorescence detection of polyphosphate in polyacrylamide gels using 4',6-diamidino-2-phenylindol.* Electrophoresis, 2007. **28**(19): p. 3461-5.

113. Ruiz, F.A., et al., *Human platelet dense granules contain polyphosphate and are similar to acidocalcisomes of bacteria and unicellular eukaryotes.* J Biol Chem, 2004. **279**(43): p. 44250-7.

114. Alcid, J., et al., *A Rare Case of Hermansky-Pudlak Syndrome Type 3.* J Hematol, 2018. **7**(2): p. 76-78.

115. Argyle, J.C., et al., *T-cell lymphoma and the Chediak-Higashi syndrome.* Blood, 1982. **60**(3): p. 672-6.

116. Jumper, J., et al., *Highly accurate protein structure prediction with AlphaFold.* Nature, 2021. **596**(7873): p. 583-589.

117. Labberton, L., et al., *A Flow Cytometry-Based Assay for Procoagulant Platelet Polyphosphate.* Cytometry B Clin Cytom, 2018. **94**(2): p. 369-373.

118. Lewis, R.S., *Calcium signaling mechanisms in T lymphocytes.* Annu Rev Immunol, 2001. **19**: p. 497-521.

119. Lavoie, H., J. Gagnon, and M. Therrien, *ERK signalling: a master regulator of cell behaviour, life and fate.* Nat Rev Mol Cell Biol, 2020. **21**(10): p. 607-632.

120. Wang, R., et al., *The transcription factor Myc controls metabolic reprogramming upon T lymphocyte activation.* Immunity, 2011. **35**(6): p. 871-82.

121. Zheng, S.G., et al., *TGF-β Requires CTLA-4 Early after T Cell Activation to Induce FoxP3 and Generate Adaptive CD4+CD25+ Regulatory Cells1.* The Journal of Immunology, 2006. **176**(6): p. 3321-3329.

122. Müller, F., et al., *Platelet Polyphosphates Are Proinflammatory and Procoagulant Mediators In Vivo.* Cell, 2009. **139**(6): p. 1143-1156.

123. Suess, P.M., et al., *Extracellular Polyphosphate Promotes Macrophage and Fibrocyte Differentiation, Inhibits Leukocyte Proliferation, and Acts as a Chemotactic Agent for Neutrophils.* J Immunol, 2019. **203**(2): p. 493-499.

124. Summers, C., et al., *Neutrophil kinetics in health and disease.* Trends Immunol, 2010. **31**(8): p. 318-24.

125. Brinkmann, V., et al., *Neutrophil extracellular traps kill bacteria.* Science, 2004. **303**(5663): p. 1532-5.

126. Papayannopoulos, V., *Neutrophil extracellular traps in immunity and disease.* Nat Rev Immunol, 2018. **18**(2): p. 134-147.

127. Hou, Q., et al., *Inhibition of IP6K1 suppresses neutrophil-mediated pulmonary damage in bacterial pneumonia.* Sci Transl Med, 2018. **10**(435).

128. Pirttiniemi, A., et al., *Long-chain polyphosphates inhibit type I interferon signaling and augment LPS-induced cytokine secretion in human leukocytes.* Journal of Leukocyte Biology, 2023. **114**(3): p. 250-265.

129. Roewe, J., et al., *Bacterial polyphosphates interfere with the innate host defense to infection.* Nat Commun, 2020. **11**(1): p. 4035.

130. Ito, T., et al., *Inorganic polyphosphate potentiates lipopolysaccharide-induced macrophage inflammatory response.* J Biol Chem, 2020. **295**(12): p. 4014-4023.

131. Segawa, S., et al., *Probiotic-derived polyphosphate enhances the epithelial barrier function and maintains intestinal homeostasis through integrin-p38 MAPK pathway.* PLoS One, 2011. **6**(8): p. e23278.

132. Fujiya, M., et al., *Long-Chain Polyphosphate Is a Potential Agent for Inducing Mucosal Healing of the Colon in Ulcerative Colitis.* Clin Pharmacol Ther, 2020. **107**(2): p. 452-461.

133. Moreno-Sanchez, D., et al., *Polyphosphate is a novel pro-inflammatory regulator of mast cells and is located in acidocalcisomes.* J Biol Chem, 2012. **287**(34): p. 28435-44.

134. Jin, J., et al., *CISH impairs lysosomal function in activated T cells resulting in mitochondrial DNA release and inflammaging.* Nature Aging, 2023. **3**(5): p. 600-616.

135. Abramov, A.Y., et al., *Targeted polyphosphatase expression alters mitochondrial metabolism and inhibits calcium-dependent cell death.* Proc Natl Acad Sci U S A, 2007. **104**(46): p. 18091-6.

136. Bru, S., et al., *Improvement of biochemical methods of polyP quantification.* Microb Cell, 2016. **4**(1): p. 6-15.

137. Christ, J.J. and L.M. Blank, *Analytical polyphosphate extraction from Saccharomyces cerevisiae.* Anal Biochem, 2018. **563**: p. 71-78.

138. Francis, D.M. and R. Page, *Strategies to optimize protein expression in E. coli.* Curr Protoc Protein Sci, 2010. **Chapter 5**(1): p. 5.24.1-5.24.29.

139. Rao, N.N. and A. Kornberg, *Inorganic polyphosphate supports resistance and survival of stationary-phase Escherichia coli.* J Bacteriol, 1996. **178**(5): p. 1394-400.

140. Gori, A., et al., *Cell Penetrating Peptides: Classification, Mechanisms, Methods of Study, and Applications.* ChemMedChem, 2023. **18**(17): p. e202300236.

141. Trabulo, S., et al., *Cell-Penetrating Peptides-Mechanisms of Cellular Uptake and Generation of Delivery Systems.* Pharmaceuticals (Basel), 2010. **3**(4): p. 961-993.

142. Fretz, Marjan M., et al., *Temperature-, concentration- and cholesterol-dependent translocation of L- and D-octa-arginine across the plasma and nuclear membrane of CD34+ leukaemia cells.* Biochemical Journal, 2007. **403**(2): p. 335-342.

143. Futaki, S. and I. Nakase, *Cell-Surface Interactions on Arginine-Rich Cell-Penetrating Peptides Allow for Multiplex Modes of Internalization.* Acc Chem Res, 2017. **50**(10): p. 2449-2456.

144. Maiolo, J.R., 3rd, E.A. Ottinger, and M. Ferrer, *Specific redistribution of cell-penetrating peptides from endosomes to the cytoplasm and nucleus upon laser illumination.* J Am Chem Soc, 2004. **126**(47): p. 15376-7.

145. Maiolo, J.R., M. Ferrer, and E.A. Ottinger, *Effects of cargo molecules on the cellular uptake of arginine-rich cell-penetrating peptides.* Biochim Biophys Acta, 2005. **1712**(2): p. 161-72.

146. Quintana, A., et al., *Calcium-dependent activation of T-lymphocytes.* Pflügers Archiv, 2005. **450**(1): p. 1-12.

147. Duchen, M.R., *Ca(2+)-dependent changes in the mitochondrial energetics in single dissociated mouse sensory neurons.* Biochem J, 1992. **283 (Pt 1)**(Pt 1): p. 41-50.

148. Bhosale, G., et al., *Calcium signaling as a mediator of cell energy demand and a trigger to cell death.* Ann N Y Acad Sci, 2015. **1350**(1): p. 107-16.

149. Chalmers, S. and D.G. Nicholls, *The relationship between free and total calcium concentrations in the matrix of liver and brain mitochondria.* J Biol Chem, 2003. **278**(21): p. 19062-70.

150. Solesio, M.E., et al., *Contribution of inorganic polyphosphate towards regulation of mitochondrial free calcium.* Biochim Biophys Acta, 2016. **1860**(6): p. 1317-25.

151. Solesio, M.E., et al., *Inorganic polyphosphate is required for sustained free mitochondrial calcium elevation, following calcium uptake.* Cell Calcium, 2020. **86**: p. 102127.

152. Lorents, A., et al., *Cell-penetrating peptides split into two groups based on modulation of intracellular calcium concentration.* J Biol Chem, 2012. **287**(20): p. 16880-9.

153. Dumont, F.J., et al., *Inhibition of T cell activation by pharmacologic disruption of the MEK1/ERK MAP kinase or calcineurin signaling pathways results in differential modulation of cytokine production.* J Immunol, 1998. **160**(6): p. 2579-89.

154. Suess, P.M., et al., *Extracellular polyphosphate signals through Ras and Akt to prime Dictyostelium discoideum cells for development.* J Cell Sci, 2017. **130**(14): p. 2394-2404.

155. Labberton, L., et al., *Neutralizing blood-borne polyphosphate in vivo provides safe thromboprotection.* Nat Commun, 2016. **7**: p. 12616.

156. Lin, W., et al., *Reactive Oxygen Species in Autoimmune Cells: Function, Differentiation, and Metabolism.* Front Immunol, 2021. **12**: p. 635021.

157. Gray, M.J. and U. Jakob, *Oxidative stress protection by polyphosphate--new roles for an old player.* Curr Opin Microbiol, 2015. **24**: p. 1-6.

158. Beaufay, F., et al., *Polyphosphate Functions In Vivo as an Iron Chelator and Fenton Reaction Inhibitor.* mBio, 2020. **11**(4).

159. Tse, H.M., et al., *NADPH oxidase deficiency regulates Th lineage commitment and modulates autoimmunity.* J Immunol, 2010. **185**(9): p. 5247-58.

160. Jackson, S.H., et al., *T cells express a phagocyte-type NADPH oxidase that is activated after T cell receptor stimulation.* Nat Immunol, 2004. **5**(8): p. 818-27.

161. Shatynski, K.E., et al., *Decreased STAT5 phosphorylation and GATA-3 expression in NOX2-deficient T cells: role in T helper development.* Eur J Immunol, 2012. **42**(12): p. 3202-11.

162. Efimova, O., P. Szankasi, and T.W. Kelley, *Ncf1 (p47phox) is essential for direct regulatory T cell mediated suppression of CD4+ effector T cells.* PLoS One, 2011. **6**(1): p. e16013.

163. Kurniawan, H., et al., *Glutathione Restricts Serine Metabolism to Preserve Regulatory T Cell Function.* Cell Metab, 2020. **31**(5): p. 920-936.e7.

164. Kaminski, M.M., et al., *Mitochondrial reactive oxygen species control T cell activation by regulating IL-2 and IL-4 expression: mechanism of ciprofloxacin-mediated immunosuppression.* J Immunol, 2010. **184**(9): p. 4827-41.

165. Allan, S.E., et al., *Activation-induced FOXP3 in human T effector cells does not suppress proliferation or cytokine production.* Int Immunol, 2007. **19**(4): p. 345-54.

166. Miyara, M., et al., *Functional delineation and differentiation dynamics of human CD4+ T cells expressing the FoxP3 transcription factor.* Immunity, 2009. **30**(6): p. 899-911.

167. Polansky, J.K., et al., *Methylation matters: binding of Ets-1 to the demethylated Foxp3 gene contributes to the stabilization of Foxp3 expression in regulatory T cells.* J Mol Med (Berl), 2010. **88**(10): p. 1029-40.

168. Zhou, X., et al., *Plasticity of CD4(+) FoxP3(+) T cells.* Curr Opin Immunol, 2009. **21**(3): p. 281-5.

169. Komatsu, N., et al., *Pathogenic conversion of Foxp3+ T cells into TH17 cells in autoimmune arthritis.* Nat Med, 2014. **20**(1): p. 62-8.

170. Devlin, J.C., et al., *Single-Cell Transcriptional Survey of Ileal-Anal Pouch Immune Cells From Ulcerative Colitis Patients.* Gastroenterology, 2021. **160**(5): p. 1679-1693.

171. Yu, Q.T., et al., *Expression and functional characterization of FOXP3+CD4+ regulatory T cells in ulcerative colitis.* Inflammatory Bowel Diseases, 2007. **13**(2): p. 191-199.

172. Ostanin, D.V., et al., *T cell-induced inflammation of the small and large intestine in immunodeficient mice.* Am J Physiol Gastrointest Liver Physiol, 2006. **290**(1): p. G109-19.

173. Hovhannisyan, Z., et al., *Characterization of interleukin-17-producing regulatory T cells in inflamed intestinal mucosa from patients with inflammatory bowel diseases.* Gastroenterology, 2011. **140**(3): p. 957-65.

174. Verhoef, J.J., et al., *Polyphosphate nanoparticles on the platelet surface trigger contact system activation.* Blood, 2017. **129**(12): p. 1707-1717.

175. Dias, P.R.F., et al., *Subcellular fractionation of frozen skeletal muscle samples.* Biochem Cell Biol, 2020. **98**(2): p. 293-298.

176. Wurst, H., T. Shiba, and A. Kornberg, *The gene for a major exopolyphosphatase of Saccharomyces cerevisiae.* J Bacteriol, 1995. **177**(4): p. 898-906.

177. McLean, C.Y., et al., *GREAT improves functional interpretation of cis-regulatory regions.* Nat Biotechnol, 2010. **28**(5): p. 495-501.

178. Gholizadeh, F., et al., *Modulatory Effects of M3 Muscarinic Acetylcholine Receptor on Inflammatory Profiles of Human Memory T Helper Cells.* bioRxiv, 2024: p. 2024.09. 08.611875.

179. Yang, B., et al., *Nedd4 augments the adaptive immune response by promoting ubiquitin-mediated degradation of Cbl-b in activated T cells.* Nat Immunol, 2008. **9**(12): p. 1356-63.

180. Karaselek, M.A., et al., *Molecular investigations on T cell subsets in patients affected by hypomorphic DCLRE1C mutation.* Expert Review of Clinical Immunology, 2025. **21**(3): p. 393-399.

181. Silva-Santos, B., et al., *MicroRNAs-122 and-1247 restrain the pathogenicity of effector CD4+ T cells in autoimmune inflammation.* 2024.

182. Chan, Y.-L., et al., *TIAM2S mediates serotonin homeostasis and provokes a pro-inflammatory immune microenvironment permissive for colorectal tumorigenesis.* Cancers, 2020. **12**(7): p. 1844.

183. Zhang, H., et al., *TFAP2C exacerbates psoriasis-like inflammation by promoting Th17 and Th1 cells activation through regulating TEAD4 transcription.* Allergologia et immunopathologia, 2023. **51**(3): p. 124-134.

184. Mukohara, F., et al., *Somatic mutations in tumor-infiltrating lymphocytes impact on antitumor immunity.* Proceedings of the National Academy of Sciences, 2024. **121**(35): p. e2320189121.

185. Hou, Y., et al., *Neuropeptide signalling orchestrates T cell differentiation.* Nature, 2024: p. 1-9.

186. Lapinski, P.E. and P.D. King, *Regulation of Ras signal transduction during T cell development and activation.* Am J Clin Exp Immunol, 2012. **1**(2): p. 147-153.

187. Gomez-Rodriguez, J., Z.J. Kraus, and P.L. Schwartzberg, *Tec family kinases Itk and Rlk / Txk in T lymphocytes: cross-regulation of cytokine production and T-cell fates.* FEBS J, 2011. **278**(12): p. 1980-9.

188. Readinger, J.A., et al., *Tec kinases regulate T-lymphocyte development and function: new insights into the roles of Itk and Rlk/Txk.* Immunol Rev, 2009. **228**(1): p. 93-114.

189. Sommers, C.L., et al., *A role for the Tec family tyrosine kinase Txk in T cell activation and thymocyte selection.* J Exp Med, 1999. **190**(10): p. 1427-38.

190. Kaskow, B.J., et al., *MS AHI1 genetic risk promotes IFNgamma(+) CD4(+) T cells.* Neurol Neuroimmunol Neuroinflamm, 2018. **5**(1): p. e414.

191. Weiss, J.M., et al., *ROCK2 signaling is required to induce a subset of T follicular helper cells through opposing effects on STATs in autoimmune settings.* Sci Signal, 2016. **9**(437): p. ra73.

192. Wang, B. and Q. Bian, *SATB1 prevents immune cell infiltration by regulating chromatin organization and gene expression of a chemokine gene cluster in T cells.* Communications Biology, 2024. **7**(1): p. 1304.

193. Hong, N., et al., *In vivo overexpression of Dad1, the defender against apoptotic death-1, enhances T cell proliferation but does not protect against apoptosis.* The Journal of Immunology, 1999. **163**(4): p. 1888-1893.

194. Piroth, M., et al., *Hyaluronan synthase 3 is protective after cardiac ischemia-reperfusion by preserving the T cell response.* Matrix Biology, 2022. **112**: p. 116-131.

195. Teh, C.E., et al., *T-cell regulation by casitas B-lineage lymphoma (Cblb) is a critical failsafe against autoimmune disease due to autoimmune regulator (Aire) deficiency.* Proc Natl Acad Sci U S A, 2010. **107**(33): p. 14709-14.

196. Peer, S., G. Baier, and T. Gruber, *Cblb-deficient T cells are less susceptible to PD-L1-mediated inhibition.* Oncotarget, 2017. **8**(26): p. 41841-41853.

197. Kagami, S., et al., *Stat5a regulates T helper cell differentiation by several distinct mechanisms.* Blood, 2001. **97**(8): p. 2358-65.

198. Passerini, L., et al., *STAT5-signaling cytokines regulate the expression of FOXP3 in CD4+CD25+ regulatory T cells and CD4+CD25- effector T cells.* Int Immunol, 2008. **20**(3): p. 421-31.

199. Tarasenko, T.N., et al., *Cytochrome c oxidase activity is a metabolic checkpoint that regulates cell fate decisions during T cell activation and differentiation.* Cell metabolism, 2017. **25**(6): p. 1254-1268. e7.

200. Friesen, L.R., B. Gu, and C.H. Kim, *A ligand-independent fast function of RARalpha promotes exit from metabolic quiescence upon T cell activation and controls T cell differentiation.* Mucosal Immunol, 2021. **14**(1): p. 100-112.

201. Schneider, M.A., et al., *CCR7 is required for the in vivo function of CD4+ CD25+ regulatory T cells.* J Exp Med, 2007. **204**(4): p. 735-45.

202. Moschovakis, G.L. and R. Forster, *Multifaceted activities of CCR7 regulate T-cell homeostasis in health and disease.* Eur J Immunol, 2012. **42**(8): p. 1949-55.

203. Zhong, X.P., et al., *Enhanced T cell responses due to diacylglycerol kinase zeta deficiency.* Nat Immunol, 2003. **4**(9): p. 882-90.

204. Seki, S.M., et al., *Modulation of PKM activity affects the differentiation of T(H)17 cells.* Sci Signal, 2020. **13**(655).

205. Zheng, H., et al., *TCF12 regulates the TGF-beta/Smad2/3 signaling pathway to accelerate the progression of osteoarthritis by targeting CXCR4.* J Orthop Translat, 2024. **44**: p. 35-46.

206. Lawir, D.-F., et al., *A missense mutation in zbtb17 blocks the earliest steps of T cell differentiation in zebrafish.* Scientific reports, 2017. **7**(1): p. 44145.

207. Hu, H., et al., *Otud7b facilitates T cell activation and inflammatory responses by regulating Zap70 ubiquitination.* Journal of experimental medicine, 2016. **213**(3): p. 399-414.

208. Hu, H., et al., *OTUD7B controls non-canonical NF-kappaB activation through deubiquitination of TRAF3.* Nature, 2013. **494**(7437): p. 371-4.

209. Wiehagen, K.R., et al., *Foxp4 is dispensable for T cell development, but required for robust recall responses.* PLoS One, 2012. **7**(8): p. e42273.

210. Miyazaki, M., et al., *Id2 and Id3 maintain the regulatory T cell pool to suppress inflammatory disease.* Nat Immunol, 2014. **15**(8): p. 767-76.

211. Maruyama, T., et al., *Control of the differentiation of regulatory T cells and T(H)17 cells by the DNA-binding inhibitor Id3.* Nat Immunol, 2011. **12**(1): p. 86-95.

212. Gorczynski, R.M., *CD200: CD200R-mediated regulation of immunity.* International Scholarly Research Notices, 2012. **2012**(1): p. 682168.

213. Salmond, R.J., et al., *T-cell receptor proximal signaling via the Src-family kinases, Lck and Fyn, influences T-cell activation, differentiation, and tolerance.* Immunological reviews, 2009. **228**(1): p. 9-22.

214. Shimoda, K., et al., *Tyk2 plays a restricted role in IFNα signaling, although it is required for IL-12-mediated T cell function.* Immunity, 2000. **13**(4): p. 561-571.

215. MaruYama, T., et al., *Control of IFN-gamma production and regulatory function by the inducible nuclear protein IkappaB-zeta in T cells.* J Leukoc Biol, 2015. **98**(3): p. 385-93.

216. Okamoto, K., et al., *IkappaBzeta regulates T(H)17 development by cooperating with ROR nuclear receptors.* Nature, 2010. **464**(7293): p. 1381-5.

217. Bonnin, E., et al., *CD74 supports accumulation and function of regulatory T cells in tumors.* Nat Commun, 2024. **15**(1): p. 3749.

218. Sun, X., et al., *MTMR7 suppresses the phenotypic switching of vascular smooth muscle cell and vascular intimal hyperplasia after injury via regulating p62/mTORC1-mediated glucose metabolism.* Atherosclerosis, 2024. **390**: p. 117470.

219. Weidner, P., et al., *Myotubularin-related-protein-7 inhibits mutant (G12V) K-RAS by direct interaction.* Cancer Letters, 2024. **588**: p. 216783.

220. Guo, L., et al., *Lipid phosphatases identified by screening a mouse phosphatase shRNA library regulate T-cell differentiation and protein kinase B AKT signaling.* Proceedings of the National Academy of Sciences, 2013. **110**(20): p. E1849-E1856.

221. Yu, L., et al., *PDCD4 promotes inflammation/fibrosis by activating the PPAR-γ/NF-κB pathway in mouse atrial myocytes.* Molecular Medicine Reports, 2024. **30**(5): p. 209.

222. Lingel, H., et al., *CTLA-4-mediated posttranslational modifications direct cytotoxic T-lymphocyte differentiation.* Cell Death & Differentiation, 2017. **24**(10): p. 1739-1749.

223. Choi, H., et al., *Dual effects of Sprouty1 on TCR signaling depending on the differentiation state of the T cell.* The Journal of Immunology, 2006. **176**(10): p. 6034-6045.

224. Cekic, C., et al., *Extracellular adenosine regulates naive T cell development and peripheral maintenance.* Journal of Experimental Medicine, 2013. **210**(12): p. 2693-2706.

225. Wu, D., et al., *Unfolded protein response factor ATF6 augments T helper cell responses and promotes mixed granulocytic airway inflammation.* Mucosal immunology, 2023. **16**(4): p. 499-512.

226. Ngoenkam, J., et al., *Non-overlapping functions of Nck1 and Nck2 adaptor proteins in T cell activation.* Cell Commun Signal, 2014. **12**: p. 21.

227. Gamara, J., et al., *Arf6 regulates energy metabolism in neutrophils.* Free radical biology and medicine, 2021. **172**: p. 550-561.

228. Uechi, Y., et al., *[ORIGINAL CONTRIBUTIONS] Impaired Th2 differentiation of CD4+ T cells from Rap2b knockout mice.* 2015, 琉球大学.

229. Qiu, X., et al., *Homoharringtonine promotes heart allograft acceptance by enhancing regulatory T cells induction in a mouse model.* Chin Med J (Engl), 2024. **137**(12): p. 1453-1464.

230. Li, X., et al., *Max interacting protein 1 induces IL-17-producing T helper/regulatory T imbalance in osteoarthritis by upregulating tectonic family member 2.* Tissue Cell, 2022. **78**: p. 101906.

231. Iyer, V.S., et al., *Modulating T-cell activation with antisense oligonucleotides targeting lymphocyte cytosolic protein 2.* Journal of Autoimmunity, 2022. **131**: p. 102857.

232. Bollyky, P.L., et al., *CD44 costimulation promotes FoxP3+ regulatory T cell persistence and function via production of IL-2, IL-10, and TGF-beta.* J Immunol, 2009. **183**(4): p. 2232-41.

233. Bruck, C., et al., *Th1 and Th17 cells are resistant towards T cell activation-induced downregulation of CD6.* Clin Immunol, 2022. **238**: p. 109025.

234. Reinwald, S., et al., *CD83 expression in CD4+ T cells modulates inflammation and autoimmunity.* The Journal of Immunology, 2008. **180**(9): p. 5890-5897.

235. Lieu, Y.K., et al., *Requirement of c-myb in T cell development and in mature T cell function.* Proceedings of the National Academy of Sciences, 2004. **101**(41): p. 14853-14858.

236.	Cibrian, D. and F. Sanchez-Madrid, *CD69: from activation marker to metabolic gatekeeper.* Eur J Immunol, 2017. **47**(6): p. 946-953.

237.	Cortes, J.R., et al., *Maintenance of immune tolerance by Foxp3+ regulatory T cells requires CD69 expression.* J Autoimmun, 2014. **55**: p. 51-62.

238.	Smida, M., et al., *PAG/Cbp suppression reveals a contribution of CTLA-4 to setting the activation threshold in T cells.* Cell Communication and Signaling, 2013. **11**: p. 1-13.

239.	Owen, D.L., et al., *Identification of cellular sources of IL-2 needed for regulatory T cell development and homeostasis.* The Journal of Immunology, 2018. **200**(12): p. 3926-3933.

240.	Newton, R.H., et al., *Maintenance of CD4 T cell fitness through regulation of Foxo1.* Nat Immunol, 2018. **19**(8): p. 838-848.

241.	Jost, P., et al., *Acute Downregulation but Not Genetic Ablation of Murine MCU Impairs Suppressive Capacity of Regulatory CD4 T Cells.* Int J Mol Sci, 2023. **24**(9).

242.	Kanai, T., et al., *Identification of STAT5A and STAT5B target genes in human T cells.* PLoS One, 2014. **9**(1): p. e86790.

243.	Umhoefer, J.M., et al., *Deciphering regulation of FOXP3 expression in human conventional T cells.* bioRxiv, 2024.

244.	Wang, L., et al., *Mbd2 promotes foxp3 demethylation and T-regulatory-cell function.* Mol Cell Biol, 2013. **33**(20): p. 4106-15.

245.	Walker, L.S. and D.M. Sansom, *The emerging role of CTLA4 as a cell-extrinsic regulator of T cell responses.* Nat Rev Immunol, 2011. **11**(12): p. 852-63.

246.	Alegre, M.L., et al., *Regulation of surface and intracellular expression of CTLA4 on mouse T cells.* The Journal of Immunology, 1996. **157**(11): p. 4762-4770.

247.	Tang, A.L., et al., *CTLA4 expression is an indicator and regulator of steady-state CD4+ FoxP3+ T cell homeostasis.* J Immunol, 2008. **181**(3): p. 1806-13.

248.	Scherlinger, M., et al., *Phosphofructokinase P fine-tunes T regulatory cell metabolism, function, and stability in systemic autoimmunity.* Science Advances, 2022. **8**(48): p. eadc9657.

249.	Wan, Y.Y., *GATA3: a master of many trades in immune regulation.* Trends Immunol, 2014. **35**(6): p. 233-42.

250.	Wohlfert, E.A., et al., *GATA3 controls Foxp3(+) regulatory T cell fate during inflammation in mice.* J Clin Invest, 2011. **121**(11): p. 4503-15.

251.	Layland, L.E., et al., *Pronounced phenotype in activated regulatory T cells during a chronic helminth infection.* J Immunol, 2010. **184**(2): p. 713-24.

252.	Ding, Y., et al., *Interleukin-21 promotes germinal center reaction by skewing the follicular regulatory T cell to follicular helper T cell balance in autoimmune BXD2 mice.* Arthritis & rheumatology, 2014. **66**(9): p. 2601-2612.

253.	Jandl, C., et al., *IL-21 restricts T follicular regulatory T cell proliferation through Bcl-6 mediated inhibition of responsiveness to IL-2.* Nature communications, 2017. **8**(1): p. 14647.

254.	Tortola, L., et al., *IL-21 promotes allergic airway inflammation by driving apoptosis of FoxP3+ regulatory T cells.* Journal of Allergy and Clinical Immunology, 2019. **143**(6): p. 2178-2189. e5.

255.	Mognol, G.P., et al., *The transcriptional cofactor IRF2BP2 plays a key role in T cell homeostasis and Treg cell expansion.* bioRxiv, 2021: p. 2021.07. 29.454283.

256.	Bodor, J., et al., *ICER/CREM-mediated transcriptional attenuation of IL-2 and its role in suppression by regulatory T cells.* Eur J Immunol, 2007. **37**(4): p. 884-95.

257. Choi, S.-C., et al., *The lupus susceptibility gene Pbx1 regulates the balance between follicular helper T cell and regulatory T cell differentiation.* The Journal of Immunology, 2016. **197**(2): p. 458-469.

258. Sun, H., et al., *Distinct integrin activation pathways for effector and regulatory T cell trafficking and function.* J Exp Med, 2021. **218**(2).

259. Sun, H., et al., *IL-2 can signal via chemokine receptors to promote regulatory T cells' suppressive function.* Cell Rep, 2023. **42**(8): p. 112996.

260. Ullah, U., et al., *Transcriptional repressor HIC1 contributes to suppressive function of human induced regulatory T cells.* Cell reports, 2018. **22**(8): p. 2094-2106.

261. Ma, J., et al., *CD226 maintains regulatory T cell phenotype stability and metabolism by the mTOR/Myc pathway under inflammatory conditions.* Cell Rep, 2023. **42**(10): p. 113306.

262. Lozano, E., et al., *The TIGIT/CD226 axis regulates human T cell function.* J Immunol, 2012. **188**(8): p. 3869-75.

263. Lo Re, O., et al., *Loss of histone macroH2A1 in hepatocellular carcinoma cells promotes paracrine-mediated chemoresistance and CD4(+)CD25(+)FoxP3(+) regulatory T cells activation.* Theranostics, 2020. **10**(2): p. 910-924.

264. Richer, M.J., M.L. Lang, and N.S. Butler, *T Cell Fates Zipped Up: How the Bach2 Basic Leucine Zipper Transcriptional Repressor Directs T Cell Differentiation and Function.* The Journal of Immunology, 2016. **197**(4): p. 1009-1015.

265. Yang, L., et al., *The Critical Role of Bach2 in Shaping the Balance between CD4(+) T Cell Subsets in Immune-Mediated Diseases.* Mediators Inflamm, 2019. **2019**: p. 2609737.

266. Cho, J.W., et al., *Systems biology analysis identifies TNFRSF9 as a functional marker of tumor-infiltrating regulatory T-cell enabling clinical outcome prediction in lung cancer.* Comput Struct Biotechnol J, 2021. **19**: p. 860-868.

267. Kaminskiy, Y., et al., *Neglected, yet significant role of FOXP1 in T-cell quiescence, differentiation and exhaustion.* Front Immunol, 2022. **13**: p. 971045.

268. Ren, J., et al., *Foxp1 is critical for the maintenance of regulatory T-cell homeostasis and suppressive function.* PLoS Biology, 2019. **17**(5): p. e3000270.

269. Luo, X., et al., *Rnf20 inhibition enhances immunotherapy by improving regulatory T cell generation.* Cell Mol Life Sci, 2022. **79**(12): p. 588.

270. Bhairavabhotla, R., et al., *Transcriptome profiling of human FoxP3+ regulatory T cells.* Hum Immunol, 2016. **77**(2): p. 201-13.

271. Mehta, A.K., D.T. Gracias, and M. Croft, *TNF activity and T cells.* Cytokine, 2018. **101**: p. 14-18.

272. Lin, L., et al., *Oleic acid availability impacts thymocyte preprogramming and subsequent peripheral T(reg) cell differentiation.* Nat Immunol, 2024. **25**(1): p. 54-65.

273. Li, D., et al., *Knockdown of PELI1 promotes Th2 and Treg cell differentiation in juvenile idiopathic arthritis.* Exp Cell Res, 2024. **444**(2): p. 114360.

274. Yang, G., et al., *Insulin-like growth factor 2 enhances regulatory T-cell functions and suppresses food allergy in an experimental model.* J Allergy Clin Immunol, 2014. **133**(6): p. 1702-8 e5.

275. Fernandez, I., et al., *CD101 surface expression discriminates potency among murine FoxP3+ regulatory T cells.* J Immunol, 2007. **179**(5): p. 2808-14.

276. Ohnuma, K., et al., *Role of CD26/dipeptidyl peptidase IV in human T cell activation and function.* Front Biosci, 2008. **13**: p. 2299-310.

277. Salgado, F.J., et al., *CD26: a negative selection marker for human Treg cells.* Cytometry A, 2012. **81**(10): p. 843-55.

278. Pierson, W., et al., *Antiapoptotic Mcl-1 is critical for the survival and niche-filling capacity of Foxp3(+) regulatory T cells.* Nat Immunol, 2013. **14**(9): p. 959-65.

279. Gan, X., et al., *PRR5L degradation promotes mTORC2-mediated PKC-delta phosphorylation and cell migration downstream of Galpha12.* Nat Cell Biol, 2012. **14**(7): p. 686-96.

280. Charbonnier, L.M., et al., *Functional reprogramming of regulatory T cells in the absence of Foxp3.* Nat Immunol, 2019. **20**(9): p. 1208-1219.

281. Guo, T., et al., *PARP11 regulates total levels of type-I interferon receptor IFNAR1.* Nature microbiology, 2019. **4**(11): p. 1771-1773.

282. Basavaraja, R., et al., *PARP11 inhibition inactivates tumor-infiltrating regulatory T cells and improves the efficacy of immunotherapies.* Cell Rep Med, 2024. **5**(7): p. 101649.

283. Konkel, J.E., et al., *Transforming Growth Factor-beta Signaling in Regulatory T Cells Controls T Helper-17 Cells and Tissue-Specific Immune Responses.* Immunity, 2017. **46**(4): p. 660-674.

284. Nakatsukasa, H., et al., *Loss of TET proteins in regulatory T cells promotes abnormal proliferation, Foxp3 destabilization and IL-17 expression.* Int Immunol, 2019. **31**(5): p. 335-347.

285. Carter, N.M. and J.L. Pomerantz, *CARD11 signaling in regulatory T cell development and function.* Adv Biol Regul, 2022. **84**: p. 100890.

286. Shi, H., et al., *Amino acids license kinase mTORC1 activity and Treg cell function via small G proteins Rag and Rheb.* Immunity, 2019. **51**(6): p. 1012-1027. e7.

287. Chen, X.L., et al., *IL-15 trans-presentation regulates homeostasis of CD4(+) T lymphocytes.* Cell Mol Immunol, 2014. **11**(4): p. 387-97.

288. Zaman, T.S., et al., *Notch Balances Th17 and Induced Regulatory T Cell Functions in Dendritic Cells by Regulating Aldh1a2 Expression.* J Immunol, 2017. **199**(6): p. 1989-1997.

289. Vitali, R., et al., *PARP1 inactivation increases regulatory T / Th17 cell proportion in intestinal inflammation. Role of HMGB1.* Immunol Lett, 2024. **270**: p. 106912.

290. Vaeth, M., et al., *Tissue resident and follicular Treg cell differentiation is regulated by CRAC channels.* Nat Commun, 2019. **10**(1): p. 1183.

291. Ma, J., et al., *T-cell-specific deletion of STIM1 and STIM2 protects mice from EAE by impairing the effector functions of Th1 and Th17 cells.* Eur J Immunol, 2010. **40**(11): p. 3028-42.

292. Patterson, S.J., et al., *Cutting edge: PHLPP regulates the development, function, and molecular signaling pathways of regulatory T cells.* J Immunol, 2011. **186**(10): p. 5533-7.

293. Isomura, I., et al., *c-Rel is required for the development of thymic Foxp3+ CD4 regulatory T cells.* J Exp Med, 2009. **206**(13): p. 3001-14.

294. Wang, Y., et al., *LRCH1 suppresses migration of CD4+ T cells and refers to disease activity in ulcerative colitis.* International journal of medical sciences, 2020. **17**(5): p. 599.

295. Su, W., et al., *Protein Prenylation Drives Discrete Signaling Programs for the Differentiation and Maintenance of Effector T(reg) Cells.* Cell Metab, 2020. **32**(6): p. 996-1011 e7.

296. Dong, C., et al., *ICOS co-stimulatory receptor is essential for T-cell activation and function.* Nature, 2001. **409**(6816): p. 97-101.

297. Busse, M., et al., *ICOS mediates the generation and function of CD4+CD25+Foxp3+ regulatory T cells conveying respiratory tolerance.* J Immunol, 2012. **189**(4): p. 1975-82.

298. Wan, Y.Y., et al., *The kinase TAK1 integrates antigen and cytokine receptor signaling for T cell development, survival and function.* Nature Immunology, 2006. **7**(8): p. 851-858.

299. Lei, Y., et al., *Aire-dependent production of XCL1 mediates medullary accumulation of thymic dendritic cells and contributes to regulatory T cell development.* Journal of Experimental Medicine, 2011. **208**(2): p. 383-394.

300. Nguyen, K.D., et al., *XCL1 enhances regulatory activities of CD4+CD25highCD127low/− T cells in human allergic asthma.* The Journal of Immunology, 2008. **181**(8): p. 5386-5395.

301. Pokhrel, R.H., et al., *AMPK promotes antitumor immunity by downregulating PD-1 in regulatory T cells via the HMGCR/p38 signaling pathway.* Mol Cancer, 2021. **20**(1): p. 133.

302. Plaza-Sirvent, C., et al., *c-FLIP Expression in Foxp3-Expressing Cells Is Essential for Survival of Regulatory T Cells and Prevention of Autoimmunity.* Cell Rep, 2017. **18**(1): p. 12-22.

303. Schumann, K., et al., *Functional CRISPR dissection of gene networks controlling human regulatory T cell identity.* Nat Immunol, 2020. **21**(11): p. 1456-1466.

304. Xu, Q., et al., *Deubiquitinase OTUD3: a double-edged sword in immunity and disease.* Front Cell Dev Biol, 2023. **11**: p. 1237530.

305. Liu, Z., et al., *PDK3 drives colorectal carcinogenesis and immune evasion and is a therapeutic target for boosting immunotherapy.* Am J Cancer Res, 2024. **14**(6): p. 3117-3129.

306. Dinkel, B.A., et al., *GRK2 mediates TCR-induced transactivation of CXCR4 and TCR-CXCR4 complex formation that drives PI3Kgamma/PREX1 signaling and T cell cytokine secretion.* J Biol Chem, 2018. **293**(36): p. 14022-14039.

307. Pompura, S.L. and M. Dominguez-Villar, *The PI3K/AKT signaling pathway in regulatory T-cell development, stability, and function.* J Leukoc Biol, 2018.

308. Fu, Y., et al., *TMEM158 promotes pancreatic cancer aggressiveness by activation of TGFβ1 and PI3K/AKT signaling pathway.* J Cell Physiol, 2020. **235**(3): p. 2761-2775.

309. Li, J., et al., *TMEM158 promotes the proliferation and migration of glioma cells via STAT3 signaling in glioblastomas.* Cancer Gene Ther, 2022. **29**(8-9): p. 1117-1129.

310. Zhou, Q.L., et al., *A novel pleckstrin homology domain-containing protein enhances insulin-stimulated Akt phosphorylation and GLUT4 translocation in adipocytes.* J Biol Chem, 2010. **285**(36): p. 27581-9.

311. Sun, D., et al., *CXCL5 impedes CD8(+) T cell immunity by upregulating PD-L1 expression in lung cancer via PXN/AKT signaling phosphorylation and neutrophil chemotaxis.* J Exp Clin Cancer Res, 2024. **43**(1): p. 202.

312. Li, C., et al., *Decreasing of serine/threonine kinase 39 has tumour inhibiting effects on acute myeloid leukaemia by impacting the PI3K/AKT and Wnt/beta-catenin signalling cascades.* Toxicol Appl Pharmacol, 2024. **489**: p. 116982.

313. Jin, Y., et al., *Comprehensive analysis of the expression, prognostic significance, and function of FAM83 family members in breast cancer.* World J Surg Oncol, 2022. **20**(1): p. 172.

314. Ellis, G.I., et al., *Mitochondrial and cytosolic roles of PINK1 shape induced regulatory T-cell development and function.* Eur J Immunol, 2013. **43**(12): p. 3355-60.

315. Chaudhari, A., et al., *ARAP2 promotes GLUT1-mediated basal glucose uptake through regulation of sphingolipid metabolism.* Biochim Biophys Acta, 2016. **1861**(11): p. 1643-1651.

316. Tosello, V., et al., *Calcineurin complex isolated from T-cell acute lymphoblastic leukemia (T-ALL) cells identifies new signaling pathways including mTOR/AKT/S6K whose inhibition synergize with calcineurin inhibition to promote T-ALL cell death.* Oncotarget, 2016. **7**(29): p. 45715-45729.

317. Huang, M., et al., *Sestrin 3 Protects Against Diet-Induced Nonalcoholic Steatohepatitis in Mice Through Suppression of Transforming Growth Factor beta Signal Transduction.* Hepatology, 2020. **71**(1): p. 76-92.

318. Saxton, R.A. and D.M. Sabatini, *mTOR Signaling in Growth, Metabolism, and Disease.* Cell, 2017. **169**(2): p. 361-371.

319. Hoxhaj, G., et al., *The E3 ubiquitin ligase ZNRF2 is a substrate of mTORC1 and regulates its activation by amino acids.* Elife, 2016. **5**.

320. del Rio, R., et al., *Histamine H4 receptor optimizes T regulatory cell frequency and facilitates anti-inflammatory responses within the central nervous system.* J Immunol, 2012. **188**(2): p. 541-7.

321. Chuang, H.C. and T.H. Tan, *MAP4K Family Kinases and DUSP Family Phosphatases in T-Cell Signaling and Systemic Lupus Erythematosus.* Cells, 2019. **8**(11).

322. Ren, X., et al., *SLC39A10 promotes malignant phenotypes of gastric cancer cells by activating the CK2-mediated MAPK/ERK and PI3K/AKT pathways.* Exp Mol Med, 2023. **55**(8): p. 1757-1769.

323. Wang, Q.-L., et al., *Frontiers | T Cell Receptor (TCR)-Induced PLC-γ1 Sumoylation via PIASxβ and PIAS3 SUMO E3 Ligases Regulates the Microcluster Assembly and Physiological Function of PLC-γ1.* Frontiers in Immunology, 2019/02/28. **10**.

324. Shen, Y., et al., *Inactivation of KLF4 promotes T-cell acute lymphoblastic leukemia and activates the MAP2K7 pathway.* Leukemia, 2017. **31**(6): p. 1314-1324.

9 Appendix

9.1 <u>List of genes identified in ATAC-seq. with association to T-cell functions</u>

Table 6: List of genes identified among the top 100 DAR in ATAC-seq. associated to T-cell activation and differentiation.

Closest gene	Log2FoldChange	P value	Padj	Reference
Chrm3	4.51	0.04	0.99	[178]
Nedd4	4.41	0.04	0.99	[179]
Dclre1c	3.70	0.03	0.99	[180]
Nudt4	3.59	0.03	0.99	[181]
Tiam2	3.26	0.01	0.99	[182]
Tfap2c	3.02	0.03	0.99	[183]
Sh2d2a	2.98	0.04	0.99	[184]
Calcrl	2.51	0.04	0.99	[185]
Rasa1	1.82	0.04	0.99	[186]
Txk	1.81	0.00	0.99	[187-189]
Ahi1	1.80	0.00	0.99	[190]
Rock2	1.77	0.02	0.99	[191]
Satb1	1.43	0.02	0.99	[192]
Dad1	1.16	0.03	0.99	[193]
Has3	1.08	0.03	0.99	[194]
Cblb	1.01	0.04	0.99	[195, 196]
Stat5a	0.89	0.01	0.99	[197, 198]
Cox10	0.88	0.01	0.99	[199]
Rara	0.76	0.01	0.99	[200]
Ccr7	0.62	0.03	0.99	[201, 202]
Dgkz	0.54	0.03	0.99	[203]
Pkm	-0.47	0.03	0.99	[204]
Zbtb17	-0.47	0.04	0.99	[205, 206]
Otud7b	-0.49	0.02	0.99	[207, 208]
Foxp4	-0.51	0.02	0.99	[209]

(continued)

Id3	-0.52	0.04	0.99	[210, 211]
Cd200	-0.53	0.03	0.99	[212]
Fyn	-0.53	0.02	0.99	[213]
Tyk2	-0.54	0.01	0.99	[214]
Nfkbiz	-0.54	0.02	0.99	[215, 216]
Cd74	-0.55	0.04	0.99	[217]
Mtmr7	-0.58	0.04	0.99	[218-220]
Pdcd4	-0.58	0.02	0.99	[221, 222]
Spry1	-0.62	0.01	0.99	[223]
Adora2a	-0.63	0.03	0.99	[224]
Atf6	-0.68	0.04	0.99	[225]
Nck2	-0.75	0.00	0.99	[226]
Arf6	-0.76	0.00	0.99	[227]
Rap2b	-0.78	0.01	0.99	[228]
Trat1	-0.81	0.03	0.99	[229]
Mxi1	-0.83	0.01	0.99	[230]
Lcp2	-0.87	0.03	0.99	[231]
Cd44	-0.88	0.02	0.99	[232]
Cd6	-0.88	0.03	0.99	[233]
Cd83	-0.93	0.03	0.99	[234]
Myb	-0.98	0.00	0.99	[235]
Cd69	-1.12	0.02	0.99	[236, 237]
Pag1	-1.31	0.04	0.99	[238]
Il15	-1.31	0.00	0.99	[239]
Foxo1	-1.82	0.01	0.99	[240]

Table 7: List of genes identified among the top 1000 DAR in ATAC-seq. associated to Treg-cell functions.

Closest gene	Log2FoldChange	P value	Padj	reference
Mcu	3.19	0.02	0.99	[241]
Stat5b	2.35	0.03	0.99	[242]
Mbd2	1.85	0.03	0.99	[243, 244]
Ctla4	1.69	0.03	0.99	[245-247]
Pfkp	1.42	0.01	0.99	[248]
Gata3	1.33	0.02	0.99	[249, 250]
Gbp4	1.33	0.02	0.99	[251]
Il21	1.26	0.03	0.99	[252-254]
Irf2bp2	1.16	0.02	0.99	[255]
Crem	1.10	0.04	0.99	[256]
Pbx1	0.92	0.02	0.99	[257]
Stat5a	0.89	0.01	0.99	[197, 198]
Apbb1ip	0.85	0.04	0.99	[258, 259]
Hic1	0.77	0.03	0.99	[260]
Cd226	0.77	0.03	0.99	[261, 262]
H2afy	0.77	0.01	0.99	[263]
Ccr7	0.62	0.03	0.99	[201, 202]
Bach2	-0.42	0.02	0.99	[264, 265]
Tnfrsf9	-0.48	0.03	0.99	[266]
Foxp1	-0.49	0.04	0.99	[267, 268]
Rnf20	-0.49	0.02	0.99	[269]
Rtkn2	-0.49	0.03	0.99	[270]
Tnf	-0.52	0.02	0.99	[271]
Peli1	-0.53	0.02	0.99	[272, 273]
Fyn	-0.53	0.02	0.99	[213]
Igf2r	-0.54	0.02	0.99	[274]
Cd74	-0.55	0.04	0.99	[217]
Cd101	-0.59	0.03	0.99	[275]
Dpp4	-0.61	0.02	0.99	[276, 277]
Mcl1	-0.62	0.02	0.99	[278]
Prr5l	-0.65	0.01	0.99	[279, 280]

(continued)

Parp11	-0.68	0.01	0.99	[281, 282]
Tgfbr1	-0.69	0.04	0.99	[283]
Tet3	-0.69	0.01	0.99	[284]
Card11	-0.71	0.03	0.99	[285]
Rheb	-0.76	0.02	0.99	[286]
Il15ra	-0.79	0.00	0.99	[287]
Rbpj	-0.79	0.04	0.99	[288]
Parp1	-0.88	0.00	0.99	[289]
Cd44	-0.88	0.02	0.99	[232]
Cd6	-0.88	0.03	0.99	[233]
Stim2	-0.89	0.03	0.99	[290, 291]
Phlpp1	-0.91	0.01	0.99	[292]
Rel	-0.99	0.01	0.99	[293]
Lrch1	-1.02	0.01	0.99	[294]
Fntb	-1.07	0.02	0.99	[295]
Icos	-1.08	0.01	0.99	[296, 297]
Map3k7	-1.09	0.00	0.99	[298]
Xcl1	-1.10	0.01	0.99	[299, 300]
Cd69	-1.12	0.02	0.99	[236, 237]
Hmgcr	-1.23	0.01	0.99	[301]
Cflar	-1.49	0.01	0.99	[302]
Hivep2	-1.58	0.03	0.99	[303]

Table 8: List of genes identified among the top 1000 DAR in ATAC-seq. associated to T-cell signalling pathways.

Pi3K/AKT-signalling				
Closest gene	Log2FoldChange	P value	Padj	Ref.
Otud3	3.17	0.02	0.99	[304]
Pdk3	2.91	0.01	0.99	[305]
Grk4	2.88	0.04	0.99	[306]
Pik3r6	2.55	0.02	0.99	[307]
Tmem158	2.52	0.04	0.99	[308, 309]
Rara	0.76	0.01	0.99	[200]
Phldb1	-0.54	0.02	0.99	[310]
Pxn	-0.55	0.04	0.99	[311]
Stk39	-0.62	0.01	0.99	[312]
Fam83g	-0.69	0.03	0.99	[313]
Pink1	-0.70	0.04	0.99	[314]
Arap2	-0.78	0.03	0.99	[315] [269]
mTOR-signalling				
Ppp3ca	2.31	0.04	0.99	[316]
Sesn3	-0.47	0.03	0.99	[317]
Mlst8	-0.51	0.02	0.99	[318]
Znrf2	-0.64	0.01	0.99	[319]
Rps6ka1	-0.57	0.04	0.99	
ERK				
Hrh4	5.64	0.00	0.99	[320]
Dusp10	2.49	0.02	0.99	[321]
Slc39a10	1.62	0.03	0.99	[322]
Other signalling pathways				
Jak2	1.77	0.00	0.00	
Pias3	-0.44	0.04	0.99	[323]
Klf4	-0.62	0.02	0.99	[324]

9.2 List of potentially hazardous substances

Table 9: List of potentially hazardous substances

Substance	GHS symbol	Hazard statement	Precautionary statement
2-Mercaptoethanol		H301+H331, H310, H315, H317, H318, H361f, H373, H410	P273, P280, P301+P310, P302+P352+P310, P304+P340+P311, P305+P351+P338
4',6-Diamidino-2-phenylindol		H315, H317, H335	P261, P264, P271, P272, P280, P302+P352
Acetic acid		H226, H314	P210, P280, P301+P330+P331, P303+P362+P353, P305+P351+P338
Acrylamide		H301, H312, H332, H315, H317, H319, H340, H350, H361f, H372	P201, P280, P301+P310, P302+P352+P312, P304+P340+P312, P305+P351+P338
Ammonium chloride		H302, H319	P270, P305+P351+P338
Boric acid		H360FD	P201, P304+P340, P308+P313
Calcium chloride		H319	P280, P305+P351+P338, P337+P313

(continued)

Chloroform	H302, H331, H315, H319, H351, H361d, H336, H372, H421	P201, P273, P301+P312+P330, P302+P352+, P304+P340+P311, P308+P313
Diammonium peroxodisulfate	H272, H302, H315, H317, H319, H334, H335	P210 , P280, P301+P312, P302+P352, P304+P340+P312, P305+P351+P338
Ethanol	H225, H319	P210, P233, P240, P241, P242, P305+P251+P338
Ethylenediamine-tetraacetic acid	H319, H332, H373	P280, P304+P340, P312, P305+P351+P338, P337+P313
Formaldehyde	H301+H311+H331, H314, H317, H335, H341, H350, H370	P201, P280, P301+P330+P331, P303+P361+P353, P304+P340, P305+P351+P338, P308+P310
Hydrchloric acid	H290, H314, H335	P234, P261, P271, P280, P303+ P361+ P353, P305+P351+P338

(continued)

Imidazole		H302, H314, H360D	P260, P280, P301+P312, P303+ P361+P353, P304+P340+P310, P305+P351+P338
Sodium-iodacetate		H301, H314	P260, P270, P280, P303+P361+P353, P304+P340+P310, P305+P351+P338
Isoflurane		H336	P261, P271, P304+P340+P312, P403+P233, P501
Isopropanol		H225, H319, H336	P210, P233, P240, P241, P242, P305+P351+P338
Isopropyl β-D-1-thiogalactopyranoside ≤ 0.1% Dioxan		H350	P201, P202, P280, P308+P313, P405, P501
Methanol		H225, H301+H311+H331, H370	P210, P233, P280, P301+P310, P303+P361+P353, P304+P340+P311
N,N' Methylendiacrylamide		H301, H312, H340, H350, H361fd, H372	P202, P260, P264, P280, P301+P310, P302+P352+P312
N,N,N,N'-Tetramethylethylenediamine		H225, H302+H332, H314	P210, P280, P301+P330+P331, P303+P361+P353, P305+P351+P338, P310

(continued)

Oligomycin		H301, H302	P264, P270, P330, P405, P501
Paraformaldehyde		H228, H302+H332, H315, H317, H318, H335, H341, H350	P210, P280, P301+P312, P304+P340+P312, P305+P351+P337, P308+P313
Penicillin/streptomycin		H317, H361fd	P201, P202, P261, P272, P280, P302+P352, P308+P313, P333+P313, P362+P364, P501
Phenole TE		H301+H311+H331, H314, H341, H373, H411	P202, P273 , P280, P303+P361+P353, P304+P340+P310, P305+P351+P338
Phenole/Chloroform/ Isoamylalcohol		H301+H331, H312, H314, H341, H351, H361d, H372, H411	P201, P270, P280, P304+P340, P305+P351+P338, P308+P313
Phorbol-12-mysistate-13-acetate		H315	P280, P302+P352
Sodium hydroxide		H290, H314	P234, P260, P280, P303+P361+P353, P304+P340+P310, P305+P351+P338

(continued)

Sulfuric acid		H290, H314	P234, P280, P303+P361+P353, P304+P340+P310, P305+P351+P338, P363
Triton X-100		H302, H318, H411	P270, P273, P280, P305+P351+P338, P310
Trypan Blue solution		H350, H361	P201, P280, P202, P308+P313, P501

9.3 List of abbreviations

Abbreviation	Description
°C	Degree Celsius
2-DG	2-Deoxy-D-glucose
a.u.	Arbitrary units
ANOVA	Analysis of variance
APC	Antigen presenting cells
ATAC-seq.	Assay for transposase-accessible chromatin sequencing
ATP	Adenosine triphosphate
Ca^{2+}	Calcium
cDNA	Complementary DNA
CNS2	Non-coding region 2
COX IV	Cytochrome c oxidase subunit IV
CPP-Ppx1	Cell-penetrating peptide - polyphosphatase
CTLA4	Cytotoxic T-lymphocyte-associated protein 4
DAMP	Damage-associated molecular patterns
DAPI	4',6-Diamidino-2-phenylindole
DAR	Differentially accessible genomic regions
ECAR	Extracellular acidification rate
EDX	Electron dispersive X-ray spectroscopy
ELISA	Enzyme-linked immunosorbent assay
ERK	Extracellular signal regulated kinase
FCS	Fetal calf serum
Foxp3	Forkhead box P3
FSC	Forward scatter
FXII	Factor XII
GAPDH	Glycerinaldehyd-3-phosphate-dehydrogenase
Gls2	Glutaminase 2
Glut1	Glucose transporter 1
GO	Gene ontology
HBSS	Hanks balanced salt solution
HPH-1	Polyhomeotic-like protein 1

(continued)

Hif1α	Hypoxia-inducible factor 1α
HIV	human immunodeficiency virus
Hk2	Hexokinase 2
IDO	Indoleamine 2,3-dioxygenase
IFNγ	Interferon γ
IL	Interleukin
IPTG	Isopropyl-β-D-thiogalactopyranoside
iTreg	Induced regulatory T cell
MACS	Magnetic activated cell sorting
MDR	MitoTracker DeepRed
MEM NEAA	Minimum Essential Medium Non-Essential Amino Acids
MFI	Median fluorescent intensity
MG	MitoTracker Green
MHC	Major histocompatibility complex
Mtc4	Monocarboxylate-transporter 4
mTOR	Mammalian target of rapamycin
Myc	Myelocytomatosis oncogene
NET	Neutrophil extracellular trap
NFAT	Nuclearfactor of activated T-Cells
NFκB	Nuclear factor of kappa-light-chain-enhancer of activated B cells
NK cells	Natural killer cells
nTreg	Natural regulatory T cells
OCR	Oxygen consumption rate
OXPHOS	Oxidative phosphorylation
Padj	Adjusted p-value
PAGE	Polyacrylamide gel electrophoresis
PC	Principle component
PD1	Programmed cell death
PMA	Phorbol 12-myristate 13-acetate
PolyP	Polyphosphate
Ppk	Polyphosphate kinase
Ppx	Polyphosphatase

(continued)

Rorγt	Retinoic acid receptor-related orphan receptor gamma
ROS	Reactive oxygen species
RT	Room temperature
RT-qPCR	Real-time quantitative polymerase chain reaction
SDS	Sodium dodecyl sulphate
SEM	Standard error of the mean
SSC	Side scatter
STAT	Signal transducer and activator of transcription
T-bet	T-box expressed in T cells
TCR	T-cell receptor
Teff	Effector T cells
TEM	Transmission electron microscopy
TGF-β	Transforming growth factor beta
Th	T helper
TMB	3.3',5,5' Tetramethylbenzidine
TNFα	Tumour necrosis factor α
Tpi1	Triose phosphate isomerase 1
Treg	Regulatory T cell
Tresp	Responder T cells
TSS	Transcription start side
ZMNH	Center for Molecular Neurobiology Hamburg

9.4 <u>Acknowledgements</u>

Ein weiterer Dank geht an meine Eltern, Marcel und Martin für eure ausnahmslose Unterstützung in meinem wissenschaftlichen Werdegang und dafür, dass ihr immer an mich geglaubt habt. Vor allem dafür, dass ihr mich immer wieder aufgefangen habt, wenn ich einen weiteren Tiefpunkt erreicht habe. Aber ganz besonders möchte ich dir danken, Martin, für die wunderbare Zeit außerhalb der Arbeit: Du zeigst mir immer wieder was im Leben wirklich wichtig ist und wofür es sich gelohnt hat diesen Weg einzuschlagen.

10 Statement of contribution by others

Electron microscopy was performed by Dr. Michaela Schweizer at the Center for Molecular Neurobiology Hamburg (ZMNH). ATAC-seq. and demethylation analyses were performed by external companies as described. In some experiments, technical assistance for urea PAGE, malachite green assays, cell culture, ELISAs and T-cell isolations were provided through cooperational work practice within the Molecular T-cell Immunology group, namely Mandy Malle, M.Sc Marion Mengel and PD Dr. Reiner Mailer.

11 Eidesstattliche Versicherung

Hiermit versichere ich an Eides statt, die vorliegende Dissertationsschrift selbst verfasst und keine anderen als die angegebenen Quellen und Hilfsmittel benutzt zu haben. Sofern im Zuge der Erstellung der vorliegenden Dissertationsschrift generative Künstliche Intelligenz (gKI) basierte elektronische Hilfsmittel verwendet wurden, versichere ich, dass meine eigene Leistung im Vordergrund stand und dass eine vollständige Dokumentation aller verwendeten Hilfsmittel gemäß der Guten wissenschaftlichen Praxis vorliegt. Ich trage die Verantwortung für eventuell durch die gKI generierte fehlerhafte oder verzerrte Inhalte, fehlerhafte Referenzen, Verstöße gegen das Datenschutz- und Urheberrecht oder Plagiate.

Hamburg, 31.07.2025